

LEVEL II

(12)

DNA 3964F-21-1

THE ROSCOE MANUAL

Volume 21-1: Optics Model

Joel Garbarino
John Ise

General Research Corporation
P.O. Box 6770
Santa Barbara, California 93111

V1-A13

V20-...

1 January 1980

Final Report for Period 9 November 1977-1 January 1980

CONTRACT No. DNA 001-78-C-0002

APPROVED FOR PUBLIC RELEASE;
DISTRIBUTION UNLIMITED.

DTIC
SELECTED
MAR 25 1981

A

THIS WORK SPONSORED BY THE DEFENSE NUCLEAR AGENCY
UNDER RDT&E RMSS CODE B322078464 S99QAXHC30101 H2590D.

Prepared for
Director
DEFENSE NUCLEAR AGENCY
Washington, D. C. 20305

81 3 25 065

AD A 096823

DTIC FILE COPY

Destroy this report when it is no longer
needed. Do not return to sender.

PLEASE NOTIFY THE DEFENSE NUCLEAR AGENCY,
ATTN: STTI, WASHINGTON, D.C. 20305, IF
YOUR ADDRESS IS INCORRECT, IF YOU WISH TO
BE DELETED FROM THE DISTRIBUTION LIST, OR
IF THE ADDRESSEE IS NO LONGER EMPLOYED BY
YOUR ORGANIZATION.



UNCLASSIFIED

SECURITY CLASSIFICATION OF THIS PAGE (When Data Entered)

19 REPORT DOCUMENTATION PAGE			READ INSTRUCTIONS BEFORE COMPLETING FORM
1 REPORT NUMBER 18) DNA 3964F-21-1 ✓	2 GOVT ACCESSION NO AD-A096	3 RECIPIENT'S CATALOG NUMBER 823	
4 TITLE (and Subtitle) 6) THE ROSCOE MANUAL • Volume 21-1 Optics Model •		5 TYPE OF REPORT & PERIOD COVERED 9) Final Report for Period 9 Nov '77-1 Jan 80	
7 AUTHOR(s) 10) Joel Garbarino John Ise		6 PERFORMING ORG. REPORT NUMBER CR-1-520, Vol. 21-1 ✓	
9 PERFORMING ORGANIZATION NAME AND ADDRESS General Research Corporation ✓ P. O. Box 6770 Santa Barbara, California 93111		8 CONTRACT OR GRANT NUMBER(s) 15) DNA 001-78-C-0002 ✓	
11 CONTROLLING OFFICE NAME AND ADDRESS Director Defense Nuclear Agency Washington, D.C. 20305		10 PROGRAM ELEMENT PROJECT TASK AREA & WORK UNIT NUMBERS 16) Subtask S99QAXHC301-01	17) 2307
14 MONITORING AGENCY NAME & ADDRESS (if different from Controlling Office) 14) GRC-CR-1-520-VOL-21-1		12 REPORT DATE 11) 1 January 1980	
		13 NUMBER OF PAGES 98	12) 99/
		15 SECURITY CLASS (of this report) UNCLASSIFIED	
16 DISTRIBUTION STATEMENT (of this Report) Approved for public release; distribution unlimited.			
17 DISTRIBUTION STATEMENT (of the abstract entered in Block 20, if different from Report)			
18 SUPPLEMENTARY NOTES This work sponsored by the Defense Nuclear Agency under RDT&E RMSS Code B322078464 S99QAXHC30101 H2590D.			
19 KEY WORDS (Continue on reverse side if necessary and identify by block number) Nuclear Effects Simulation Optics Ballistic Missile Defense Computer Program			
20 ABSTRACT (Continue on reverse side if necessary and identify by block number) The ROSCOE computer code is designed specifically to be the laboratory standard for evaluating nuclear effects on radar and optical sensors. This paper presents (1) a description of the optical code interface structure; and (2) a review of the major tasks performed by GRC--the modeling of inhomogeneous regions. The first part describes the optics code structure and the system simulation methodology, and presents some sample outputs of targets detected against inhomogeneous (striated)			

DD FORM 1 JAN 73 1473

EDITION OF 1 NOV 65 IS OBSOLETE

A

UNCLASSIFIED

SECURITY CLASSIFICATION OF THIS PAGE (When Data Entered)

402754

llw

UNCLASSIFIED

SECURITY CLASSIFICATION OF THIS PAGE(When Data Entered)

20. ABSTRACT (Continued)

↙ nuclear debris, whose characterization is in terms of an exponential autocorrelation function for integrated radiance. Separate exponentiation decorrelation lengths are used along and perpendicular to the earth's magnetic field, and time decorrelation is also exponential. ↗

UNCLASSIFIED

B
SECURITY CLASSIFICATION OF THIS PAGE(When Data Entered)

TABLE OF CONTENTS

<u>Section</u>		<u>Page</u>
	LIST OF ILLUSTRATIONS	2
1	INTRODUCTION	3
2	SUMMARY OF CODE DEVELOPMENT	4
	2.1 Optics Code Structure	4
	2.2 Systems Simulation Methodology and Sample Output	8
3	MODELING OF INHOMOGENEOUS REGIONS	37
	3.1 Introduction	37
	3.2 Generation of Radiant Intensities in the Ideal Focal Plane	39
	3.3 Differentiability of First-Order Markov Processes	48
	3.4 Autocorrelation Function for Gaussian Striations	54
	REFERENCES	60
	APPENDIX A: EXTRAPOLATION AND INTERPOLATION OF RANDOM SEQUENCE	61
	APPENDIX B: FLOW DIAGRAMS	65

A

LIST OF ILLUSTRATIONS

<u>Figure</u>		<u>Page</u>
1	Systems Function Interaction Chart	5
2	Physics Function Interaction Chart	6
3	Surveillance Sensor Dynamics (OLOOK)	9
4	Object Dynamics (OPROP)	10
5	Object Characterization	12
6	Number of Paths/Object	13
7	Example Sight Paths for Fireball	14
8	Path Integration (SPCALC)	16
9	Example Cell List	18
10	Focal Plane Generation (OPSIM)	21
11	Variation in Mean Intensity	23
12	Spatial Correlation	25
13	Time Correlation	26
14	Time Correlation	27
15	Multiple Fireballs	28
16	Multiple Objects	30
17	Multiple Objects--Growth With Time	31
18	Sensor Scan	32
19	Optics Data Processing	33
20	Surveillance Sensor Example	35
21	Surveillance Sensor--Example Output	36
22	Extrapolation of Gaussian Sequence in Three Dimensions	46
23	"Derivative" of First-Order Markov Sequence	51
24	Autocorrelation Function For Distribution of Gaussian Striations	59

1 INTRODUCTION

As part of a continuing effort to supply the user community with the best phenomenology codes available for the evaluation of nuclear effects on sensors, DNA has undertaken the task of expanding the ROSCOE (Radar and Optical Systems Code with Nuclear Effects) computer program¹ to include an optical/SWIR capability.

An initial program planning phase was initiated in 1976 to formulate the objectives of this model, place bounds on the scope and level of detail required, and suggest a plan for its development. The plan called for code development during 1977 and 1978, with a completion date of approximately January 1979, followed by a code validation and documentation effort.

General Research Corporation, as part of a team of contractors, has participated in this program development effort. GRC's responsibilities have been primarily concerned with the development of the optics system model and the interfacing of the optics package (both systems and physics) with the code as a whole.

This paper presents a summary of the optics code structure. In Section 2, a description of the optical code interface structure is given; Section 3 presents a review of one of the major tasks performed by GRC-- the modeling of inhomogeneous regions. Appendix A provides some analytical backup material for Section 3, and Appendix B contains flow diagrams for the major programs and subroutines which comprise the optics code interface structure.

2 SUMMARY OF CODE DEVELOPMENT

The following sections describe the optics code structure, the system simulation methodology, and some sample outputs.

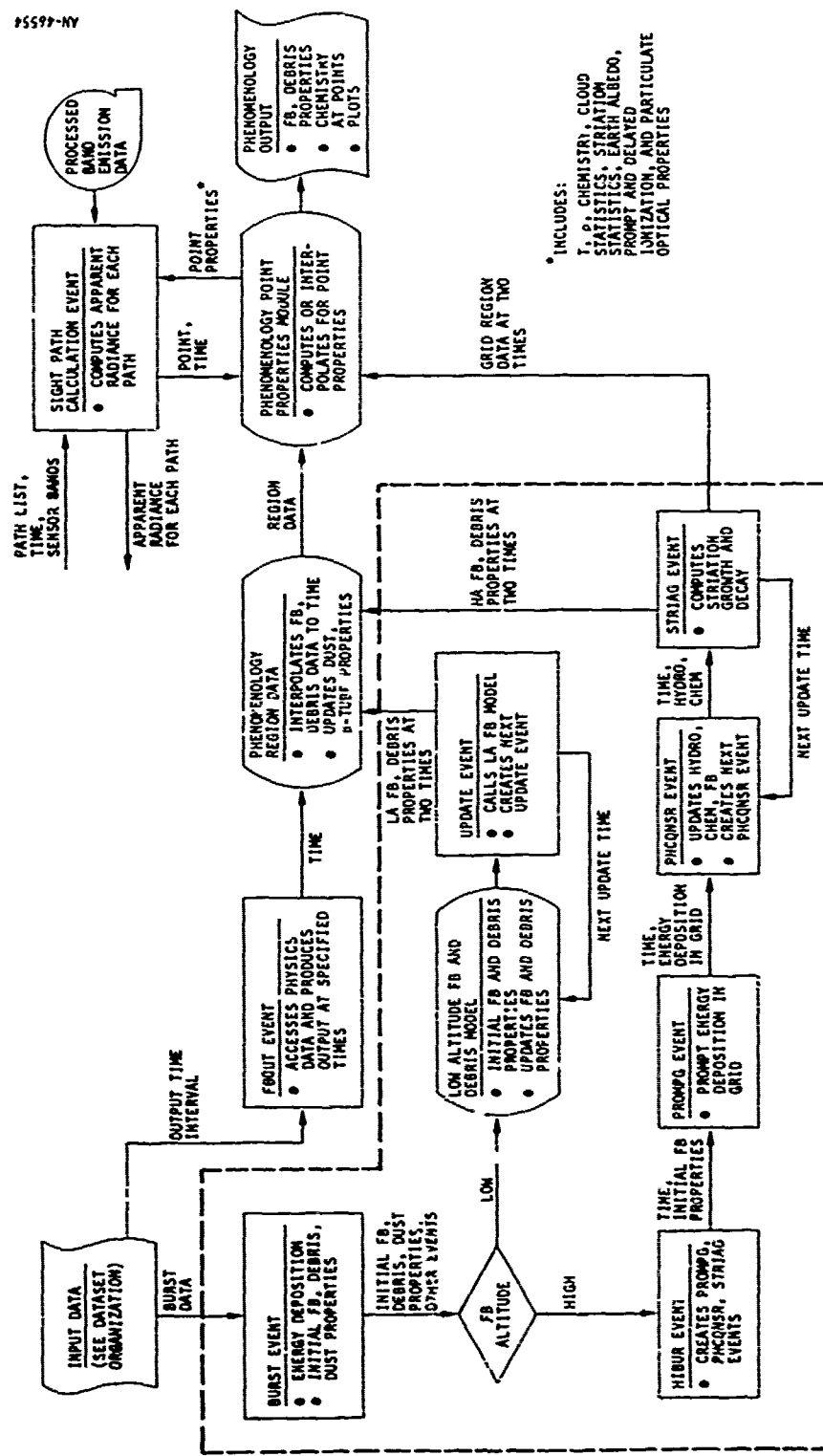
2.1 OPTICS CODE STRUCTURE

The ROSCOE code is divided into a number of separate computational blocks which perform various parts of the systems or physics simulation. Each block is made up of a number of subroutines, and is stored in a separate overlay. These blocks are referred to as "events." In the execution of the code, a series of computations, or events, is set up. Each of these events is given a calculation time, and they are processed (i.e., the proper overlay is called and executed) in a time-ordered fashion. An initial list of events is set up in the input deck by the user. Additional events may be added to the list as computations are carried out to complete the simulation specified.

A block diagram showing the major computational blocks and information flow for the optics code is shown in Figs. 1* and 2. The optics systems blocks, or events, are shown in Fig. 1, and the physics events in Fig. 2. Some interface blocks which feed phenomenology data to the systems blocks are shown in both figures.

The physics portion of the model (Fig. 2) is comprised of a burst event which creates the initial burst parameters and several update events to update the nuclear environment in time. In the low-altitude region (<90 km), an update event is used to maintain the fireball and debris region data at two times. The update event calls the fireball and debris model routines at specified times to update these data, and then they are interpolated at intermediate times as requested for systems calculations or for printout.

* A similar diagram for the ROSCOE radar code is given in Volume 1 of The ROSCOE Manual.



* INCLUDES:
 T, P, CHEMISTRY, CLOUD
 STATISTICS, STRIATION
 STATISTICS, AERIAL ALBEDO,
 PROMPT AND DELAYED
 IONIZATION, AND PARTICULATE
 OPTICAL PROPERTIES

Figure 2. Physics Function Interaction Chart

The high-altitude data are also maintained at two times. Here, because the nuclear effects may be more widespread, a grid of physical data (chemistry, striations) is computed in addition to fireball and debris properties (which are treated as overlays on the grid).

The optics system portion of the code consists of (1) an attack generation event, which initializes the ambient atmosphere and magnetic field models and creates objects to be viewed by the sensor; (2) an optics look event (OLOOK), which sets up the sensor look geometry; (3) an optics propagation path event (OPROP), which sets up the number and position of sight paths in the sensor field of view for creating the "scene" at the focal plane; (4) a sight path calculation event (SPCALC), which performs the integration of the radiation transport equation along each sight path; (5) a simulated optics event (OPSIM), which generates a focal plane array using the sight path data and simulates the scanning and signal processing functions of the optical sensor; and (6) a set of system events (currently there is only an optical track function (OTRACK) modeled here) to simulate various system functions such as track, homing, or discrimination.

The systems/physics interface structure is much the same as for the radar code. The propagation and sight path calculation events access phenomenology region data (e.g., fireball, debris, dust, beta tube parameters) by calling a subroutine which interpolates these data in time. The sight path calculation event also accesses a point properties module. It supplies the time and location of the point in space, and the point properties module returns the appropriate data requested. These data include temperature, mass density, chemical composition, cloud statistics, striation statistics, earth albedo, prompt and delayed ionization, and particulate optical properties. In addition, the sight path calculator accesses preprocessed band emission data from external data blocks.

2.2 SYSTEMS SIMULATION METHODOLOGY AND SAMPLE OUTPUT

This section describes the optical system simulation methodology. The discussion which follows describes the use of the SWIR code by guiding the reader through the simulation procedure block by block, and displaying some intermediate code outputs.

1. Surveillance Sensor Dynamics (OLOOK).^{*} An example of how the optics look (OLOOK) event sets up the look geometry for a surveillance-type sensor is illustrated in Fig. 3. The boresight of the sensor is determined from the satellite position and a reference position, as shown. The frame time (the time it takes for the sensor to complete its circular scan) is input, and must be consistent with the scan rate desired.

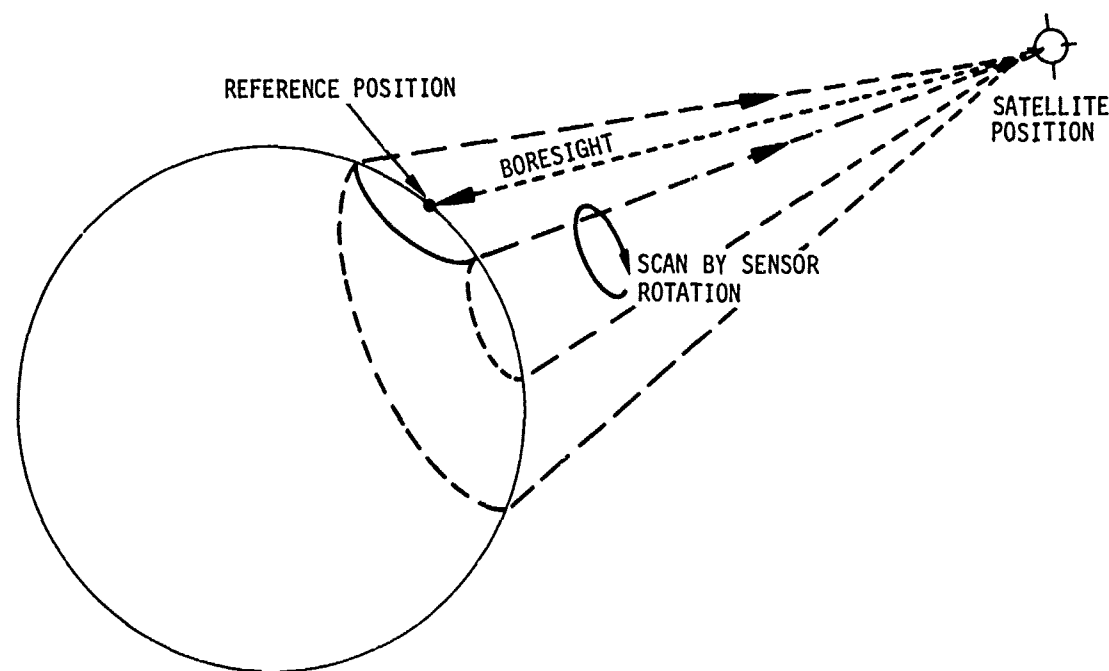
Scanning motion is simulated by creating a frozen frame of the environment at a selected engagement time and then sweeping over this frame in a circular fashion at the appropriate rate.

2. Object Dynamics (OPROP). In the optics propagation (OPROP) event, the object motion in the sensor field of view is treated by interpolating in time for the position of each object, and then transforming these coordinates to the sensor coordinate frame. Objects treated include nuclear bursts and their associated ionization regions, booster plumes, and natural clouds (see Fig. 4).

The sensor coordinate frame[†] is defined by setting the z-vector anti-parallel to the boresight. The y-vector is in the plane formed by the z-vector and the satellite position vector, and is directed as close to the satellite position vector as possible. The x-vector is chosen to complete the right-hand system.

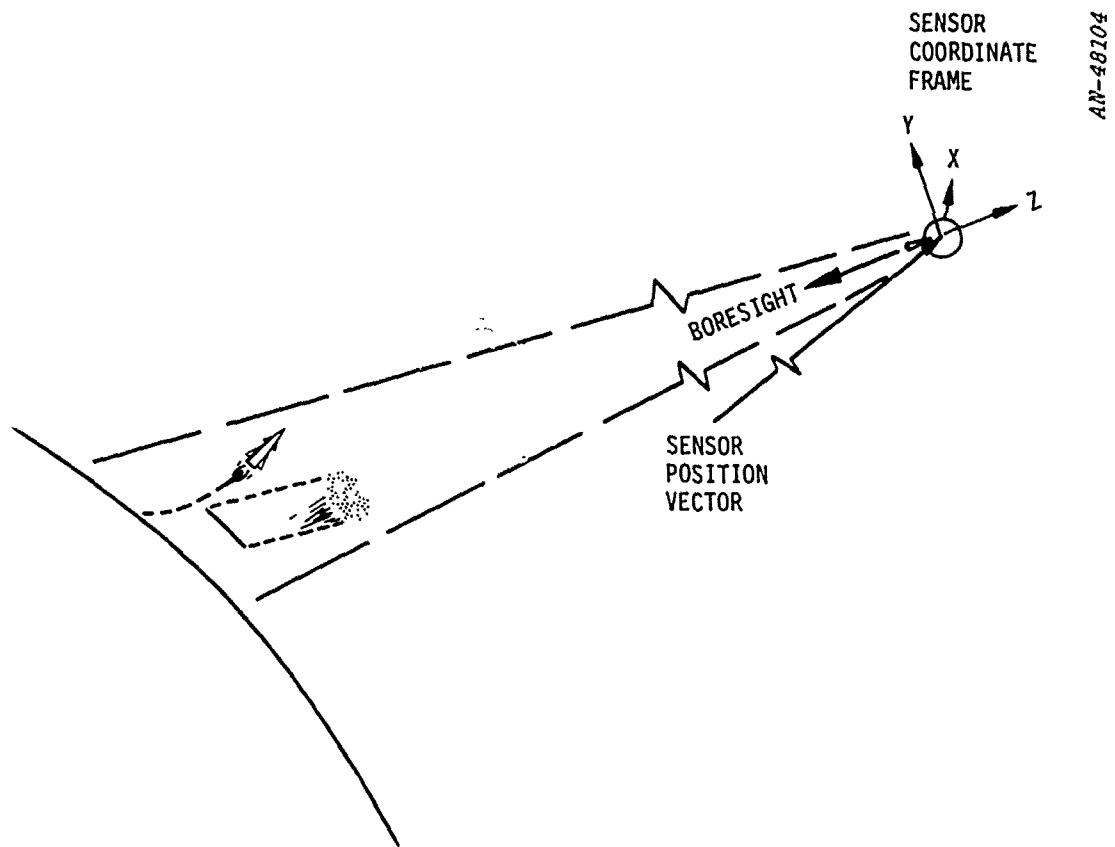
* The block names are given here so that the radar can refer back to the block diagrams shown in Figs. 1 and 2.

† This coordinate system is used in generating the focal plane array.



- BORESIGHT ESTABLISHED BY POINTING AT REFERENCE POSITION
- FRAME TIME BASED ON ROTATION RATE
- CIRCULAR SCAN SIMULATES SENSOR MOTION

Figure 3. Surveillance Sensor Dynamics (OLOOK)



- OBJECTS INCLUDE - NUCLEAR BURSTS (ASSOCIATED REGIONS)
 - BOOSTER PLUMES
 - NATURAL CLOUDS
- SENSOR COORDINATE FRAME

Figure 4. Object Dynamics (OPROP)

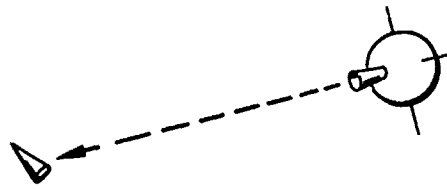
3. Object Characterization (OPROP). To characterize the objects in the focal plane of the sensor, the code integrates the radiation transport along a number of paths from the sensor which intersect each object. Since these path integrations can be time-consuming, an attempt is made to minimize the number of paths used by selecting a relatively few paths and interpolating between them later to generate finer detail in the focal plane.

Objects or regions are divided into three types: (1) point objects, which are objects whose dimensions are small compared to the sensor resolution; (2) extended objects (such as fireballs), which may be bright and cover many resolution cells; and (3) background, or other regions which are less bright or very extensive (cover the entire field of view).

Point objects can be characterized by a single path, as shown in Fig. 5. Extended objects are treated by taking the object projection in a plane normal to the vector between the sensor and the object, and selecting a set of points within this boundary. Finally, the background is treated in as much (or as little) detail as the user feels is warranted by setting up a grid of points within the sensor field of view. The user selects the grid spacing in the input deck. A default value of four points is used as a minimum.

4. Number of Paths/Object (OPROP). The number of paths used to characterize an extended object is a function of the object size and the sensor resolution, as shown in Fig. 6. One, five, seven, or thirteen paths through the region are set up for integration using the scaling rules shown.

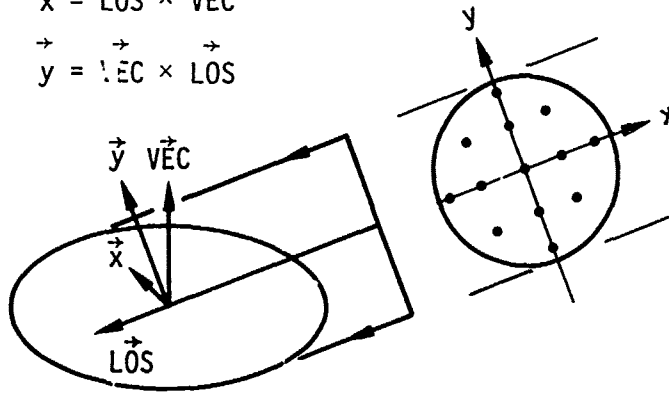
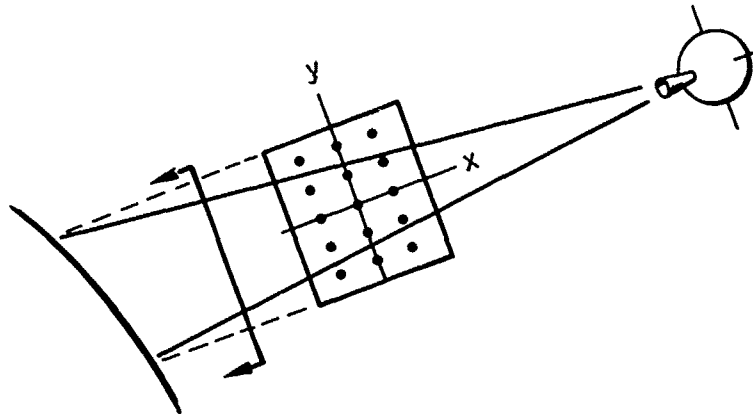
5. Example Sight Paths to a Fireball (OPROP). An example set of sight paths used in generating the focal plane image of a fireball is shown in Fig. 7. Here a striated fireball is viewed by a sensor on a synchronous satellite. The sensor resolution was small compared to the



POINT OBJECT--SINGLE PATH

$$\vec{x} = \vec{LOS} \times \vec{VEC}$$

$$\vec{y} = \vec{VEC} \times \vec{LOS}$$

EXTENDED OBJECT--MULTIPLE PATHS TO POINTS
ON OBJECT PROJECTION

BACKGROUND--GRID OF POINTS

Figure 5. Object Characterization

$NPX = \text{IFIX} (\Delta X / \text{RESOL}) - 1$
 $NPY = \text{IFIX} (\Delta Y / \text{RESOL}) - 1$
 WHERE: $\Delta X, \Delta Y$ = OBJECT ANGULAR SUBTENSE
 RESOL = SENSOR ANGULAR RESOLUTION

AN-48106

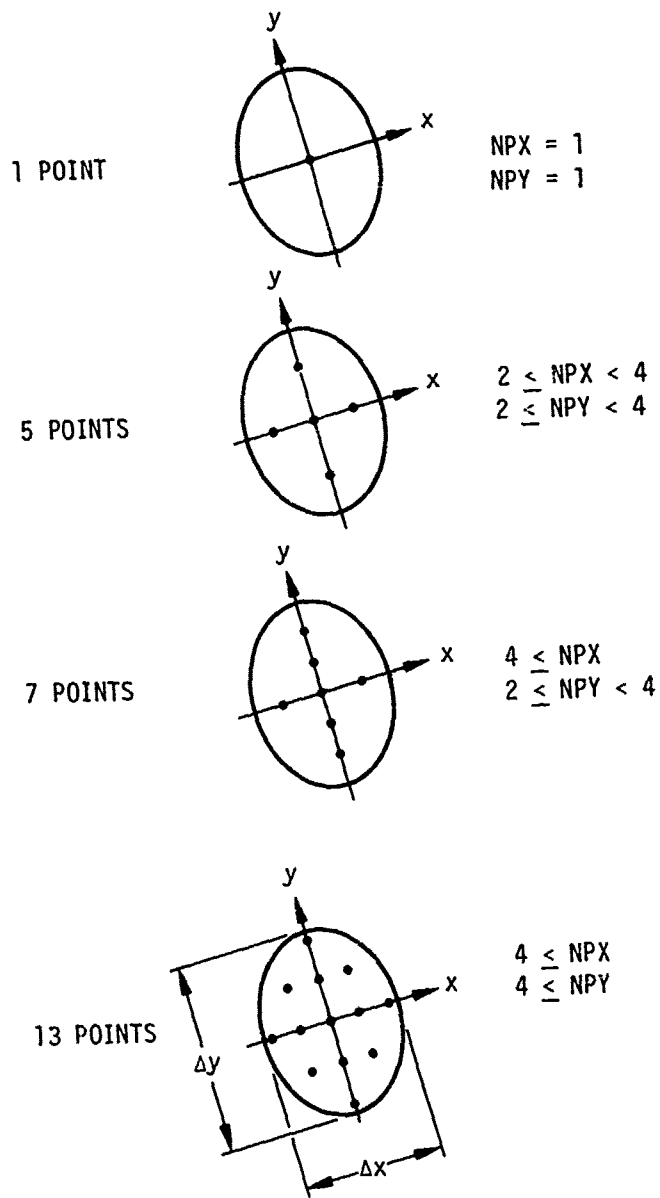


Figure 6. Number of Paths/Object

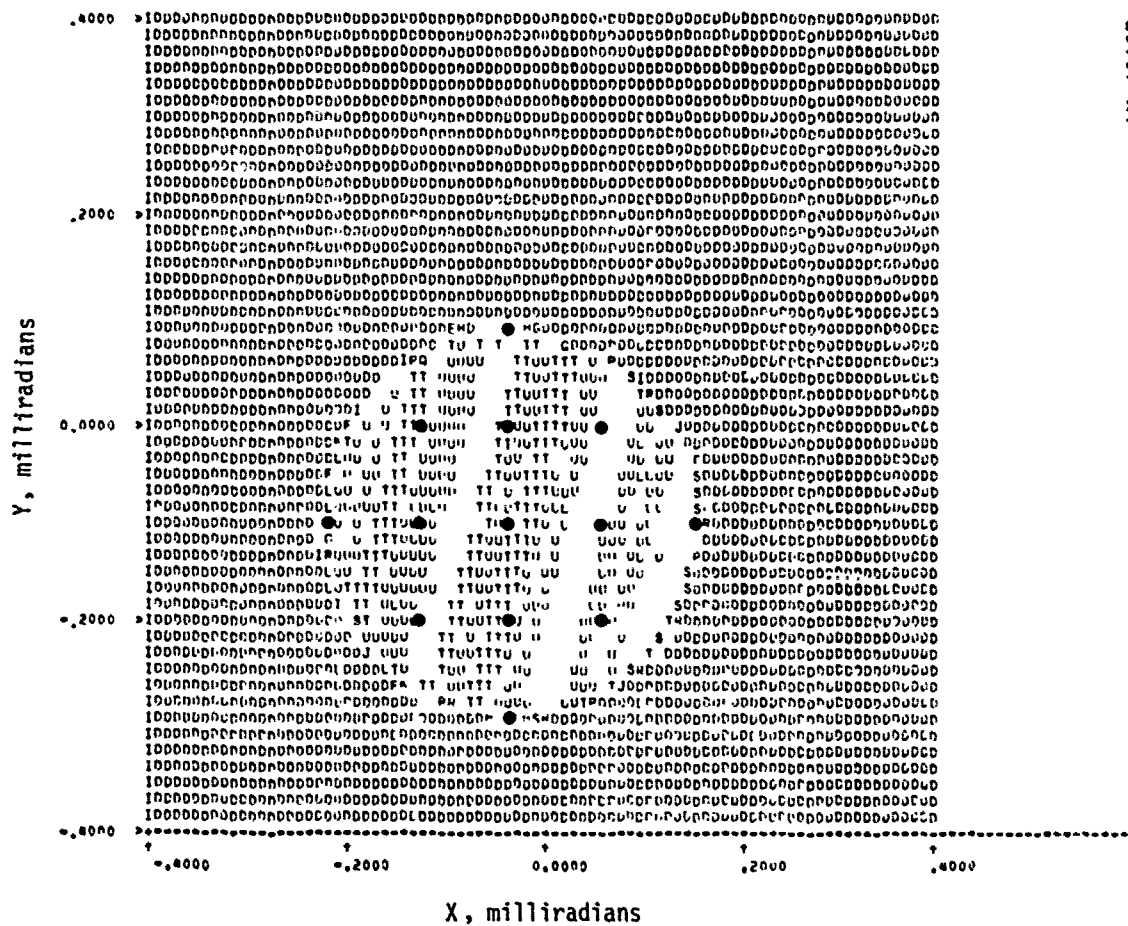


Figure 7. Example Sight Paths for Fireball

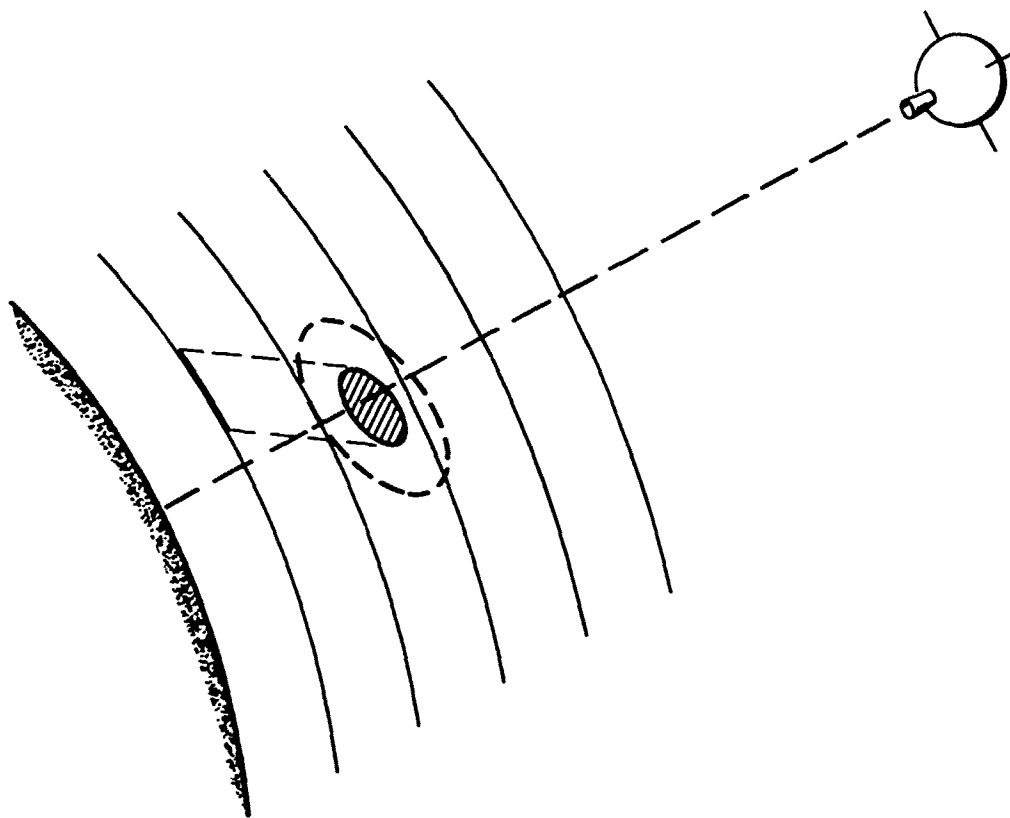
object dimensions, so thirteen paths were used (denoted by dots in the figure). A symmetric set of paths were set up in this case to model the spherical region.

6. Path Integration (SPCALC). As mentioned, for each sight path specified within the field of view, the equation of radiation transport must be integrated from the satellite to the ground. The methodology developed in WOE II² for optical sight path integration through multiple overlapping regions of disturbance has been adopted for use in ROSCOE.

The methodology involves generating a cell list of integration regions along the path (Fig. 8). These regions may be further subdivided into integration elements. The cell list consists of bounding cells at the sensor and at some terminator (the ground, in this case), atmospheric shells of about a scale height in width, and disturbed region cells. A ranking scheme for determining the relative importance of overlapping regions has also been taken from WOE.

7. Sight Path List Cell Types (SPCALC). Table 1 shows the various sight path cell types that may be generated in the code and the logical rules used in overlapping regions. Each cell type has a region code and is given a rank; the higher the rank, the more important the region. The region codes for all nuclear disturbed regions are identified by the number 1000 and distinguished by adding a region index. The region index is merely a counter of the number of "region kinds" intersected. For example, the first disturbed region intersection has an index of 1 and a region code of 1001, and so forth.

8. Example Cell List (SPCALC). An example cell list generated in the code for a typical sight path is shown in Fig. 9. The following information is given:



- CELL LISTS CONSIST OF -- (1) BOUNDING CELLS
(2) ATMOSPHERIC SHELLS
(3) DISTURBED REGION CELLS
- RANKING SCHEME USED FOR OVERLAPPING REGIONS

Figure 8. Path Integration (SPCALC)

TABLE 1
SIGHT-PATH LIST CELL TYPES

Sight Path Region	Region Code	Disturbed Region KIND	Associated $t=t_0$ RANK ^a	Geometric Overlap Logical Rules LKEEP ^b
Sun	-1	--	100	None of lower RANK
Moon	-2	--	100	None of lower RANK
Earth	-3	--	100	None of lower RANK
Cloud layer	-4	--	100	None of lower RANK
Galaxy	-5	--	100	None of lower RANK
Target	-50	--	50	All regions of lower RANK except ambient atmosphere
Vacuum	0	--	0	All
Ambient atmosphere	Shell index	--	6.0	All regions of lower RANK
Ambient chemiluminescent pancake	NDR + 1001	--	2.5	Debris particulates
Fireball	Region index + 1000	11 to 15	10.5	None of lower RANK
Ion-leak and CHEX patch	"	16	3.5	Debris particulates
Low-altitude chemiluminescent sphere	"	17	3.5	Debris particulates
High-altitude chemiluminescent pancake	"	18	3.5 ^c	Debris particulates
Beta tube	"	19	5.5	Debris particulates, fireball wake, and all other beta regions
Beta sheath	"	20	5.5	Debris particulates, fireball wake, and all other beta regions
Shock heated vortex	"	21	8.5	Debris particulates, chemiluminescent regions, fireball wake, and beta regions
Dust cloud stem	"	22	1.5	All other dust and particulate regions
Dust cloud cap and condensed debris particulates	"	23	1.5	All other dust and particulate regions
Spheroidal weapon debris, vapor and particulates	"	24	12.5	All regions of lower RANK except ambient atmosphere
Toroidal weapon debris, vapor and particulates	"	25	12.5	All regions of lower RANK except ambient atmosphere
Fireball wake	"	26	4.5	All regions of lower RANK
Debris loss-cone patch	"	27	3.5	Debris particulates

NOTES:
^aThe RANK of disturbed regions decreases linearly with age to a value that is almost one below the initial value when the age reaches one hour and thereafter remains constant.
^bAppend to all entries "and regions of greater RANK."
^cThe chemiluminescent pancake is given a fixed age of ten minutes.

T	LINK	DSP=0	ICMEG	OISTIC	KEEPR			
1	01120100111730011200	0000020000070000000	0	0.	0	0		
2	01337700111770011202	00200100000070000000	0	3.5723E+00	0	0		
3	01340100112010013400	01313700000070000000	20	3.5724E+00	0	0		
4	01120300133770013402	01313000000070000000	50	3.5724E+00	0	0		
5	01337300134010011204	00377600000070000000	20	3.5731E+00	0	0		
6	01331100112030013374	01315500000070000000	10	3.5738E+00	0	0		
7	01337100133730013312	00405700000070000000	10	3.5739E+00	0	0		
8	01331300133110013372	01314000000070000000	10	3.5746E+00	0	0		
9	01331500133710013314	00474500000070000000	10	3.5747E+00	150	0	3	
10	01336300133130013316	00565100000070000000	17	3.5748E+00	150	0	3	
11	01336500133150013318	01322000000070000000	1002	3.5749E+00	150	0	3	21
12	01336100133630013316	01321100000070000000	1002	3.5749E+00	150	0	3	21
13	01335700133650013312	01322700000070000000	1001	3.5756E+00	0	0		11
14	01337500133610013310	01320200000070000000	1002	3.5757E+00	0	0		21
15	01336700133570013370	01314000000070000000	1002	3.5757E+00	0	0		21
16	01331700133750013370	01317300000070000000	1002	3.5758E+00	0	0		21
17	01332100133670013320	00645400000070000000	16	3.5763E+00	0	0		
18	01332300133170013322	01195100000070000000	15	3.5771E+00	0	0		
19	01332500133210013324	01194200000070000000	14	3.5779E+00	0	0		
20	01332700133230013326	01193300000070000000	13	3.5788E+00	0	0		
21	01333100133250013330	01192400000070000000	12	3.5796E+00	0	0		
22	01333300133270013332	01191500000070000000	11	3.5804E+00	0	0		
23	01333500133310013334	01190600000070000000	10	3.5806E+00	0	0		
24	01333700133330013336	01187700000070000000	9	3.5808E+00	0	0		
25	01334100133350013340	01187000000070000000	8	3.5810E+00	0	0		
26	01334300133370013342	01186100000070000000	7	3.5812E+00	0	0		
27	01334500133410013344	01185200000070000000	6	3.5814E+00	0	0		
28	01334700133430013346	01330100000070000000	5	3.5816E+00	0	0		
29	01334900133450013350	01327200000070000000	4	3.5818E+00	0	0		
30	01335300133470013352	01326300000070000000	3	3.5820E+00	0	0		
31	01335500133510013354	01325400000070000000	2	3.5822E+00	0	0		
32	01117900133530013356	01324500000070000000	1	3.5824E+00	0	0		
33	00172400133550011170	00000100000070000000	0	1.0000E+15	0	0		
34	01117300111750011170	00012100000070000000	-5	1.0000E+16	0	0		

AN-10741

Figure 9. Example Cell List

I	Cell number
LINK	A packed word used to find addresses of the previous and next cells (datasets)
DSPWRD	Pointer word in the DSA scheme which allows one to access the dataset for this cell
ICREG	Region code for sight path cell terminating on this boundary
DISTIC	Distance along the sight path from the sensor to this cell boundary
KEEPR	A packed word containing subordinate region indices (up to five subordinate region indices can be stored)
KIND	(last column shown) Disturbed region KIND

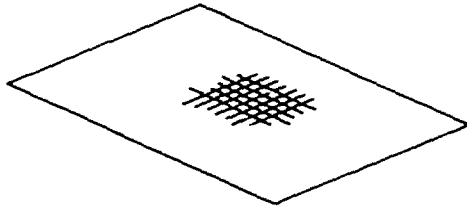
The cell list contains null cells (ICREG = 0) at the sensor and at the ground (DISTIC = 3.5824E9) and twenty atmospheric cells (ICREG = 1-20) from the ground to 100 km (DISTIC = 3.5724E9). A target cell (ICREG = -50) of zero length has been inserted at 100 km, and six disturbed region cells (ICREG \geq 1000) have been added between 66 km and 75 km.

The cell list would then be used as a guide for the integration of the radiation transport along this path. Each path would be integrated and the resulting information passed to the focal plane generation block of the code.

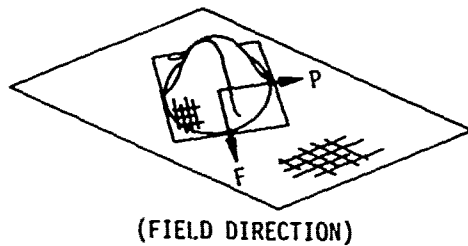
9. Focal Plane Generation (OPSIM). To create a focal plane image of the environment, the code grids the field of view into a fine mesh (the mesh size is taken as something smaller than a detector diameter), and then uses the sight path data computed at selected points to map the intensity. Recall that we previously mentioned that objects or regions in the field of view are divided into three types: background (grid), extended objects, or point objects, and that each type was characterized

by one or more sight paths. These are used as follows in the focal plane development (Fig. 10):

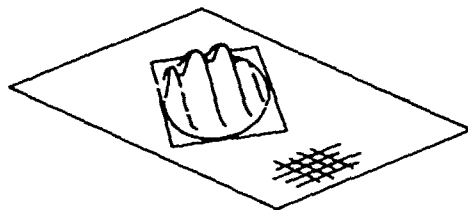
- a. The background is generated by taking the sight paths associated with the grid and using bivariate linear interpolation to compute the values at each cell in the mesh.
- b. Extended objects are then added one at a time by taking the sight paths associated with each object and following this procedure:
 - A rotated, magnetic, field-aligned coordinate system is set up, called the F-P frame.
 - The maximum and minimum region dimensions in the F-P frame are determined.
 - For each cell in the F-P grid, the code determines if the sight path through this point intersects the object. If it does, the three path datasets nearest this point are found and used to interpolate for the mean, the standard deviation, and the correlation lengths of the intensity distribution at the point. A normalized random sample is generated using the correlation lengths and a one-point recursion formula. The intensity is then computed as the mean plus the standard deviation times the random sample.
 - The point is transformed back to the sensor coordinate frame and the intensity at this point is taken as the maximum of the computed value and the old array value.
- c. Finally, point objects are added to the array at the appropriate locations specified by their sight path location in the field of view.

BACKGROUND

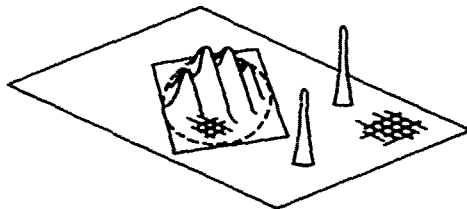
- PLANAR INTERPOLATION OF GRID DATA

OBJECTS -- MEAN

- OBJECTS ADDED ONE AT A TIME
- PLANAR INTERPOLATION OF OBJECT DATA FOR MEAN INTENSITY
- CONSTRUCTED IN COORDINATE SYSTEM ALIGNED WITH FIELD

-- STRUCTURE

- PLANAR INTERPOLATION FOR SIGMA AND CORRELATIONS
- RANDOM SAMPLES GENERATED USING ONE-POINT RECURSION AND CORRELATIONS
- INTENSITY AT POINT FOUND BY COMBINING MEAN AND RANDOM COMPONENTS
- TRANSFORMATION BACK TO SENSOR FRAME
- FINAL VALUE AT GRID POINT TAKEN AS MAX OF CURRENT AND OLD VALUES

POINTS

- ADDED AT APPROPRIATE LOCATIONS IN ARRAY

Figure 10. Focal Plane Generation (OPSIM)

10. Examples--Focal Plane Array (OPSIM). A number of test runs were conducted to determine whether the code structure up to this point produced reasonable outputs. The procedure used in this verification process consisted of (1) inputting fictitious values for the mean and variation of the integrated intensity for each sight path,* (2) using these data to generate the focal plane array, and (3) producing contour plots of the array. The contour plots are produced by plotting an alpha-numeric character or blank for successive increments of intensity ("A" being the lowest intensity, and "Z" the highest). Thus in a region of increasing intensity, one would see a character (or a repetition of the same character), followed by a blank region, followed by a repetition of a higher-order character, and so forth. A number of these example outputs follow.

Variation in Mean Intensity (Fig. 11). Contour maps were produced for a case where a single fireball was being viewed by the sensor. Two sets of inputs were assumed for the fireball intensity; the first assumed the mean was constant and the variation was about 10 percent of the mean, and the second assumed that the mean varied with the depth of the region intersected, and again the variation was taken as 10 percent of the mean. Several key points are shown in these plots:

- A reasonable representation of the fireball projection has been produced. In this case, the fireball dimensions are large with respect to the sensor resolution, so the maximum number of paths (13) were used.
- The striated nature of the fireball is easily seen in the first plot. The field direction is about -103° ccw from the horizontal x-axis, and correlation distances of 0.6 km (equivalent to 0.0167 mrad in this example) across the field and 1000 km along the field were assumed. This shows that the one-point recursion formula produces reasonable outputs in the two spatial dimensions.

* By inputting the data, the mean can be held constant and the variation displayed relative to this focal background.

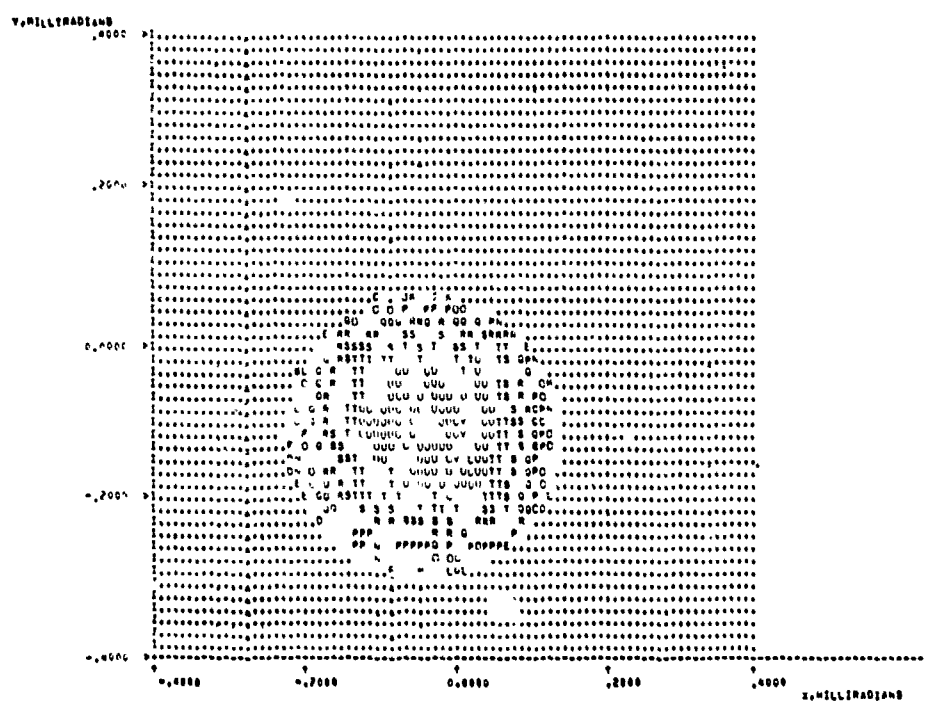
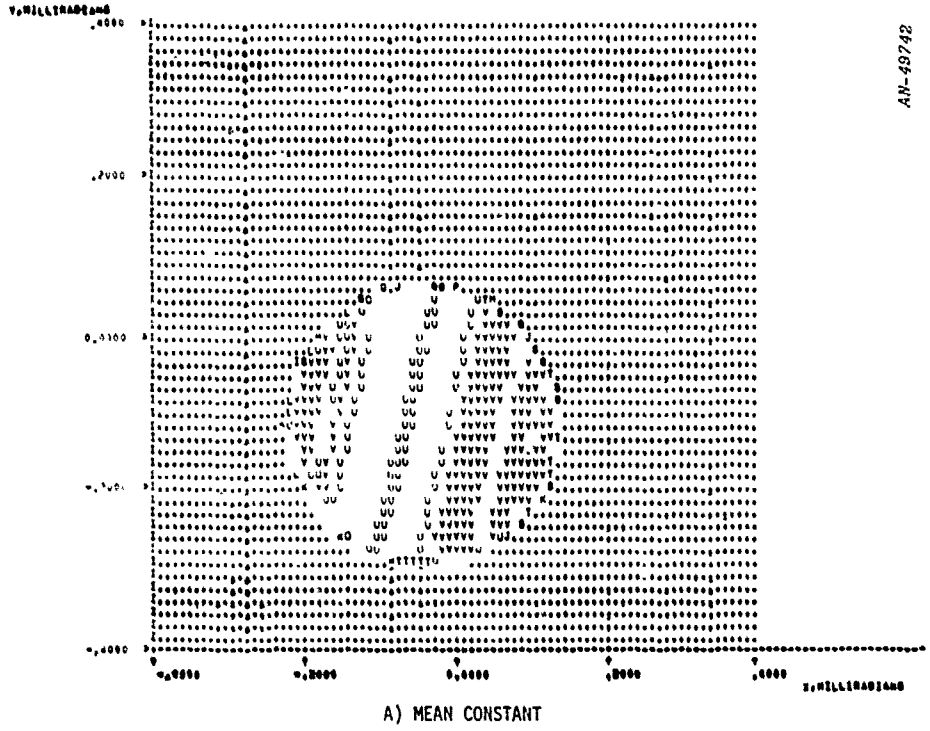


Figure 11. Variation in Mean Intensity

- The striations are somewhat less distinctive in the second case where the mean falls off from the fireball center; but the representation appears to be reasonable.

Spatial Correlation (Fig. 12). The correlation distance across the field was varied to further test the recursion formula. The plots show the same fireball with assumed correlation distances of 0.06 km and 0.6 km, respectively. As one could expect, the plots show that as the correlation distance increases, the spacing between striations in the realization increases.

Time Correlation (Figs. 13 and 14). To test the third dimension of the recursion formula (i.e., time correlation), contour plots at look times of 0 and 1 second were made with two assumed correlation times.

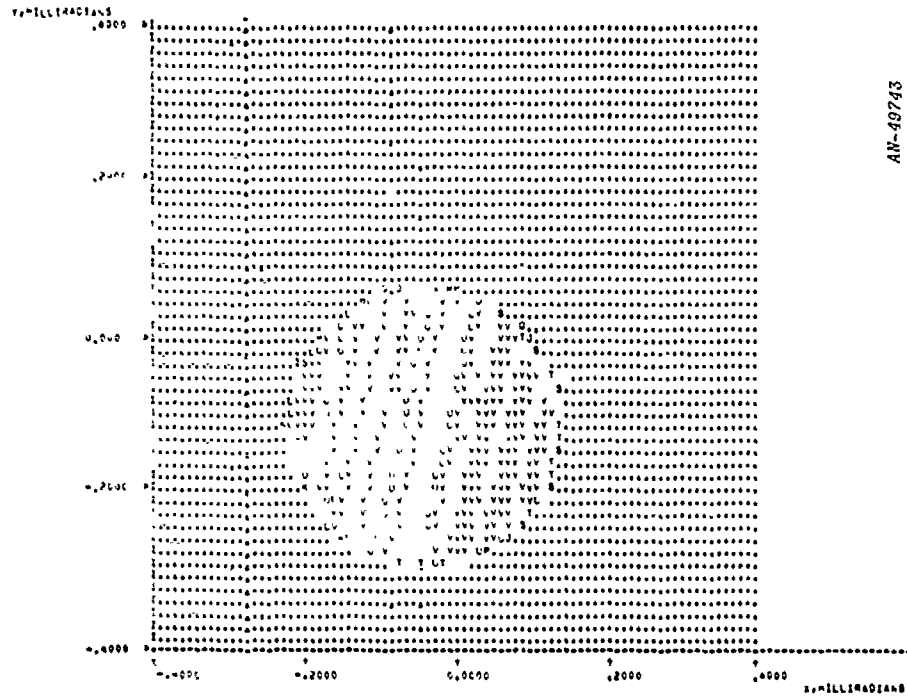
The first set (Fig. 13) shows contours for a case where the correlation time (10 s) is large in comparison to the look interval (1 s). As one would expect, the structure within the fireball changes only slightly.

The next set (Fig. 14) shows contours for a correlation time much smaller (0.1 s) than the look interval. Here, the random samples generated at the two look times are nearly independent, so that the realizations of the structure are completely different.

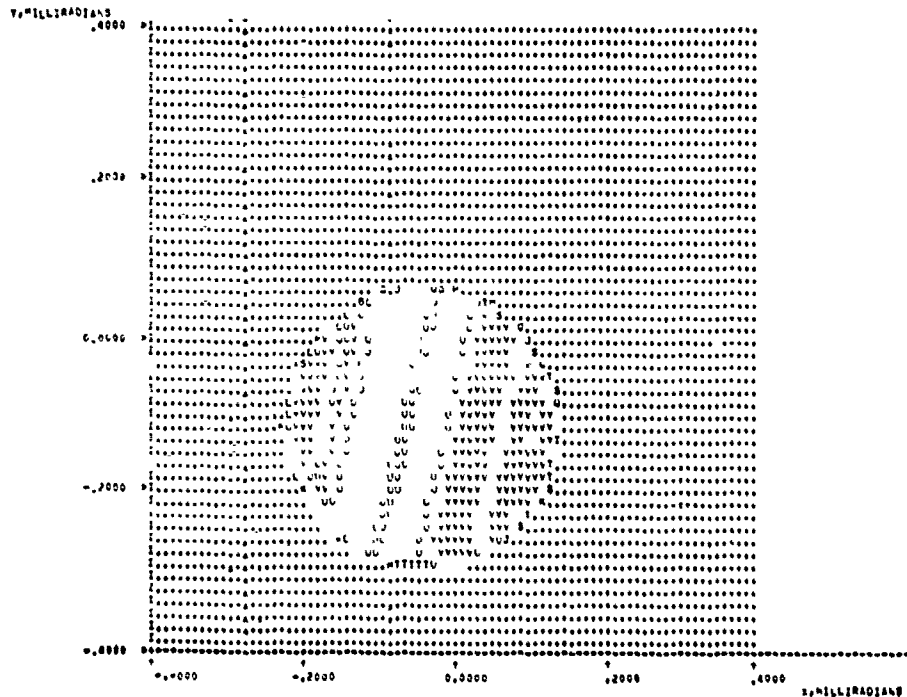
Multiple Fireballs (Fig. 15). Next, a run was performed to test the logic for generating overlapping fireballs. In the upper part of the figure, the single fireball used previously is shown. In the lower figure, a second fireball of the same size but displaced to the side has been generated. This second fireball has the same mean intensity and structure.

The plot shows that the fireball profiles are clearly defined, and a reasonable realization of the structure has been generated.

AN-40743



A) CORRELATION DISTANCE = .06 km



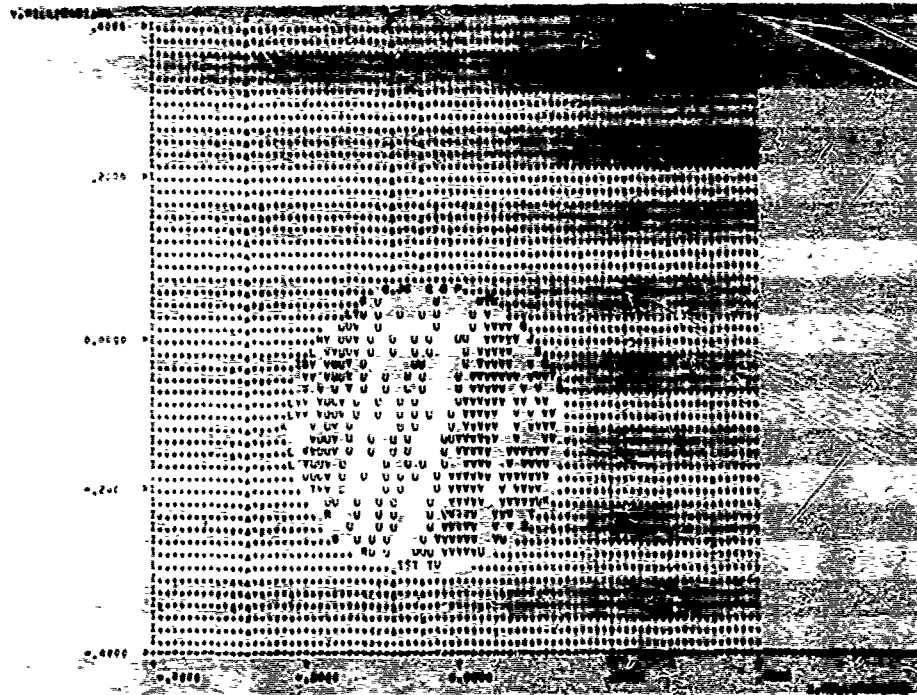
B) CORRELATION DISTANCE = .6 km

Figure 12. Spatial Correlation

CORRELATION TIME = 10 SEC

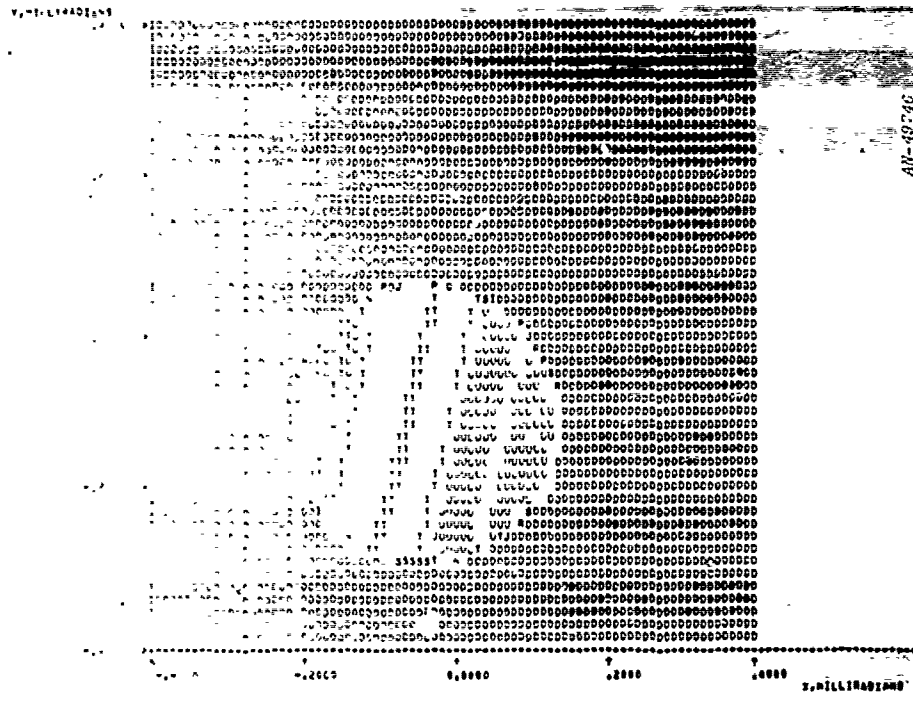


A) $t = 0$ SEC

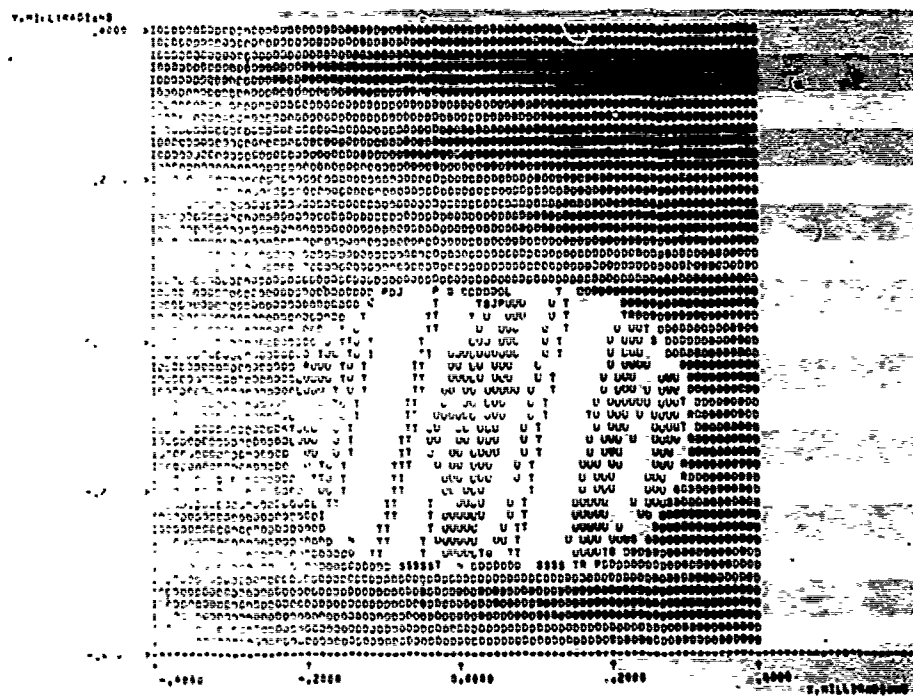


B) $T = 1$ SEC

Figure 13. Time Correlation



A) SINGLE FIREBALL



B) TWO OVERLAPPING FIREBALLS

Figure 15. Multiple Fireballs

Multiple Objects--growth with time (Figs. 16 and 17). Another test of the multiple object logic was made where two different object types were assumed: a fireball and a beta tube. For simplicity, the fireball and beta tube were assumed to have the same mean intensity and intensity variation due to structure. The plots (Fig. 16) show (1) the fireball alone, and (2) the fireball and beta tube together at a time 10 seconds after burst.

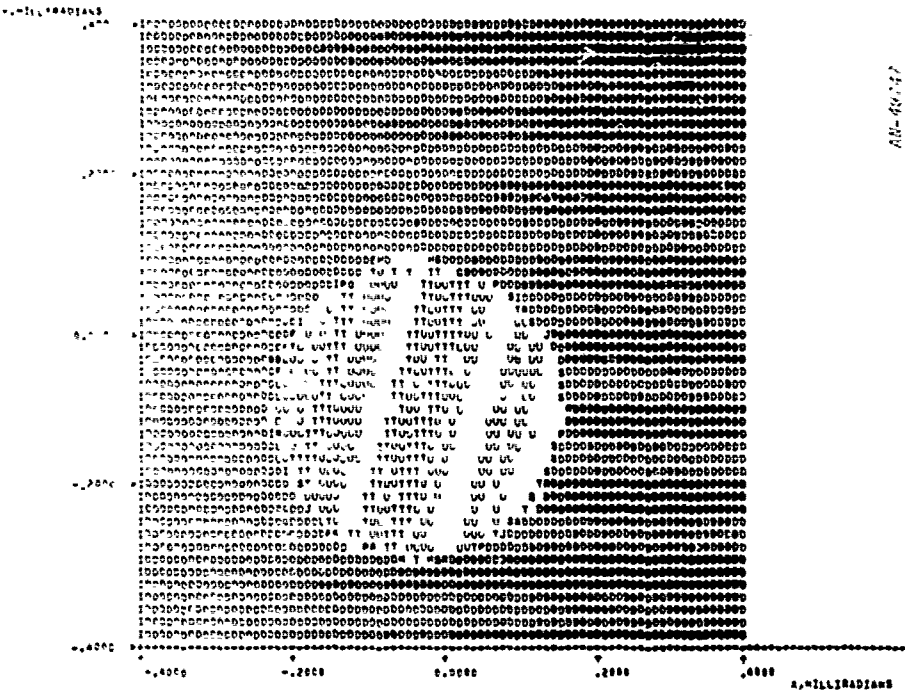
A second set of plots are shown in Fig. 17 at a later time (20 seconds after burst) to show that the program can produce reasonable object representations as the regions grow with time. Note here that both the fireball and beta tube have expanded radially about 30 percent.

11. Sensor Scan (SPIRE). As mentioned above, once a realization of the environment has been created in the focal plane, the sensor scanning motion is simulated by sweeping over this frame with a detector array. The scanning motion and number and position of the detectors in the array are specified by the user. In the example depicted in Fig. 18, a surveillance sensor which uses a circular scan and a simple linear alignment of four detectors is assumed. Because the focal plane array is gridded with a spacing on the order of the sensor resolution, the scanning process merely consists of picking up focal plane array values in the proper order for each detector. The output consists of a data stream for each detector.

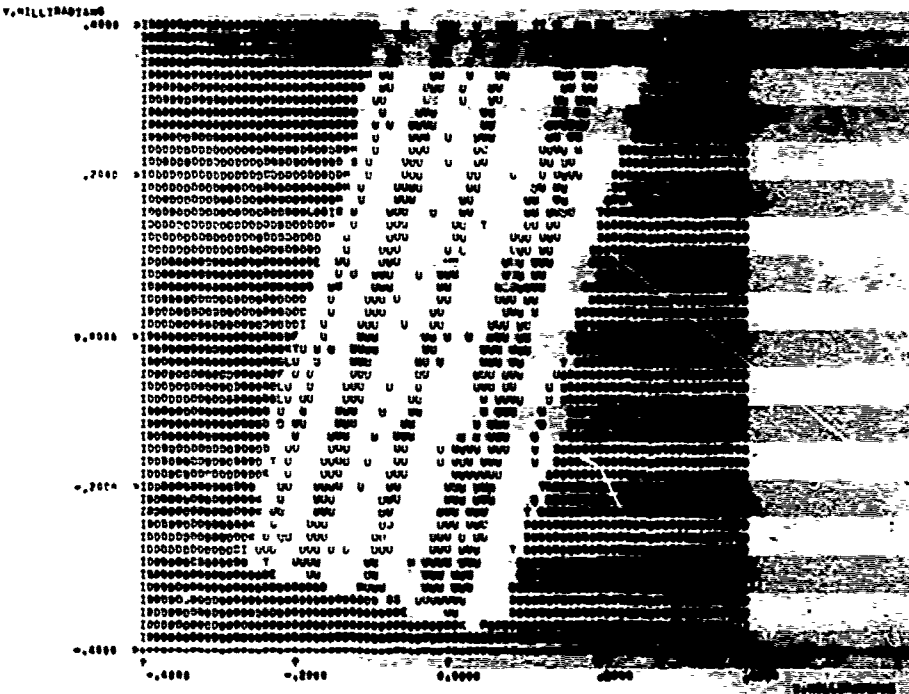
12. Optics Data Processing (SPIRE). The sensor data processing model consists of over thirty processing algorithms which can be used in a building-block approach for modeling a specific data processing system.

A simple example of this approach is shown in Fig. 19 for the surveillance sensor mentioned above. For each detector, the focal plane array is scanned to produce a data stream of samples, detector noise is added to each sample, the data stream is smoothed, adjacent samples are differenced, and a threshold test is applied to detect targets.

T = 10 SEC AFTER BURST



A) FIREBALL



B) FIREBALL AND BETATUBE

Figure 16. Multiple Objects

T = 20 SEC AFTER BURST

AN-49748

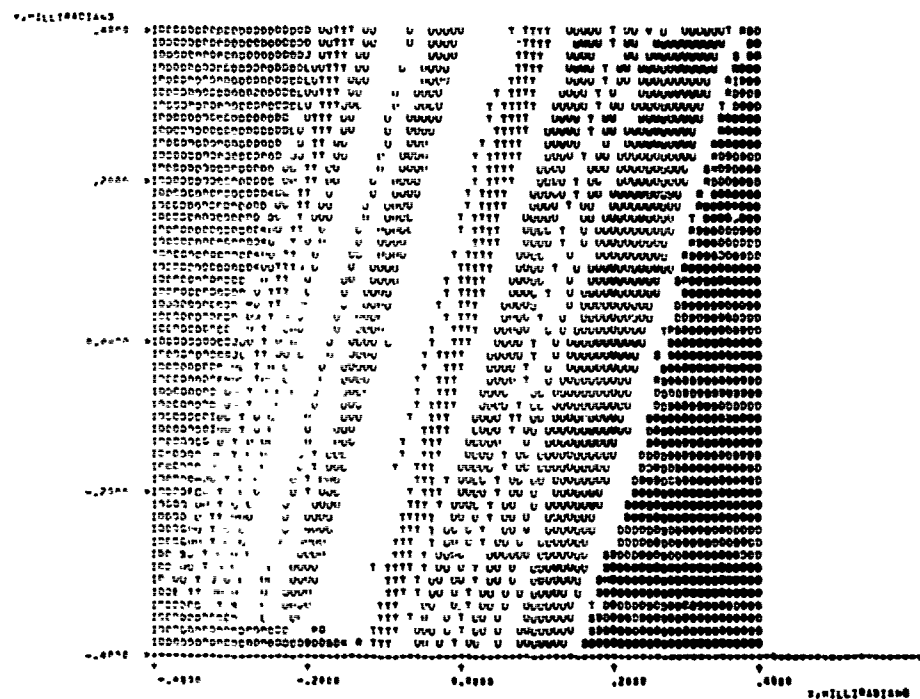
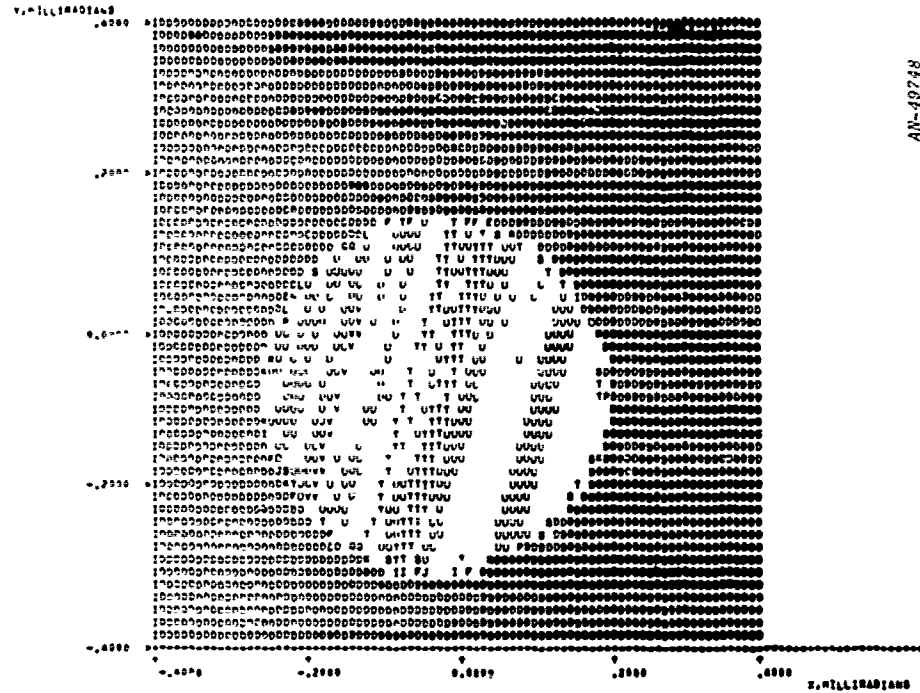


Figure 17. Multiple Objects--Growth With Time

AN-48110

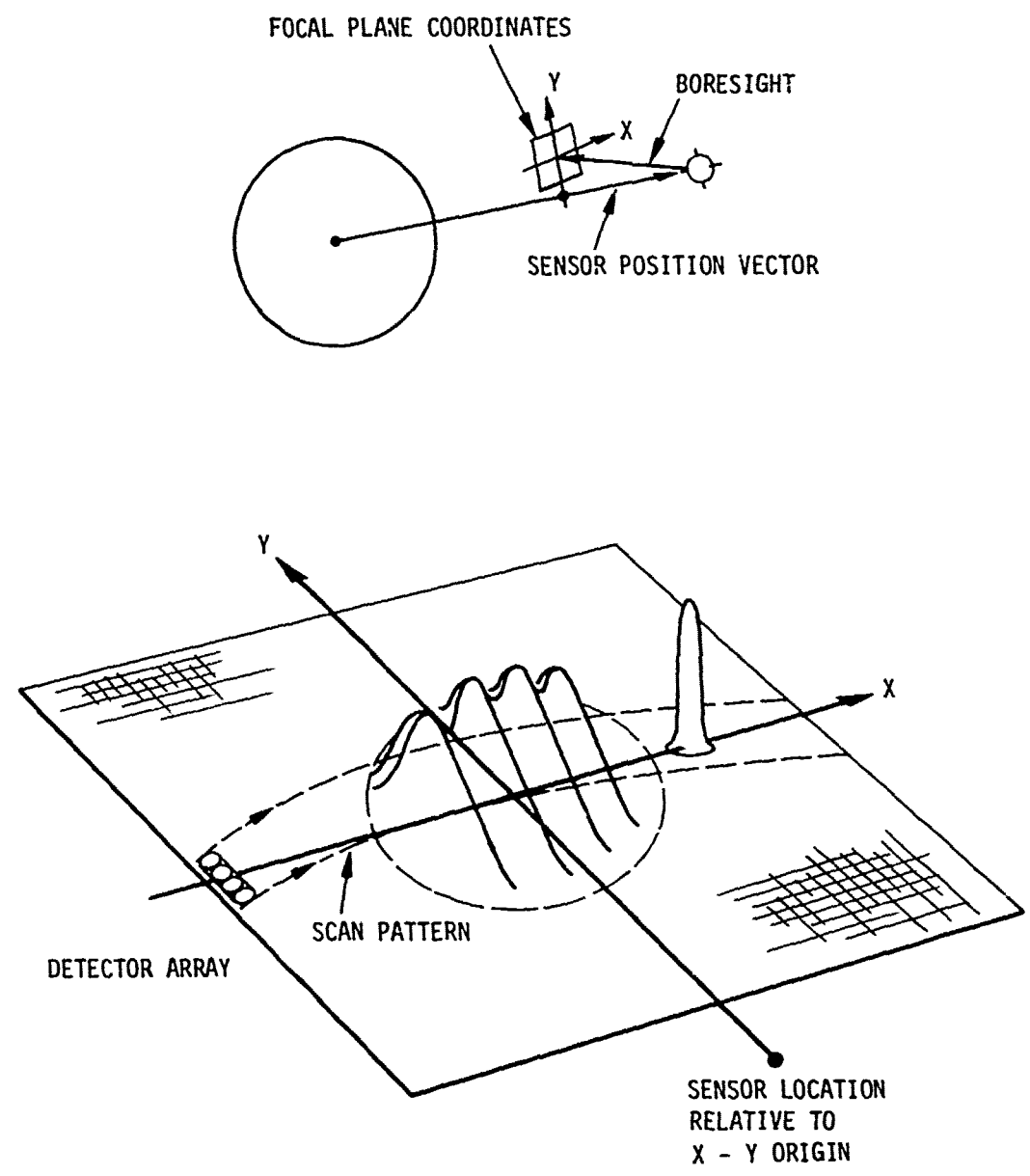


Figure 18. Sensor Scan

AN-48111

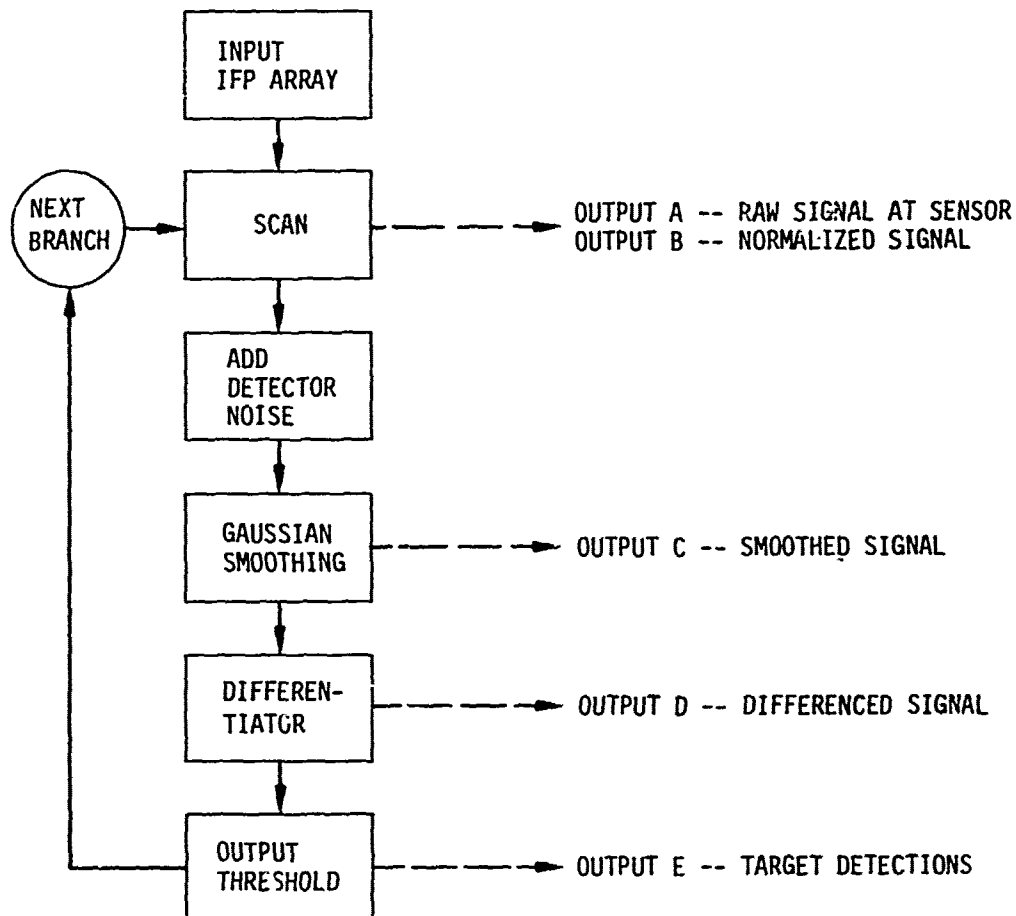


Figure 19. Optics Data Processing

Outputs are produced at several stages in this process. The raw signal as it is sampled from the focal plane is output, as well as the same signal normalized to the sensor NEFD, the signal after the addition of detector noise and smoothing has been performed, the differenced signal, and finally, a flag to denote target detections (samples that exceed an input threshold).

13. Surveillance Sensor--Example Case. The sensor scanning and processing functions were exercised for the following scenario:

A surveillance sensor attempts to detect a booster which has been launched just prior to the sensor scan of the launch site. A nuclear burst which has occurred just 10 seconds earlier is at an altitude just below the booster, and produces a high level of background radiation.

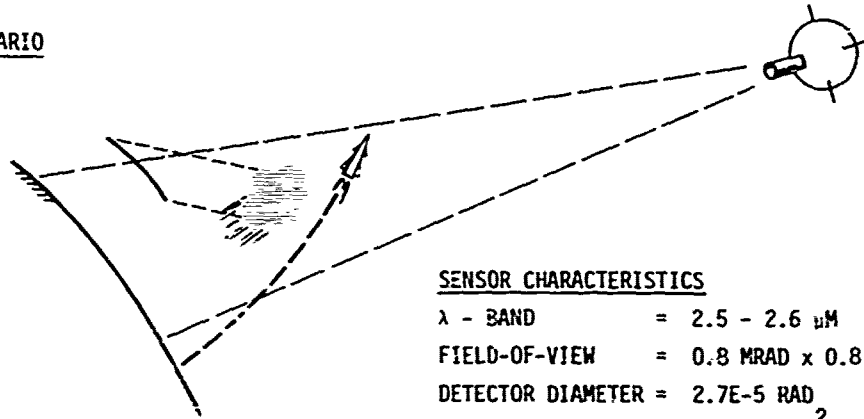
The scenario is shown in Fig. 20, along with the focal plane generated by the program. The fireball and beta tube were assumed to have constant mean intensities of 20 dB* and intensity variations due to striations of 10 dB. The booster consists of a single point in the plane (the character "D" at the center of the plot) with an intensity of 30 dB.

The data stream produced by the scanning and processing of the focal plane data is shown in Fig. 21 for one detector. The output consists of the time at which each sample is taken, the detector number, the central wavelength for this measurement, the position of the sampled point in azimuth and elevation off-boresight, and the five processing outputs mentioned above.

The data show that the sensor is able to detect the target in the presence of the noisy background created by the burst.

* The intensity contours are plotted in terms of signal/noise. Signal/noise is defined here as the irradiance/NEFD.

SCENARIO



AN-48184

SENSOR CHARACTERISTICS

- λ - BAND = 2.5 - 2.6 μ M
- FIELD-OF-VIEW = 0.8 MRAD x 0.8 MRAD
- DETECTOR DIAMETER = 2.7E-5 RAD
- NEFD = .5E-15 W/CM²
- SCAN PERIOD = 1.3E-3 SEC
- SCAN LENGTH = 0.8 MRAD

FOCAL PLANE CONTOUR MAP

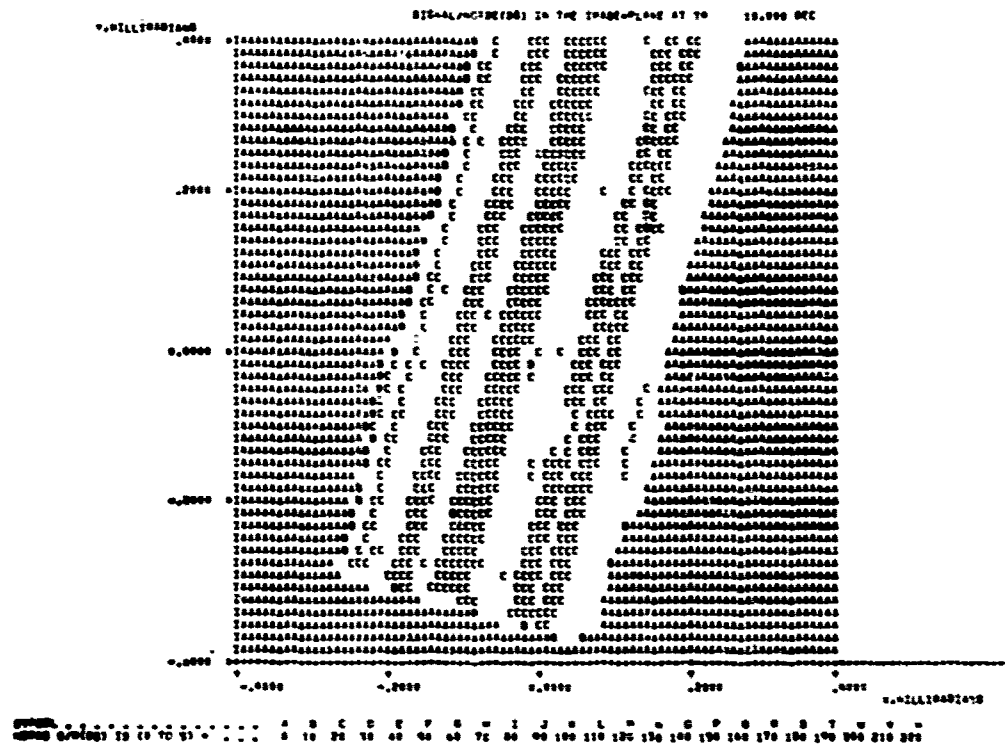


Figure 20. Surveillance Sensor Example

TIME SEC	ALTIMETER FEET	ALTITUDE FEET	ALTITUDE FEET	ALTITUDE FEET	SCANNED SIGNAL OUTPUT	NORMALIZED SIGNAL OUTPUT	SCANNED SIGNAL OUTPUT	DIFFERENCED SIGNAL OUTPUT	TARGET DETECTION FLAG
15.000000	1.000	254.000	-0.000000	0.222000	0.222000	1.110	1.363	2.223	#####
15.000015	1.000	254.000	-0.340000	0.210000	0.103000	5.033	5.596	1.560	#####
15.000030	1.000	254.000	-0.680000	0.224000	0.108000	5.203	5.806	0.753	#####
15.000045	1.000	254.000	-1.020000	0.277000	0.129000	5.346	6.357	0.222000	#####
15.000060	1.000	254.000	-1.360000	0.222000	0.107000	5.356	5.376	0.000	#####
15.000075	1.000	254.000	-1.700000	0.182000	0.100000	5.356	5.476	0.173	#####
15.000090	1.000	254.000	-2.040000	0.170000	0.104000	5.356	5.606	0.001000	#####
15.000105	1.000	254.000	-2.380000	0.140000	0.100000	5.356	5.713	-0.119000	#####
15.000120	1.000	254.000	-2.720000	0.170000	0.100000	5.356	5.632	0.154	#####
15.000135	1.000	254.000	-3.060000	0.170000	0.100000	5.356	5.705	0.196	#####
15.000150	1.000	254.000	-3.400000	0.107000	0.100000	5.356	5.907	-0.226000	#####
15.000165	1.000	254.000	-3.740000	0.207000	0.100000	5.356	5.900	0.168	#####
15.000180	1.000	254.000	-4.080000	0.222000	0.100000	5.356	5.970	-0.5535	#####
15.000195	1.000	254.000	-4.420000	0.230000	0.100000	5.356	5.916	0.1667	#####
15.000210	1.000	254.000	-4.760000	0.240000	0.100000	5.356	6.070	-0.264000	#####
15.000225	1.000	254.000	-5.100000	0.240000	0.100000	5.356	6.003	0.1710	#####
15.000240	1.000	254.000	-5.440000	0.240000	0.111000	5.377	6.014	0.333	#####
15.000255	1.000	254.000	-5.780000	0.200000	0.111000	5.450	6.148	1.560	#####
15.000270	1.000	254.000	-6.120000	0.180000	0.110000	5.800	6.207	6.266	#####
15.000285	1.000	254.000	-6.460000	0.180000	0.110000	7.500	12.00	17.00	#####
15.000300	1.000	254.000	-6.800000	0.140000	0.110000	16.33	30.33	35.00	#####
15.000315	1.000	254.000	-7.140000	0.140000	0.092000	40.50	65.03	50.47	#####
15.000330	1.000	254.000	-7.480000	0.150000	0.120000	115.6	122.4	62.67	#####
15.000345	1.000	254.000	-7.820000	0.160000	0.100000	190.5	145.1	47.01	#####
15.000360	1.000	254.000	-8.160000	0.170000	0.130000	250.7	232.5	25.06	#####
15.000375	1.000	254.000	-8.500000	0.180000	0.130000	285.4	250.3	7.350	#####
15.000390	1.000	254.000	-8.840000	0.180000	0.130000	265.6	263.7	0.001	#####
15.000405	1.000	254.000	-9.180000	0.170000	0.130000	281.0	266.6	1.225	#####
15.000420	1.000	254.000	-9.520000	0.160000	0.130000	265.4	265.0	3.707	#####
15.000435	1.000	254.000	-9.860000	0.140000	0.120000	267.7	269.6	3.832	#####
15.000450	1.000	254.000	-10.200000	0.130000	0.120000	275.6	273.6	0.2274	#####
15.000465	1.000	254.000	-10.540000	0.130000	0.120000	273.6	273.6	0.121	#####
15.000480	1.000	254.000	-10.880000	0.120000	0.120000	275.6	269.5	-0.301	#####
15.000495	1.000	254.000	-11.220000	0.120000	0.120000	269.7	265.1	1.000	#####
15.000510	1.000	254.000	-11.560000	0.120000	0.120000	250.0	266.6	11.61	#####
15.000525	1.000	254.000	-11.900000	0.120000	0.120000	271.3	278.6	278.6	#####
15.000540	1.000	254.000	-12.240000	0.120000	0.120000	265.4	302.2	55.04	#####
15.000555	1.000	254.000	-12.580000	0.120000	0.120000	322.0	357.3	175.7	TARGET
15.000570	1.000	254.000	-12.920000	0.120000	0.120000	370.2	530.0	447.6	TARGET
15.000585	1.000	254.000	-13.260000	0.120000	0.120000	606.6	674.0	655.6	TARGET
15.000600	1.000	254.000	-13.600000	0.120000	0.120000	1410.	1635.	130.0	TARGET
15.000615	1.000	254.000	-13.940000	0.120000	0.120000	2012.	1971.	350.4	#####
15.000630	1.000	254.000	-14.280000	0.120000	0.120000	1700.	1615.	6071.2	#####
15.000645	1.000	254.000	-14.620000	0.120000	0.120000	306.1	603.5	694.0	#####
15.000660	1.000	254.000	-14.960000	0.120000	0.120000	310.2	488.6	-109.7	#####
15.000675	1.000	254.000	-15.300000	0.120000	0.120000	275.7	318.0	61.06	#####
15.000690	1.000	254.000	-15.640000	0.120000	0.120000	267.0	277.0	68.025	#####
15.000705	1.000	254.000	-15.980000	0.120000	0.120000	265.0	240.0	-0.207	#####
15.000720	1.000	254.000	-16.320000	0.120000	0.120000	267.0	268.6	1.303	#####
15.000735	1.000	254.000	-16.660000	0.120000	0.120000	260.0	270.0	2.736	#####
15.000750	1.000	254.000	-17.000000	0.120000	0.120000	270.0	272.7	4.612	#####
15.000765	1.000	254.000	-17.340000	0.120000	0.120000	274.3	277.3	4.276	#####
15.000780	1.000	254.000	-17.680000	0.120000	0.120000	286.7	281.5	-0.7100	#####
15.000795	1.000	254.000	-18.020000	0.120000	0.120000	287.0	280.0	-0.790	#####
15.000810	1.000	254.000	-18.360000	0.120000	0.120000	278.0	274.1	-0.4310	#####
15.000825	1.000	254.000	-18.700000	0.120000	0.120000	262.2	265.7	-0.130	#####
15.000840	1.000	254.000	-19.040000	0.120000	0.120000	258.4	250.6	-7.600	#####
15.000855	1.000	254.000	-19.380000	0.120000	0.120000	247.2	251.0	-2.01	#####
15.000870	1.000	254.000	-19.720000	0.120000	0.120000	240.6	231.0	-65.46	#####
15.000885	1.000	254.000	-20.060000	0.120000	0.120000	285.2	195.6	-60.51	#####
15.000900	1.000	254.000	-20.400000	0.120000	0.120000	114.6	121.5	50.81	#####
15.000915	1.000	254.000	-20.740000	0.120000	0.120000	39.0	62.7	35.98	#####
15.000930	1.000	254.000	-21.080000	0.120000	0.120000	12.3	26.7	14.97	#####
15.000945	1.000	254.000	-21.420000	0.120000	0.120000	6.773	1.70	-6.531	#####
15.000960	1.000	254.000	-21.760000	0.120000	0.120000	5.645	1.283	-1.37	#####
15.000975	1.000	254.000	-22.100000	0.120000	0.120000	5.017	5.017	-0.0003	#####
15.000990	1.000	254.000	-22.440000	0.120000	0.120000	5.370	5.476	-0.1067	#####
15.001005	1.000	254.000	-22.780000	0.120000	0.120000	5.301	5.290	-0.1043	#####
15.001020	1.000	254.000	-23.120000	0.120000	0.120000	5.130	5.135	0.005500	#####
15.001035	1.000	254.000	-23.460000	0.120000	0.120000	5.130	5.176	0.240	#####
15.001050	1.000	254.000	-23.800000	0.120000	0.120000	5.130	5.330	0.819000	#####
15.001065	1.000	254.000	-24.140000	0.120000	0.120000	5.130	5.277	-0.2177	#####
15.001080	1.000	254.000	-24.480000	0.120000	0.120000	5.130	5.072	-0.1066	#####
15.001095	1.000	254.000	-24.820000	0.120000	0.120000	5.130	5.070	-0.252	#####
15.001110	1.000	254.000	-25.160000	0.120000	0.120000	5.130	5.200	0.200	#####
15.001125	1.000	254.000	-25.500000	0.120000	0.120000	5.130	5.360	-0.202000	#####
15.001140	1.000	254.000	-25.840000	0.120000	0.120000	5.130	5.516	-0.207	#####
15.001155	1.000	254.000	-26.180000	0.120000	0.120000	5.130	5.201	-0.1130	#####
15.001170	1.000	254.000	-26.520000	0.120000	0.120000	5.130	5.177	-0.2750	#####
15.001185	1.000	254.000	-26.860000	0.120000	0.120000	5.130	5.041	-0.605000	#####
15.001200	1.000	254.000	-27.200000	0.120000	0.120000	5.130	5.551	-0.002	#####
15.001215	1.000	254.000	-27.540000	0.120000	0.120000	5.201	4.806	-0.0501	#####
15.001230	1.000	254.000	-27.880000	0.120000	0.120000	5.033	5.033	-1.275	#####
15.001245	1.000	254.000	-28.220000	0.120000	0.120000	5.760	2.676	-0.687	#####

AN-49740

Figure 21. Surveillance Sensor--Example Output

3 MODELING OF INHOMOGENEOUS REGIONS

3.1 INTRODUCTION

In the ROSCOE simulation currently available for radar and satellite communications, two forms of inhomogeneities are considered for the ionized regions that affect propagation at microwave frequencies. These are the fireball surface bumpiness responsible for radar clutter at low altitudes, and field-aligned striations within and adjacent to high-altitude fireballs.*

Extension of the ROSCOE simulation to include effects of nuclear detonations on infrared systems has necessitated some additions to the set of structured regions modeled. Fireballs at all altitudes are observed to show flocculent structure inside the bright fireball, at frequencies in the visible range. This structure, usually attributed to Taylor instabilities during the initial disassembly of the warhead debris, should be present in the 2-5 μm region also, and at high altitude evolves in time to form striations aligned along the geomagnetic field.

In addition to this structure inside fireballs, other irregular regions present in the visible and SWIR include beta patch irregularities and light reflected from clouds. The beta patch irregularities are presumably causally related to corresponding structure in the fission debris at higher altitudes along the geomagnetic field lines, and will be modeled in some as yet unspecified way within the ROSCOE simulation. Reflection of solar and bomb-thermal light from fireballs is being accounted for separately, so this section deals only with the modeling of radiating structures at high altitude, the striations within and near high-altitude fireballs.

* Even the surface lumpiness at low altitudes is not modeled directly, but only through its effects in extending the reflected radar pulse length beyond the extent of the specular reflection region.

ROSCOE presently calculates the slow growth rates of striated regions, assumed field-aligned at all times, from the gradient-drift instability as described in Volumes 6 and 18 of The ROSCOE Manual. The growth rate for this instability is

$$\alpha \approx (V_i - V_n) \cdot \nabla_{\perp} \ln n_e \quad \text{seconds}^{-1} \quad (3.1)$$

where $V_i - V_n$ is the relative slip velocity between ions and neutrals and the component of the logarithmic gradient of electron density n_e perpendicular to the magnetic field is used. Thus striations should form from the gradient-drift instability, wherever a gradient in electron density and a slip velocity between neutrals and ions coexist. Initially high-altitude fireballs have strong electron density gradients near their edges (although ROSCOE treats high-altitude fireballs as geometric overlays with constant electron density across planes of equal altitude). Thus fireballs should striate on the surface soon after magnetic containment is attained. Other regions identified³ as possible sources for striation growth by this mechanism are the fireball core and the fireball bottom after this region has passed through its apogee and falls back into the atmosphere.

Thus high-altitude fireball structure of relevance to radiance variations comprises initial flocculence, presumably isotropic at early times, but growing with time along the magnetic field; surface striations around the periphery of the fireball; and volume striations throughout the body of the fireball. These may all be modeled with different parameters as regards size spectrum, degree of structure (variation of radiance), and relative correlation distances along and normal to the geomagnetic field. However, the modeling must be consonant with the current representation of generalized high-altitude structures, whose form is discussed in the next subsection.

3.2 GENERATION OF RADIANT INTENSITIES IN THE IDEAL FOCAL PLANE

During the initial structuring of the optics routines for ROSCOE, a particular concern was the question of how statistical properties of structured radiating regions should be represented in the patch plane, or ideal focal plane, and how specific realizations of how these statistics should be generated. The two basic approaches considered were:

1. Accumulation of statistics along a number of paths, each corresponding to a particular point in the patch plane. The number of paths must be sufficient to describe individual region boundaries in the plane. A specific realization is then generated from a recursion formula.
2. Calculation of statistics for a number of lines of sight within each object separately. A specific realization is then generated for each object, from a recursion formula, and superimposed on the patch plane along with the specific realization for other regions.

For the specific case of sensors at synchronous altitudes, striations in regions at 100-km altitude look about like those at 200-km altitude, because of the great distance to the satellite sensors. It would, however, be dangerous to capitalize on this fact by designing the code in such a specific way that later versions for other sensor systems would have to be restructured in some major way.

We present below a method for generating correlated intensity patterns in the patch plane, together with the equations necessary for extrapolating, interpolating, and joining different numerical sequences in several dimensions, when the variance of the computed values is permitted to be any arbitrary function of position, and when the spatial autocorrelation function has two orthogonal axes of symmetry. The only assumptions are that the statistics are Gaussian and that the autocorrelation

function is exponential,^{*} with a different (but constant) e-folding length along the two space axes. This situation is felt to be appropriate to the case of an infrared sensor scanning in some arbitrary direction along high-altitude striations, where the magnetic field produces an automatic elongation of the luminosity parallel to the field. Time decorrelation due to relative motion of the line of sight through the striations is also assumed to be exponential in time.

Consider a two-dimensional array of intensities $S_{i,j}$, which we take as having already been "detrended;" i.e., the smooth variation of intensity as the line of sight sweeps through regions of different total luminosity has been subtracted out so that we need consider only fluctuations about the mean value of zero. As the line of sight moves, the fluctuations of course change also, so we ascribe a variance $\sigma_{i,j}$ to the signal, and furthermore we assume that there exist two different exponential correlation distances in the i- and j-directions. The total intensity (which is assumed detrended) and variance are computed from the known fireball parameters along a line of sight designated as i,j , or along several lines of sight. Our problem then is to compute a "reasonable" representation of the expected intensity fluctuations at other arbitrary points, and to ensure that all points correlate properly with themselves and each other. We would like to use a simple recursion relation relating the next value at $i+n, j+m$ only to $S_{i,j}$ by an equation resembling that for stationary Markov processes. We want the computed value to have the following properties:

$$a. \quad \langle S_{i+n, j+m}^2 \rangle = \sigma_{i+n, j+m}^2 \quad (3.2)$$

where $\sigma_{i+n, j+m}$ is the variance of the signal.

$$b. \quad \langle S_{i+n, j+m} S_{i, j} \rangle = F^n P^m \sigma_{i, j} \sigma_{i+n, j+m} \quad (3.3)$$

^{*}A discussion of the possible problems engendered by this choice is given in a later section, with some suggestions for improvements, if desired.

Here,

$$F^n = e^{-n\Delta x/L_1}$$

$$p^m = e^{-m\Delta y/L_2}$$

where L_1 and L_2 are the correlation distances along the two axes, and Δx and Δy are the linear separation of two neighboring points in the mesh to be computed. The third property,

$$c. \quad \langle S_{i,j} \rangle = \langle S_{i+n,j+m} \rangle = 0 \quad (3.4)$$

is automatically satisfied by the detrending.

Let us try a recursion relation of the form

$$\frac{S_{i+n,j+m}}{\sigma_{i+n,j+m}} = F^n p^m \frac{S_{i,j}}{\sigma_{i,j}} + \sqrt{1 - F^{2n} p^{2m}} R_{i,j} \quad (3.5)$$

where $R_{i,j}$ is a random Gaussian variate of variance 1, as are the quantities $S_{i,j}/\sigma_{i,j}$. This equation is seen to satisfy the three conditions above. Furthermore, the process may be extended to the values $S_{i+n',j+m'}$, where $n' > n$ and $m' > m$, merely by successive application of Eq. 3.5. Thus

$$\begin{aligned} \frac{S_{i+n',j+m'}}{\sigma_{i+n',j+m'}} &= F^{n'-n} p^{m'-m} \frac{S_{i+n,j+m}}{\sigma_{i+n,j+m}} \\ &+ \sqrt{1 - F^{2(n'-n)} p^{2(m'-m)}} R \end{aligned} \quad (3.6)$$

This clearly satisfies condition (a), and if we compute the correlation with the previously computed $S_{i,j}$, it is seen to obey (b) too, since, from Eq. 3.6,

$$\begin{aligned} \frac{\langle S_{i+n',j+m'} S_{i,j} \rangle}{\sigma_{i+n',j+m'}} &= \frac{F^{n'-n} p^{m'-m}}{\sigma_{i+n,j+m}} \langle S_{i+n,j+m} S_{i,j} \rangle \\ &= F^{n'-n} p^{m'-m} F^n p^m \sigma_{i,j} \end{aligned} \quad (3.7)$$

Therefore the sequence may be automatically extrapolated to larger values of n, m in steps of arbitrary size. (The case where either n' or m' is less than n or m is a special case of the interpolation equations to be discussed next.) From symmetry, it is also seen that the sequence may also be extended in the other direction from the lowest values of i, j . But now the question arises as to how to interpolate; i.e., having computed $S_{i+n,j+m}$ from Eq. 3.5, what do we do about, say, $S_{i+n,j+m-1}$? The mere fact that we have computed the point at $i+n, j+m$ by drawing from the random variable R automatically sets a constraint on the value of $S_{i+n-1, j+m-1}$, since it must now correlate with $S_{i+n, j+m}$, as well as with $S_{i, j}$.

Let us compute the two other corner points, $i, j+m$ and $i+n, j$, which, by Eq. 3.5, are given by

$$(S/\sigma)_{i, j+m} = p^m (S/\sigma)_{i, j} + \sqrt{1 - p^{2m}} R_j \quad (3.8)$$

$$(S/\sigma)_{i+n, j} = F^n (S/\sigma)_{i, j} + \sqrt{1 - F^{2n}} R_i \quad (3.9)$$

where we are henceforth using the subscripts only on the quantities

$$S_{i,j}/\sigma_{i,j} \equiv (S/\sigma)_{i,j}$$

These two values have unity variance, and clearly correlate in the appropriate way with $S_{i,j}$ but not with $S_{i+n, j+m}$ in Eq. 3.5. The reason is clear. Whatever choice was made of the random variate $R_{i,j}$ in Eq. 3.5 sets a constraint on the separate values R_i and R_j in

Eqs. 3.8 and 3.9--which constraint may be easily computed. Thus, applying (3.8) and (3.9) successively,

$$\begin{aligned} (S/\sigma)_{i+n,j+m} &= P^m(S/\sigma)_{i+n,j} + \sqrt{1 - P^{2m}} R'_j \\ &= P^m F^n(S/\sigma)_{i,j} + \left\{ P^m \sqrt{1 - F^{2n}} R_i + \sqrt{1 - P^{2m}} R'_j \right\} \end{aligned} \quad (3.10)$$

This clearly satisfies conditions (a) and (b) as applied to all pairs of points. The term in brackets may then be interpreted as the second term in Eq. 3.5. A fuller discussion is given in Appendix A.

This then gives us our set of rules about forward versus backward behavior. As long as both indices increase, Eq. 3.5 may be used to extend the sequence, as long as no "leapfrogging" occurs. The sequence may be extended (in either direction) from the end point only. Going backward in either index demands an interpolation formula, now to be derived.

Let us start with S_{ij} and compute $S_{i+n,j}$ and $S_{i,j+m}$ from Eqs. 3.8 and 3.9. Then compute $S_{i+n,j+m}$ by proceeding from either $i+n,j$ using (3.8) again, or from $i,j+m$ using (3.9). Now from the four corner values we interpolate for $S_{i+l,j+k}$ ($l < n$, $k < m$) at any interior point by the following algorithm:

$$\begin{aligned} (S/\sigma)_{i+l,j+k} &= \alpha(S/\sigma)_{i,j} + \beta(S/\sigma)_{i,j+m} \\ &\quad + \gamma(S/\sigma)_{i+n,j} + \delta(S/\sigma)_{i+n,j+m} + \epsilon R \end{aligned} \quad (3.11)$$

where $\alpha, \beta, \gamma, \delta, \epsilon$ are constants to be determined, and R is again a completely random Gaussian variate of unity variance (i.e., not tied to any of the random variates used to compute the four corner points). This is an important point--we never have to "remember" any previously used random variate, in any step.

That the value of $(S/\sigma)_{i+\ell, j+k}$ correlates properly with itself and the four corner values is the condition that determines the five constants. This leads to the following equation:

$$1 = \alpha^2 + \beta^2 + \gamma^2 + \delta^2 + \epsilon^2 + 2P^m(\alpha\beta + \gamma\delta) \\ + 2F^n(\alpha\gamma + \beta\delta) + 2F^n P^m(\beta\gamma + \alpha\delta)$$

$$\left. \begin{aligned} \alpha + \beta P^m + \gamma F^n + \delta F^n P^m &= F^\ell P^k \\ \alpha P^m + \beta + \gamma F^n P^m + \delta F^n &= F^\ell P^{m-k} \\ \alpha F^n + \beta F^n P^m + \gamma + \delta P^m &= F^{n-\ell} P^k \\ \alpha F^n P^m + \beta F^n + \gamma P^m + \delta &= F^{n-\ell} P^{m-k} \end{aligned} \right\} (3.12)$$

whose solution is

$$\left. \begin{aligned} \alpha &= F^\ell P^k (1 - P^{2m-2k})(1 - F^{2n-2\ell})/\Delta \\ \beta &= F^\ell P^{m-k} (1 - P^{2k})(1 - F^{2n-2\ell})/\Delta \\ \gamma &= F^{n-\ell} P^k (1 - F^{2\ell})(1 - P^{2m-2k})/\Delta \\ \delta &= F^{n-\ell} P^{m-k} (1 - F^{2\ell})(1 - P^{2k})/\Delta \\ \Delta &= (1 - F^{2n})(1 - P^{2m}) \end{aligned} \right\} (3.13)$$

These values are readily seen to lead to the correct correlations as ℓ, k approach any of the four corners.

Four-point interpolation may in some cases collapse to even two-point interpolation, as when $S_{2,1}$ is computed from $S_{1,1}$ and $S_{2,2}$, but Eqs. 3.13 represent the most general possible case. The proof that this solution correlates correctly with previously computed points $S_{i',j'}$ ($i' < i, j' < j$) is tedious but straightforward.

We have thus shown that two-dimensional sequences can be generated from the end points in both directions, and have given the necessary equations for interpolating, which is tantamount to joining two separately generated sequences as they near each other. Note that from the form of Eq. 3.5, it is perfectly appropriate to generate completely independent sequences in widely separated regions--the first term in (3.5) then vanishes and only the random Gaussian is used. Only when the sequences near each other need any correlation be considered.

The previous discussion may readily be generalized to more than two dimensions, but the algebra becomes tedious even under the simplifying assumptions of exponential decorrelation. Analogy with sequences in one and two dimensions would lead us to expect the following results. Extrapolation of a sequence in a single dimension involves only the end point, whereas interpolation involves the two nearest bounding values. Extrapolation in two dimensions can involve up to three previously computed values (see Eq. A.4), whereas interpolation in general demands four other points. In three dimensions, extrapolation can involve up to seven other values (to obtain the final corner of a rectangular parallelepiped), and interpolation demands in general eight other points.

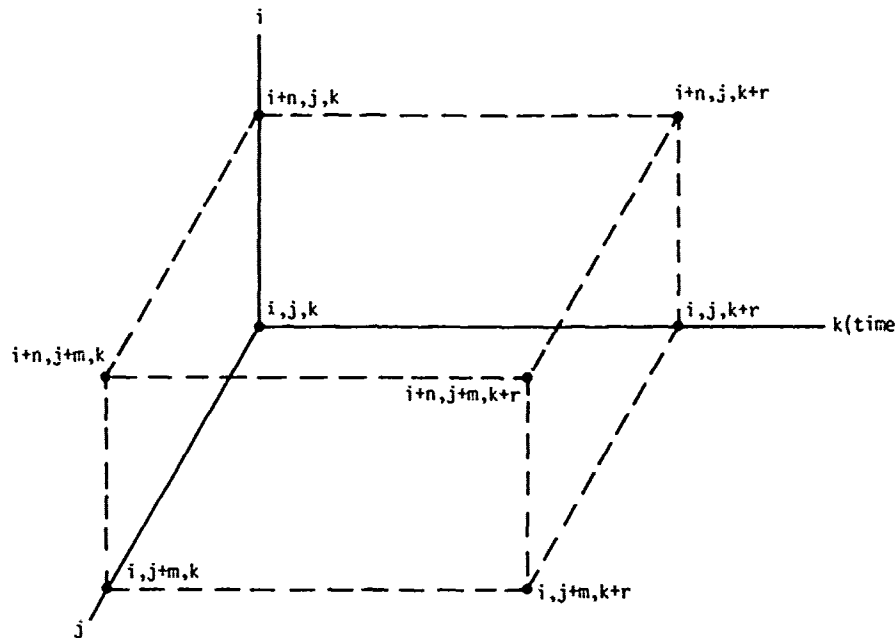
We present below the case of extrapolation in three dimensions to find the final value at the last corner of a rectangular parallelepiped. Thus we label points now with three indices, i,j,k , the last corresponding to the time. Points separated only in time are related by the equation

$$(S/\sigma)_{i,j,k+r} = \phi^r (S/\sigma)_{i,j,k} + \sqrt{1 - \phi^{2r}} R_k \quad (3.14)$$

where ϕ is the exponential time decorrelation. Equation 3.5 is replaced by

$$(S/\sigma)_{i+n,j+m,k+r} = F^n P^m \phi^r (S/\sigma)_{i,j,k} + \sqrt{1 - F^{2n} P^{2m} \phi^{2r}} R_{ijk} \quad (3.15)$$

In Fig. 22, let the axes be as labeled. Equation 3.15 is appropriate only when no "leapfrogging" over intermediate values occurs. These intermediate values (the other corners shown in Fig. 22) are computed as follows. In the plane $k = k$, corresponding to a single instant of time, we have already shown how to compute the values at $(i+n,j,k)$, $(i,j+m,k)$, and $(i+n,j+m,k)$, beginning with the point at (i,j,k) . Equation 3.14 is then used to compute the point $(i,j,k+r)$.



AN-49604

Figure 22. Extrapolation of Gaussian Sequence in Three Dimensions

Equation A.4 is then used to give $(S/\sigma)_{i+n,j,k+r}$ from the three other corner values (i,j,k) , $(i+n,j,k)$, and $(i,j,k+r)$; and similarly for the point at $(i,j+m,k+r)$ in terms of the values (i,j,k) , $(i,j,k+r)$, and $(i,j+m,k)$. Finally, to fill in the last corner $(i+n,j+m,k+r)$, we must write

$$\begin{aligned}
 (S/\sigma)_{i+n,j+m,k+r} &= A(S/\sigma)_{i,j,k+r} + B(S/\sigma)_{i,j,k} \\
 &+ C(S/\sigma)_{i+n,j,k} + D(S/\sigma)_{i,j+m,k} + E(S/\sigma)_{i+n,j+m,k} \\
 &+ G(S/\sigma)_{i+n,j,k+r} + H(S/\sigma)_{i,j+m,k+r} + \epsilon R_{ijk}
 \end{aligned} \tag{3.16}$$

Insuring the proper correlation with all other points leads to the following values for the coefficients in Eq. 3.16:

$$\begin{aligned}
 A &= -F^n P^m \\
 B &= F^n P^m \phi^r \\
 C &= -P^m \phi^r \\
 D &= -F^n \phi^r \\
 E &= \phi^r \\
 G &= P^m \\
 H &= F^n \\
 1-\epsilon^2 &= -(F^{2n} P^{2m} + P^{2m} \phi^{2r} + F^{2n} \phi^{2r}) + F^{2n} P^{2m} \phi^{2r} \\
 &\quad + F^{2n} + P^{2m} + \phi^{2r}
 \end{aligned} \tag{3.17}$$

The formulas for interpolation inside the rectangular box will correspondingly involve the solution of eighth-order determinants.

3.3 DIFFERENTIABILITY OF FIRST-ORDER MARKOV PROCESSES

The exponential correlation function assumed in the previous section is appropriate to first-order Markov processes,⁴ and is used principally for mathematical simplicity in generating random sequences in three dimensions. Before it can be adopted for use in ROSCOE, we must find a way of relating it to the expected variations in intensity, while scanning across the distribution of Gaussian striations used in ROSCOE, which is done in Sec. 3.4; we must also examine more closely another problem connected with differentiability.

In the linear extrapolation of a sequence of values of some quantity $u(x)$, the simplest is the first-order sequence for which $u(x + \tau)$ depends on the previous value $u(x)$, through

$$u(x + \tau) = k u(x) + \sqrt{1 - k^2} R \quad (3.18)$$

where $k = e^{-\nu|\tau|} < 1$ and R is a random Gaussian variate. This sequence, represented by an exponential correlation function

$$\beta(\tau) = \sigma^2 e^{-\nu|\tau|}$$

is pathological in being continuous but non-differentiable. Thus, denoting expectation values by brackets $\langle \rangle$

$$\begin{aligned} \langle [u(x + \delta) - u(x)]^2 \rangle &= \langle [u(x + \delta)]^2 \rangle + \langle [u(x)]^2 \rangle \\ &\quad - 2 \langle u(x + \delta) u(x) \rangle \\ &= 2\sigma^2(1 - e^{-\nu\delta}) \\ &= 2\sigma^2 \nu\delta \end{aligned} \quad (3.19)$$

and, as $\delta \rightarrow 0$, the left-hand side gives

$$\langle du/dx \rangle = \sigma \sqrt{2\nu} \delta^{-1/2} \quad (3.20)$$

σ^2 being the variance.

The reason for this behavior is well known⁴ to be the non-existence of the second derivative $B''(0)$, caused by the cusp in the correlation function $B(\tau)$ at $\tau = 0$. This introduces a high-frequency fuzz or jaggedness into the function $u(x)$, manifested by the comparatively slow high-frequency fall-off of the spectral density $S(\omega)$:

$$\begin{aligned} S(\omega) &= 1/2\pi \int_{-\infty}^{\infty} e^{i\omega\tau} B(\tau) d\tau \\ &= \nu / (\nu^2 + \omega^2) \end{aligned} \quad (3.21)$$

In this section we attempt to quantify how seriously this jaggedness interferes with the differentiation of $u(x)$, as described by Eq. 3.18, taking into account the finite detector width. In Sec. 3.2, we described a technique for generating a sequence of intensity values simulating a striated field of view with different correlation lengths along and across the magnetic field, and also a finite decorrelation time. We consider here only the one-dimensional case, and let the linear field of view of the slit (at the striated region) be Δ , assumed to be some multiple N of the sequence step-size δ . We shall examine the character of the (expectation value of the) derivative $u'(x)$ as a function of both Δ and N , where $u'(x)$ is defined as

$$\begin{aligned} u'(x) &= \frac{1}{(N+1)\Delta} \langle [(u_0 + u_1 \dots u_N) \\ &\quad + (u_{-N} + u_{-N+1} + \dots u_0)]^2 \rangle > 1/2 \end{aligned} \quad (3.22)$$

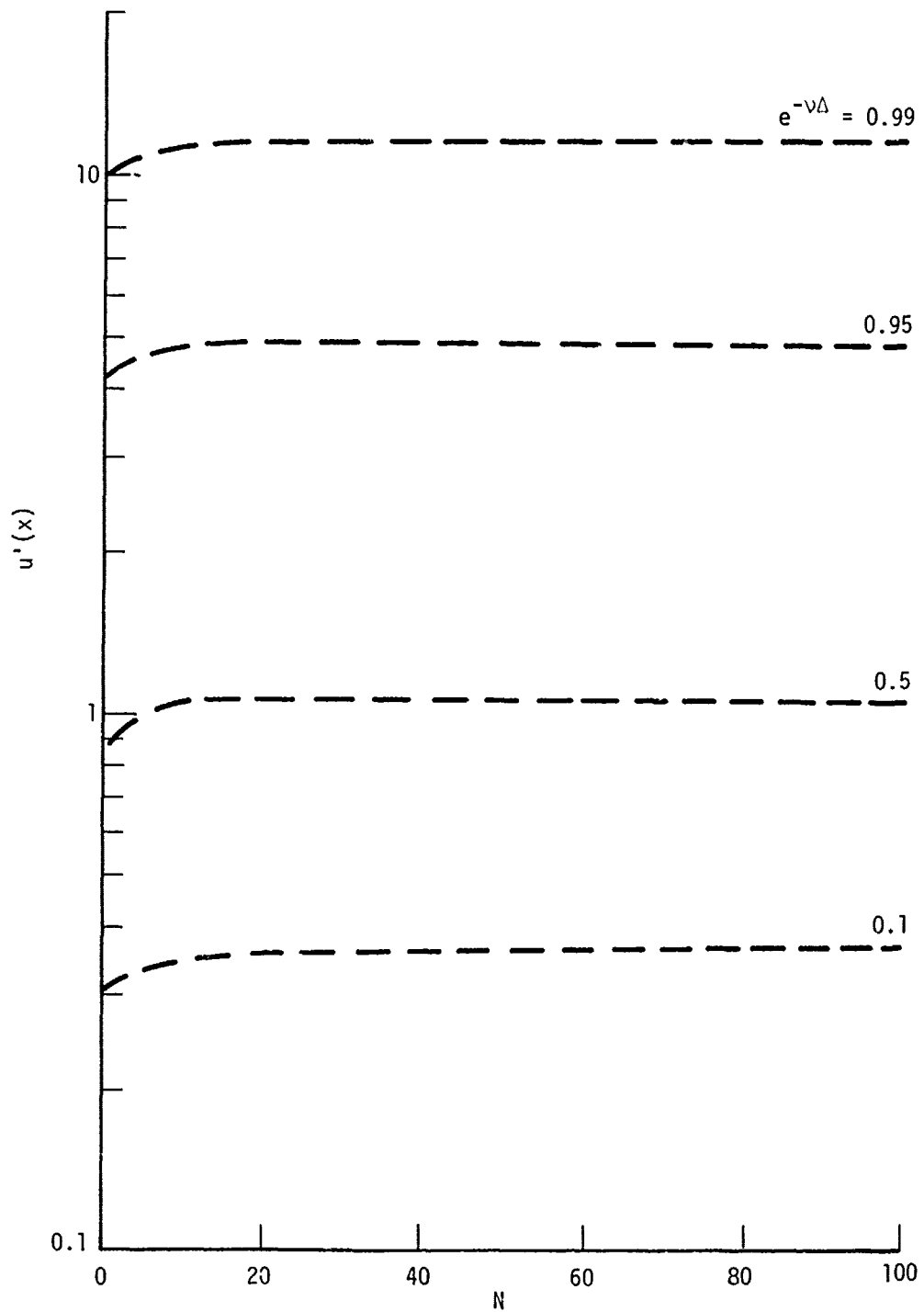
Letting $x = e^{-v\delta}$ and $\sigma^2 = 1$, this expression may be shown to reduce to

$$u'(x) = \frac{1}{(N+1)\Delta} \left\{ 2N + \frac{1}{(1-x)^2} [4(N-1)x - (4N+2)x^2 + 4x^{N+1} + 4x^{N+2} - 2x^{2N+2}] \right\}^{1/2} \quad (3.23)$$

This is plotted in Fig. 23, and is seen to be very insensitive to the number of points N in the interval Δ , but varies essentially as $\Delta^{-1/2}$ for slit widths small compared to the correlation distance v^{-1} , in accord with Eq. 3.20. Thus as the detector field of view is narrowed down to values small compared to the correlation length, the derivative (as defined by Eq. 3.22) becomes indeterminate, as expected.

It is not yet obvious, however, that this spikiness need preclude the use of an exponential correlation function for generating similar striated fields of view even in this case (narrow field of view). It must be remembered that the radiance values described by Eq. 3.18 are also contaminated by the other various sources of noise (photon noise, detector noise, etc.), and if the spectral composition of the noise is much wider in high frequencies than that of the signal, the derivative is chiefly due to the noise.⁵ Thus the high-frequency hash in Eq. 3.21 may itself be considered as a kind of noise, which must be alleviated in the smoothing process.

The central reason for trying to retain the single-point representation (Eq. 3.18), with its admitted bad features in differentiability, concerns the algebraic difficulties of extending and interpolating sequences of higher order in two and three dimensions. In Sec. 3.2, we derived the equations for extending, interpolating, and joining different numerical sequences in several dimensions, when the variance of the computed value was permitted to be any arbitrary function of position, the



AN-49605

Figure 23. "Derivative" of First-Order Markov Sequence
(of Eq. 3.23)

statistics were Gaussian, and the autocorrelation function was exponential. Even in this simplest case of a single-point sequence, extrapolation in three dimensions demanded use of seven previously computed values (to obtain the final corner value of a rectangular parallelepiped), and interpolation between previously computed values demands the solution of eight algebraic equations, in order to maintain proper three-dimensional correlation. If one were to use a more complicated recursion formula than Eq. 3.18, involving more than the last previously computed value, the difficulties of extrapolation and interpolation would clearly be increased, but it is not yet clear how severely.

Let us consider, for example, an autocorrelation function Gaussian in shape, since it is the cusp at the origin of $e^{-\nu|x|}$ that introduces the high-frequency hash that leads to problems in differentiation. Since a Gaussian correlation function falls off much more rapidly than the exponential, one might think that in this case $u(x + \tau)$ for large τ would be much less dependent on the "past" of the process than for the exponential, which already corresponds to a single-point recursion relation (Eq. 3.18). However, the situation is just the opposite:⁴ for the exponential correlation, knowledge of previous values of $u(x - n\tau)$ provides little information about $u(x + n\tau)$, whereas for a Gaussian autocorrelation function, the value of the process in the arbitrary distant future can be approximated arbitrarily closely by a linear combination of past values.

With a Gaussian correlation function

$$B(\tau) = \sigma^2 e^{-\beta^2 \tau^2 / 4} \quad (3.24)$$

corresponding to a spectral density

$$S(\omega) = (\sigma^2 / \sqrt{\pi} \beta) e^{-\omega^2 / \beta^2} \quad (3.25)$$

We may make a power series expansion of e^{ω^2/β^2} , retaining only the first $(n + 1)$ terms, so that the real random stationary process $u(x)$ is replaced by a Markov process $u_n(x)$, and Eq. 3.25 becomes

$$\left(1 + \frac{\omega^2}{\beta^2} + \dots + \frac{1}{n} \frac{\omega^{2n}}{\beta^{2n}}\right) S(u_n; \omega) = \sigma^2/\beta \sqrt{\pi} \quad (3.26)$$

The right-hand side of Eq. 3.26 is the spectral density of a delta-correlated process (white noise), and the quantities $u_n, u_n', \dots, u_n^{(n-1)}$ (i.e., the process u_n and its first $n-1$ derivatives) form the components of an n -dimensional Markov process.

The first-order approximation, with $n = 1$, gives

$$S(u_1; \omega) = \frac{\sigma^2}{\beta \sqrt{\pi} (1 + \omega^2/\beta^2)} \quad (3.27)$$

which has a correlation function

$$B_1(\tau) = \sigma^2 \sqrt{\pi} e^{-\beta|\tau|} \quad (3.28)$$

which is our familiar exponential. The next and closer approximation has a correlation function

$$B_2(\tau) = \sigma^2 \sqrt{\pi/(1 - \sqrt{2})} e^{-a|\tau|} [\cos(b) + \frac{a}{b} \sin(b|\tau|)] \quad (3.29)$$

where

$$\begin{aligned} a &= \beta \sqrt{(1 + \sqrt{2})/2} \\ b &= \sqrt{(\sqrt{2} - 1)/2} \\ a/b &= 1 + \sqrt{2} \end{aligned} \quad (3.30)$$

The two-term correlation function is seen to be regular at the origin, and indeed the quantity $u_2(x)$ may be shown to satisfy the differential equation

$$\frac{1}{\beta^2 \sqrt{2}} \ddot{u}_2 + \frac{\sqrt{1 + \sqrt{2}}}{\beta} \dot{u}_2 + u_2 = R \quad (3.31)$$

where R is a delta-correlated function, in this Gaussian case reducing to white noise. Whether this process will actually be conveniently extendable to two and three dimensions has not been examined.

3.4 AUTOCORRELATION FUNCTION FOR GAUSSIAN STRIATIONS

We now must examine how to approximate the autocorrelation function appropriate to the particular (Chesnut) distribution of Gaussian striations used in ROSCOE, by an exponential. Consider a random array of Gaussian rods, with average axial density λ (km^{-2}), and with the normalized size distribution used in ROSCOE

$$P(a) = \frac{8}{3 \sqrt{\pi} \sigma_0} (\sigma_0/a)^6 e^{-\sigma_0^2/a^2} \quad (3.32)$$

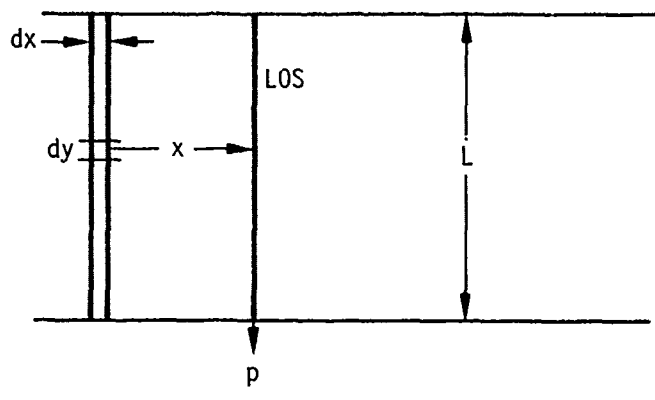
packed in a slab of thickness L (km). Let the electron density in each rod be

$$n(r) = n_0 e^{-r^2/a^2} \quad (3.33)$$

so that the light emission (cm^{-3}) is, assuming for the moment that the rods do not overlap)

$$I(r) = c n_0^2 e^{-2r^2/a^2} \quad (3.34)$$

AN-49606



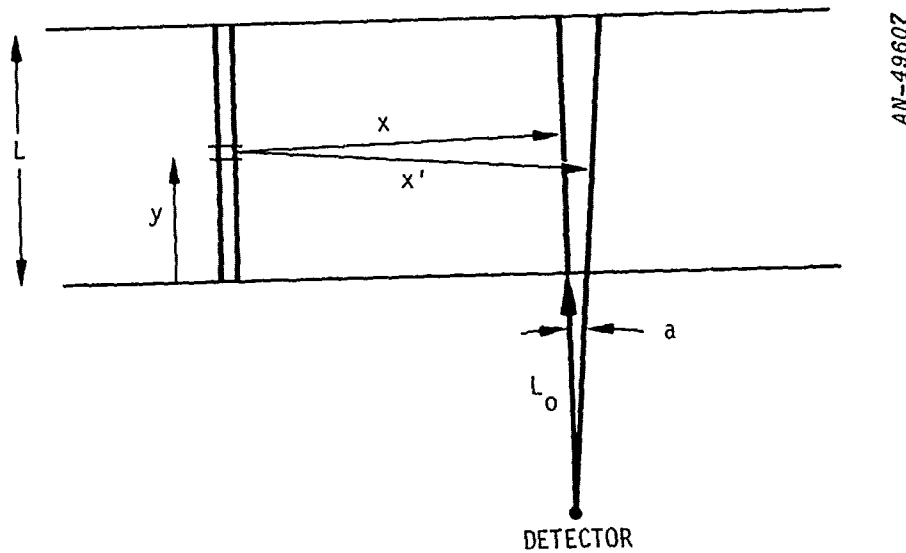
Consider the integrated intensity along a line of sight (LOS) at P, due to all the striations in a strip dx wide at a lateral distance X from P. The probability that a striation of size a is in dx dy is P(a) dx dy. The integrated intensity due to the striation of radius a is

$$\begin{aligned}
 I(a,x) &= c n_o^2 \int dy e^{-(2/a^2)(x^2 + y^2)} \\
 &= c a \sqrt{\pi/2} n_o^2 e^{-2x^2/a^2} \tag{3.35}
 \end{aligned}$$

This same expression is true for all striations, of size a in the strip, of which there are $\int L dx$. The autocorrelation function due to all striations of size a is thus

$$\begin{aligned}
 B(\tau) &= \int da P(a) \int_{-\infty}^{\infty} dx \int L c^2 n_o^4 a^2 \frac{\pi}{2} e^{-(2/a^2)(x^2 + (x+\tau)^2)} \\
 &= \int da P(a) \frac{c^2 n_o^4}{4} \pi^{3/2} \int L a^3 e^{-\tau^2/a^2} \\
 &= \frac{c^2 n_o^4 \int L \pi \sigma_o^3}{3} \left(\frac{1}{1 + \tau^2/\sigma_o^2} \right) \tag{3.36}
 \end{aligned}$$

Let us now consider the case for which the detector is so close to the striated region that the angular size of the striations differs along the line of sight.



Considering again only striations of a given size a in the area $dx dy$, the change in "impact parameter" X due to an angular rotation α of the line of sight is

$$X' = X + \alpha(L_0 + y)$$

As before (Eq. 3.35),

$$I(a, X) = cn_0^2 a \sqrt{\pi/2} e^{-(2X^2/a^2)}$$

$$I(a, X') = cn_0^2 a \sqrt{\pi/2} e^{-(2/a^2)(X^2 + 2\alpha X(L_0 + y) + a^2(L_0 + y)^2)}$$

so that

$$I(a,X) I(a,X') = (c^2 n_o^4 a^2 \pi) / 2 \cdot e^{-(1/a^2)(4X^2 + 4\alpha X(L_o+y) + \alpha^2(L_o+y)^2)} \quad (3.37)$$

Integrating over all spatial positions for the striation axis, and over the size spectrum a , gives for the autocorrelation function:

$$B(\alpha) = \int_0^\infty da P(a) \int_0^L dy \int_{-\infty}^\infty dx I(a,X) I(a,X') \quad (3.38)$$

$$B(\alpha) = \frac{c^2 n_o^4 \pi \sigma_o^4}{3\alpha} \int \left\{ \tan^{-1} \left(\frac{\alpha(L_o+L)}{\sigma_o} \right) - \tan^{-1} \left(\frac{\alpha L_o}{\sigma_o} \right) \right\} \quad (3.39)$$

which may easily be seen by L'Hopital's rule to reduce to (3.36) as $L_o \rightarrow \infty$, since αL_o in Eq. 3.39 corresponds exactly to τ in Eq. 3.36. Thus we have now formalized the procedure for integrating along a line of sight that penetrates striated regions at various distances from the detector. Thus, using a subscript i to refer to the various striated layers, we have

$$B(\alpha) = (\pi \int \sigma_o^4 c^2) / 3\alpha \cdot \sum_i n_o^4 \left\{ \tan^{-1} \left(\frac{\alpha(L_{oi}+L_i)}{\sigma_o} \right) - \tan^{-1} \left(\frac{\alpha L_{oi}}{\sigma_o} \right) \right\} \quad (3.40)$$

One of the objections to Approach 2, the simple superimposition of bright structured regions (as at different distances) was that it apparently locked into the code a technique applicable to detectors at DSP distances, but not for sensors much closer to the striated regions where nearby striations subtend a much larger angle than distant ones.

Equation 3.40 removes this objection, and in Fig. 24 we have plotted Eq. 3.40 in normalized form for a single 1000-km thick cloud at various distances L_0 from the detector, ranging from 100 km to essentially infinity, together with the single exponential. Note the similarity of all the curves; this agreement is then a measure of how well the exponential approximation of Sec. 3.2 can approximate the "true" autocorrelation function.

If the areal density \int of the rod axes becomes great enough that appreciable overlap occurs, correlations between different rods must be considered, since the intensity of light emissions is proportional to the square of the total electron density, and thus is not the same as the sum of the squares of the electron densities appropriate to the various rods. In this case, the factor $1/(1 + R^2)$ in Eq. 3.36 ($R = \tau/\sigma_0$) is replaced by the expression

$$\frac{\left\{ \frac{1}{1 + R^2} + \frac{4.35F}{(1 + 2R^2/3)} + \frac{1.11F}{(1 + R^2/2)^{2.5}} + \frac{5.03F}{(1 + R^2/2)} \right\}}{(1 + 4F/3)^2}$$

where $F = \pi \int \sigma_0^2$ is the axial packing density. For $F \approx 1$, this expression is in general a factor of two or three higher than the simple $1/(1 + R^2)$. We are indebted to Dr. Peter Redmond for carrying out the algebra for this relation.

AN-49608

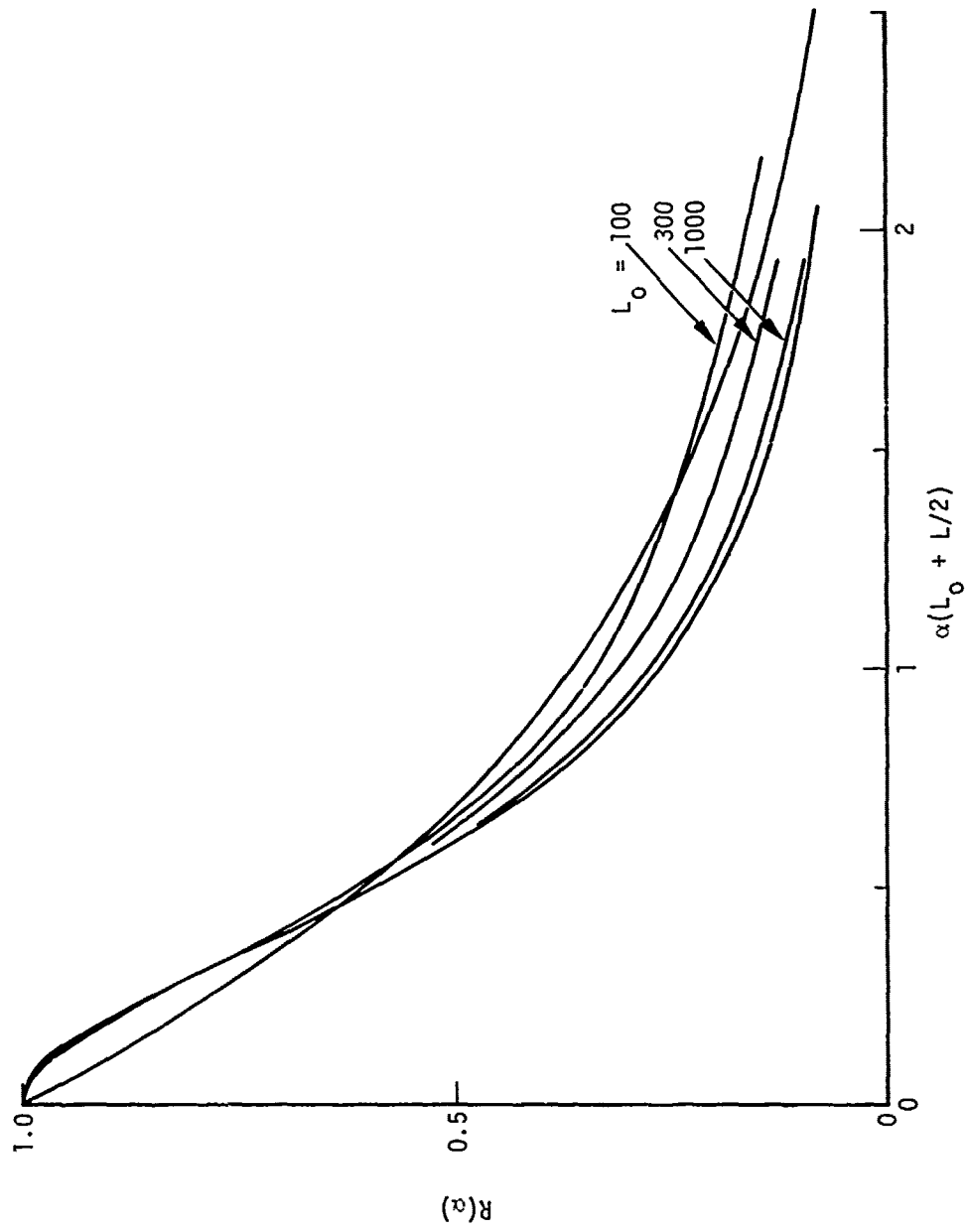


Figure 24. Autocorrelation Function for Distribution of Gaussian Striations

REFERENCES

1. The ROSCOE Manual, Volumes 1 through 20, General Research Corporation (unpublished).
2. Nuclear Induced Optical Phenomenology Program, General Electric/TEMPO (unpublished).
3. Paul Fisher, private communication.
4. A. M. Yaglom, Stationary Random Functions, Dover Publications, 1962.
5. N. Wiener, Extrapolation, Interpolation, and Smoothing of Stationary Time Series, Wiley and Sons, 1950.

APPENDIX A

EXTRAPOLATION AND INTERPOLATION OF RANDOM SEQUENCE

We have omitted several steps in the chain of proofs necessary to justify some of the statements in Sec. 3.2, which we address more fully below.

First, we must show the independence of extrapolation in two dimensions. Having computed

$$(S/\sigma)_{i+n,j} = F^n (S/\sigma)_{i,j} + \sqrt{1 - F^{2n}} R_i \quad (A.1)$$

can we project ahead in the orthogonal j direction from $S_{i,j}$ without taking account of $S_{i+n,j}$? The answer is in the affirmative, since if we try a solution for $S_{i,j+m}$ of the form

$$(S/\sigma)_{i,j+m} = \alpha (S/\sigma)_{i,j} + \beta (S/\sigma)_{i+n,j} + \gamma R_j \quad (A.2)$$

it is easy to show, using Eqs. 3.2 and 3.3 of Sec. 3.2, that

$$\begin{aligned} \beta &= 0 \\ \alpha &= p^m \end{aligned} \quad (A.3)$$

so that the point at $i+n,j$ does not influence that at $i,j+m$.

Second, we must modify Eq. 3.4 of Sec. 3.2 when any "leap-frogging" occurs, as in computing the point at $i+n,j+m$ when we have already computed the other corners of the rectangle, at $i+n,j$ and $i,j+m$, from Eqs. A.1 and A.2. In this case we can easily show that

$$\begin{aligned}
 (S/\sigma)_{i+n,j+m} &= -F^n P^m (S/\sigma)_{i,j} + P^m (S/\sigma)_{i+n,j} \\
 &\quad + F^n (S/\sigma)_{i,j+m} + \delta R_{ij}
 \end{aligned}
 \tag{A.4}$$

where R_{ij} is a random Gaussian variate of unity variance, and

$$1 - \delta^2 = F^{2n} + P^{2m} - F^{2n} P^{2m} \tag{A.5}$$

Note the negative sign of the first term on the right, which is at first sight surprising, since an exponential decorrelation demands a positive expectation value for the product of any two terms.

The answer, of course, lies in the positive correlation of all the terms on the right with each other, which must be considered when one takes the expectation value

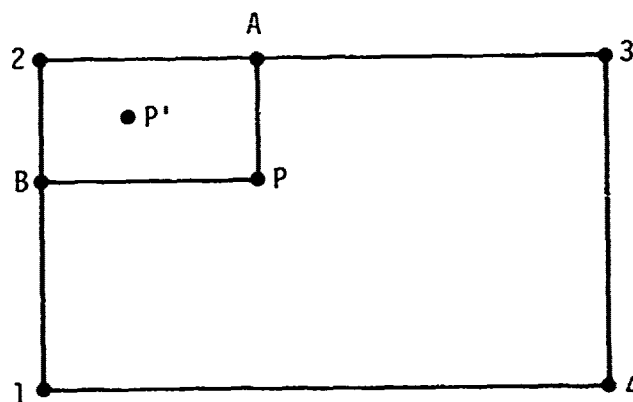
$$\langle (S/\sigma)_{i+n,j+m} (S/\sigma)_{i,j} \rangle$$

The proof that $(S/\sigma)_{i+n,j+m}$, as computed in this manner, correlates properly with previously computed values at $i-n, j-m$ is straightforward.

The interpolation formula (3.10) has some interesting features that are worthy of note. If the interpolated point lies on an edge, its value depends only on the values at the two corners 1 and 2 bounding this edge, and not at all on the opposite corners 3 and 4. But if only three corners, say 1, 3, and 4, have been computed (and not the corner S_2), in order to compute the same point P on the edge 1-2, all three values at points 1, 3, and 4 must be used in a linear combination, as in Eq. A.4.

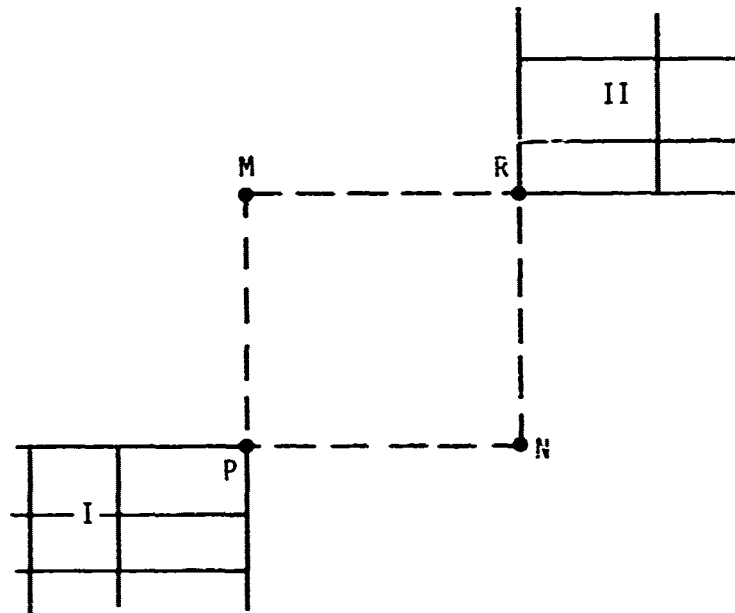
Successive interpolation for points in a rectangle is straightforward, but cannot be done blindly. Having once computed a point P inside a rectangle, an auxiliary constraint has been set for a subsequent point P' since these must correlate properly with each other. Thus Eq. 3.10 cannot simply be reapplied for P' . Instead the two points A and B must be found (A from a linear combination of 2, 3, and P , and B from a linear combination of 2, A , and P , as in Eq. A.4), and then the interpolation (Eq. 3.10) reapplied. At each step it must be shown that any computed point correlates properly with other values than those used in its determination. See Fig. A.1.

The final step, of joining two widely separated regions computed wholly independently, is now seen to be straightforward, by a process of computing successive corner points of the rectangle between the two regions. Thus if region I has a limiting point P in its upper right-hand corner, and region II a limiting point R in the lower left-hand corner, the other two corners M (a linear combination of P and R) and N (a linear combination of P , M , and R) are then computed and intermediate values interpolated as previously discussed. See Fig. A.2.



AN-49609

Figure A.1. Multiple Interpolation Inside a Rectangle

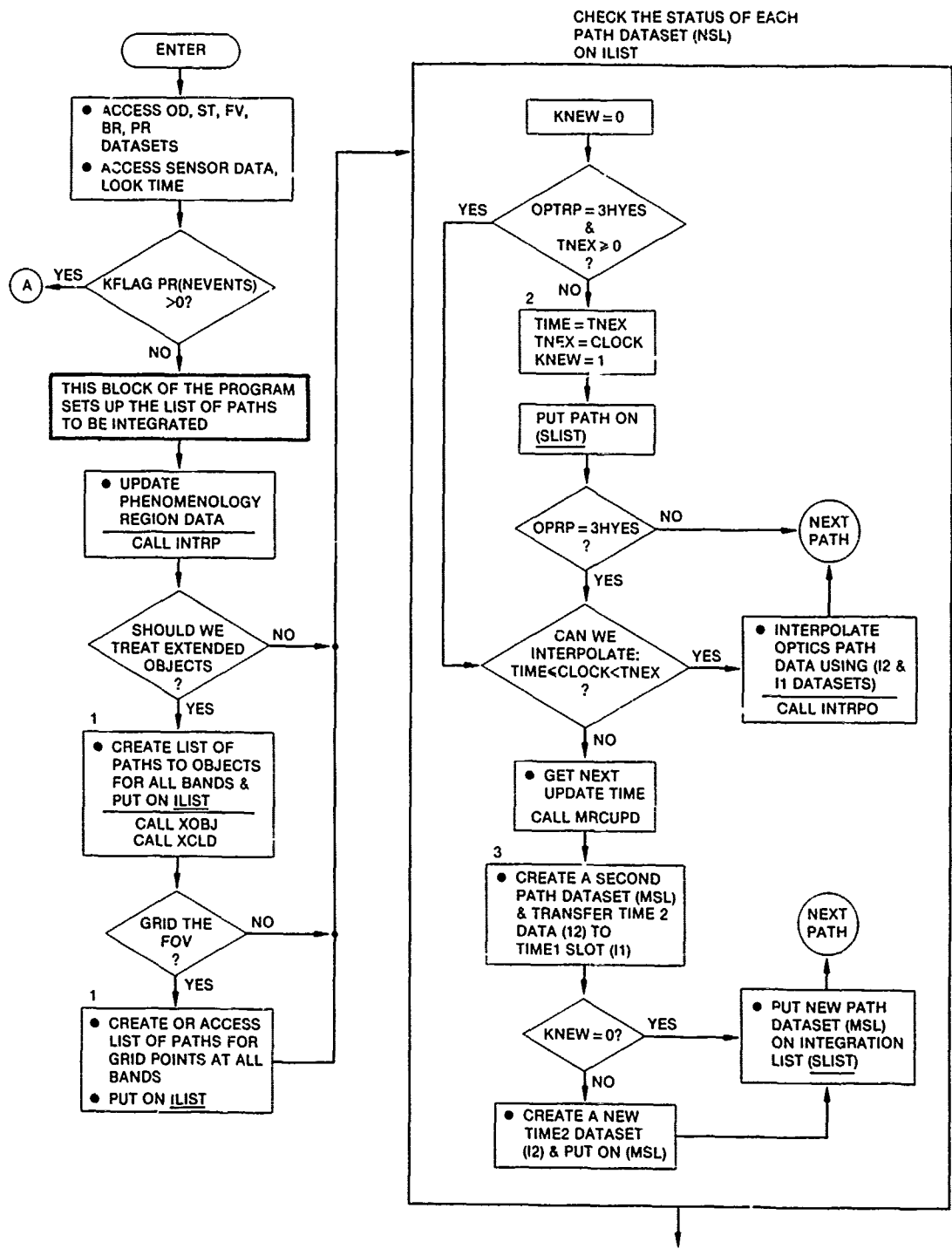


AN-49610

Figure A.2. Joining Separate Regions

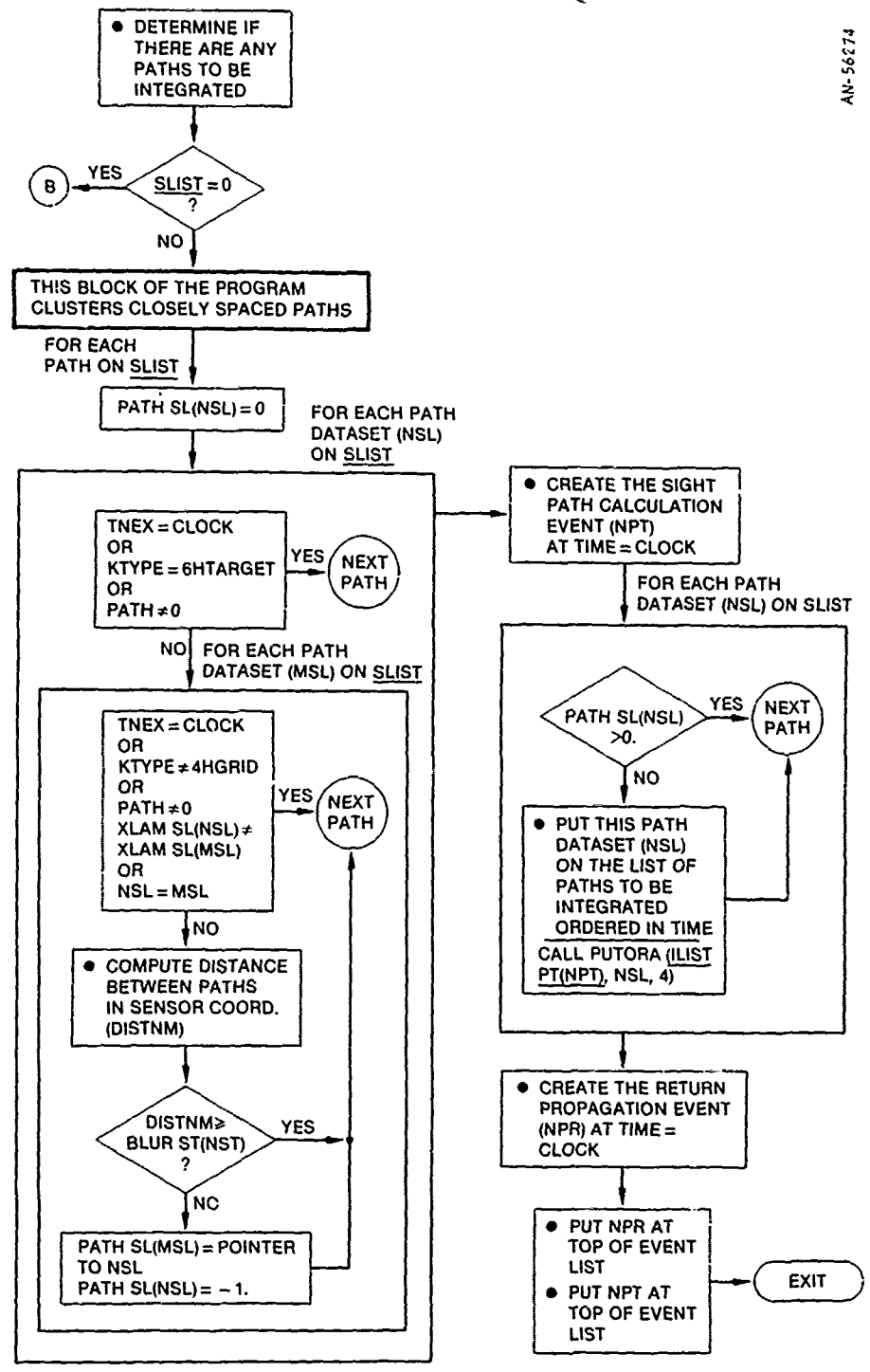
APPENDIX B

FLOW DIAGRAMS

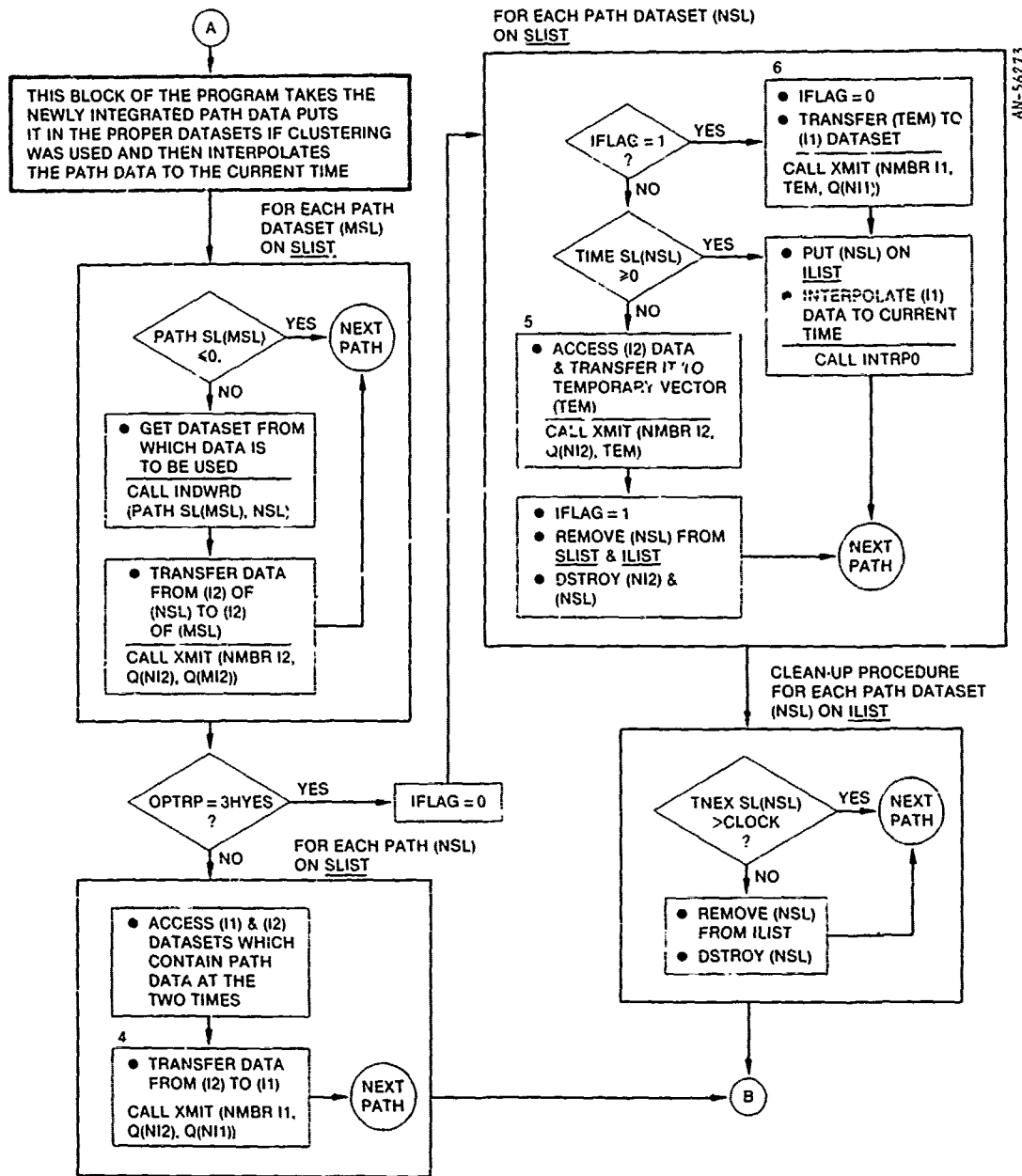


AN-56275

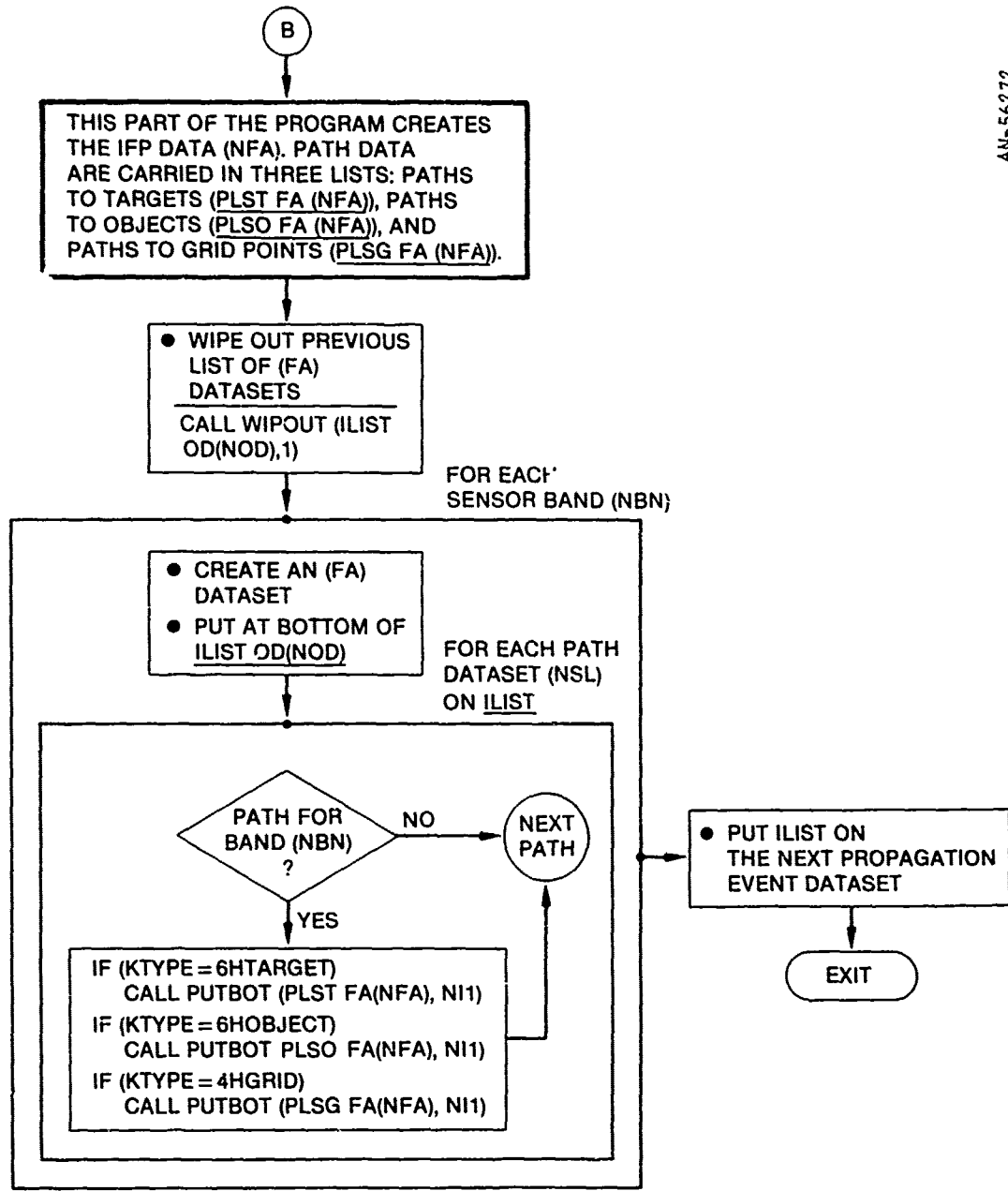
PROGRAM OPROP: Optics propagation event. Sets up paths to be integrated and/or interpolates these data



PROGRAM OPROP (continued)



PROGRAM OPROP (continued)



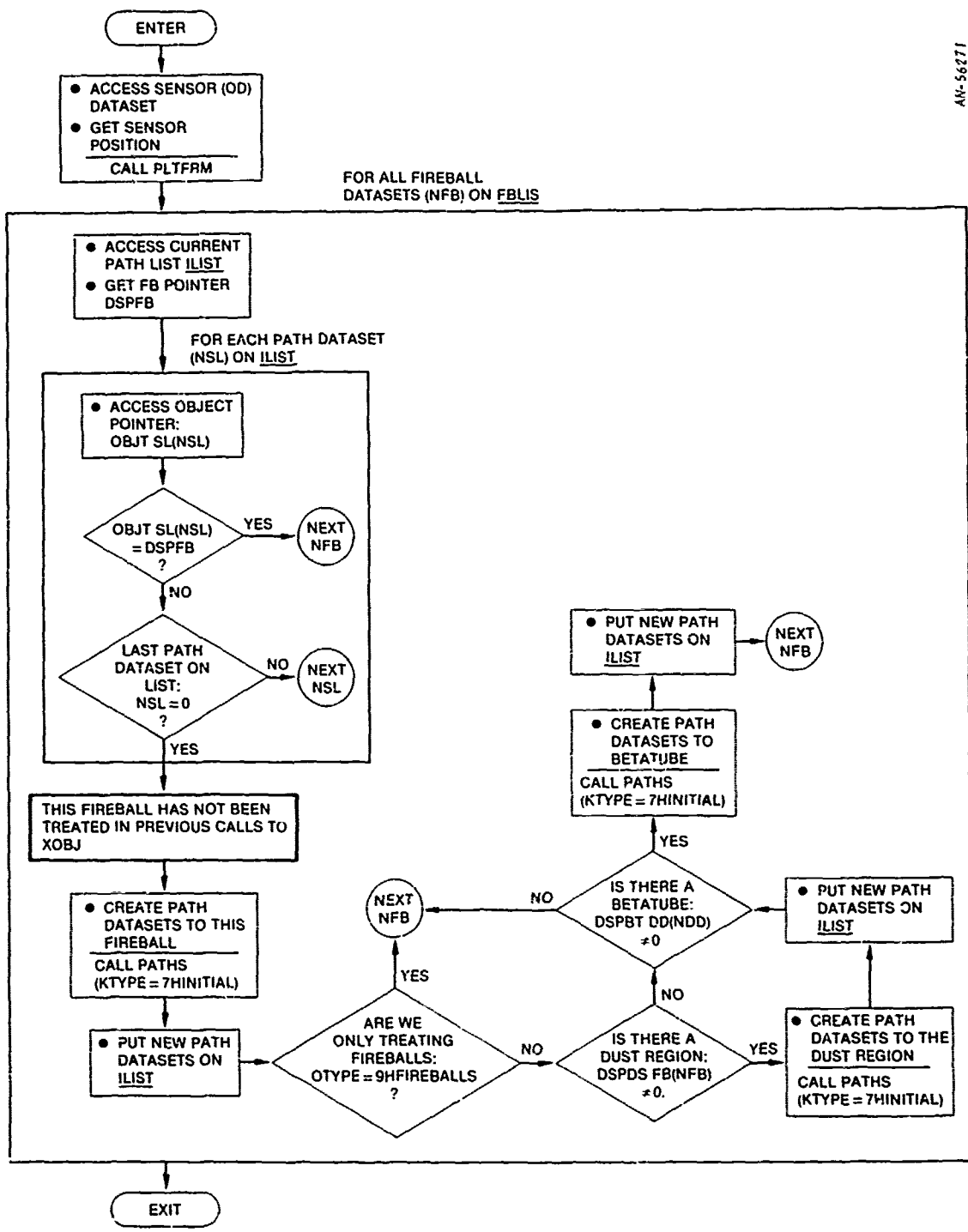
PROGRAM OPROP (continued)

NOTES

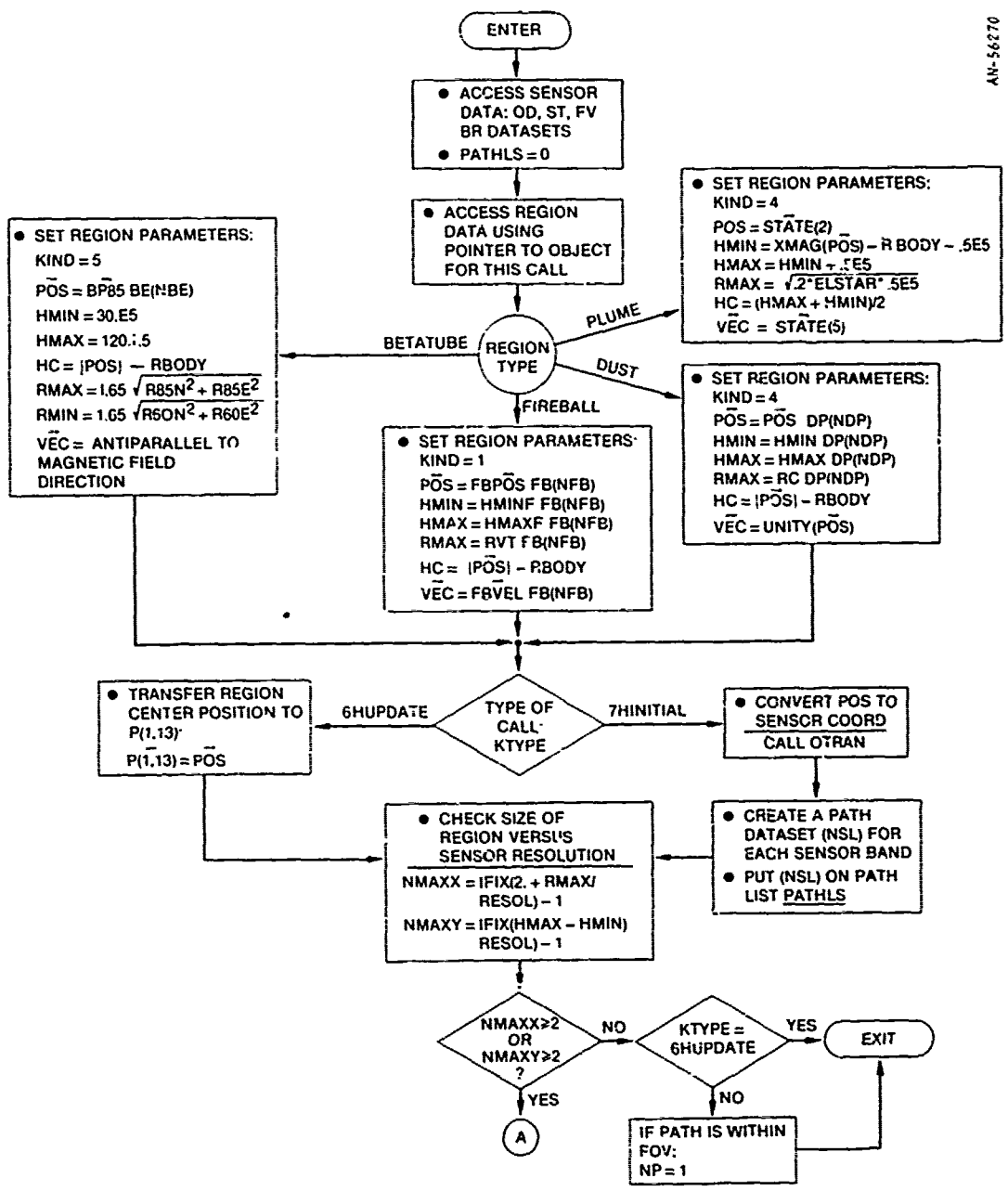
1. For all new path datasets, we set:
 TIME = CLOCK
 TNEX = -5000.
2. This part is computed only when path data is to be initialized.
3. The second path dataset contains the same data as the first for normal updates. For initialization, however, a new O21 dataset is required since integrations at two times are required.
4. The (I1) dataset always carries the path data at the current time used in the optics simulation.
5. This part is computed only when path data is initialized. It sets up the (I1) data for interpolation.
6. The path datasets on SLIST are ordered such that initialization data at two times for the same path are sequential. A single path dataset (NSL) with pointers to the datasets carrying the time-varying parameters at two times (I1 and I2) is then formed.

PROGRAM OPROP (concluded)

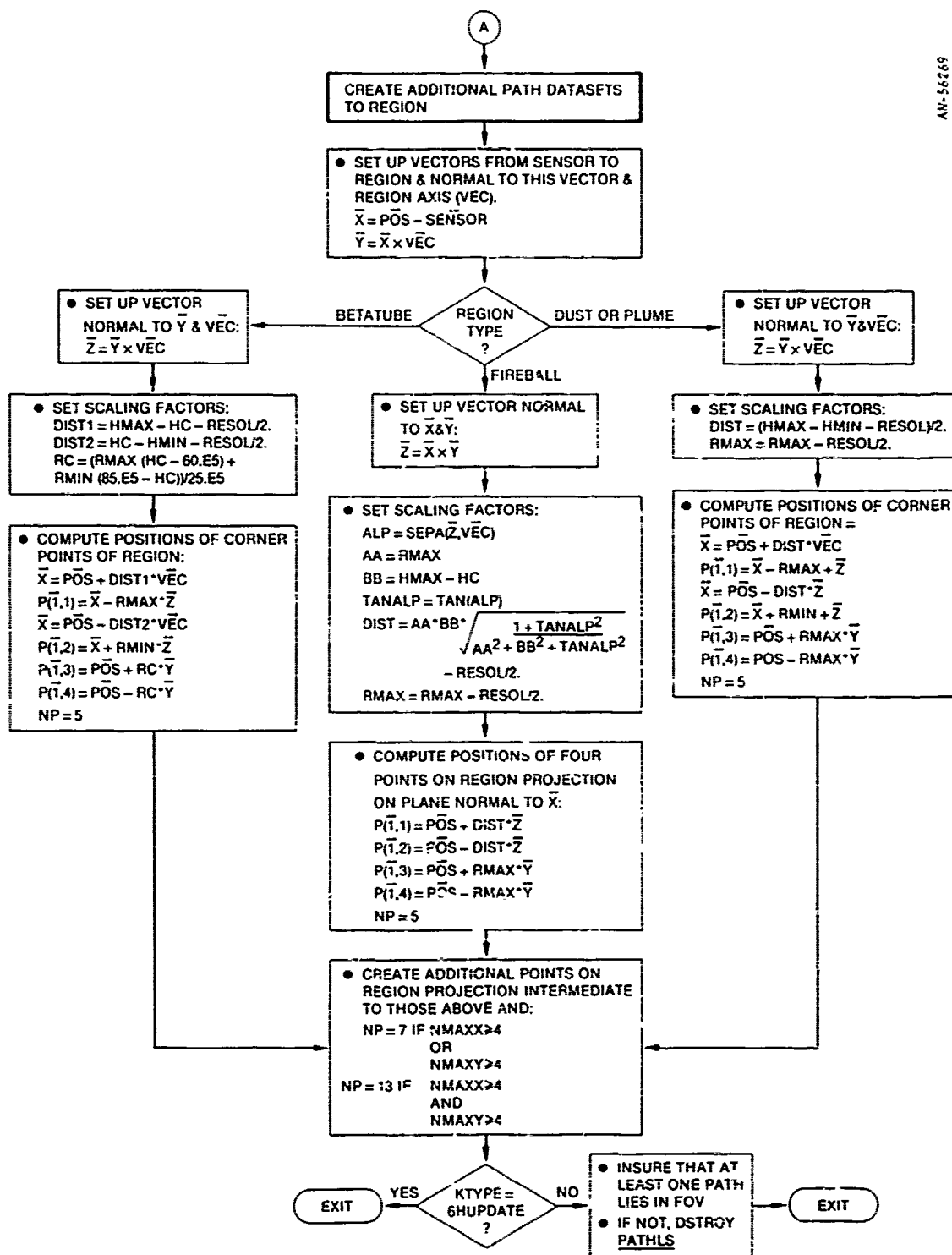
AN-56271



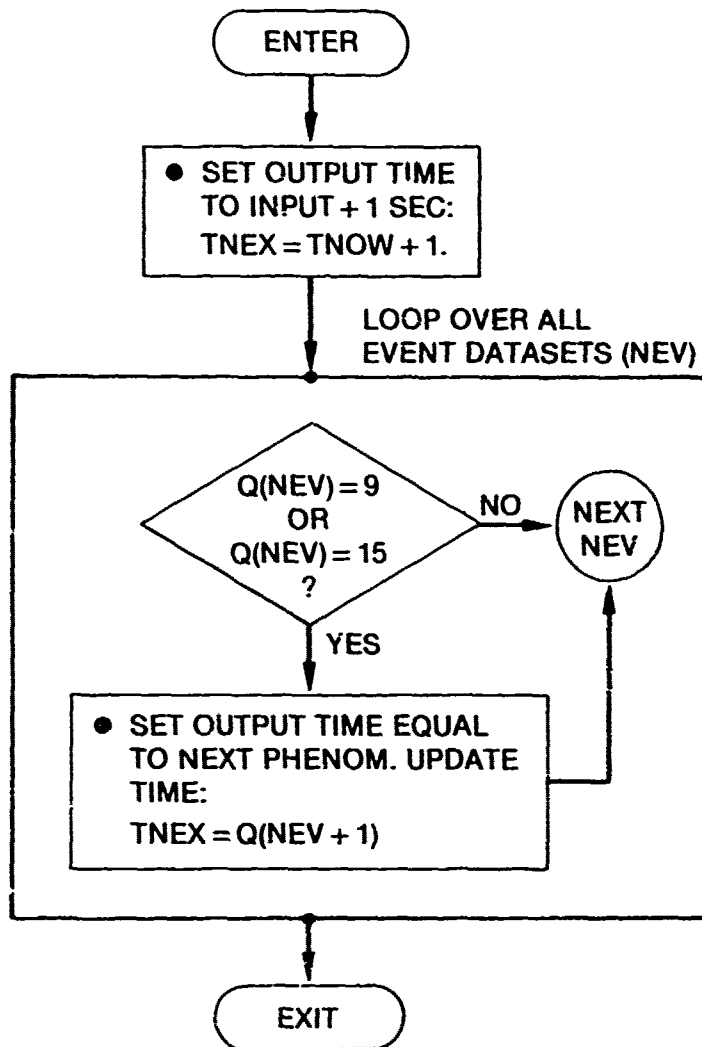
SUBROUTINE XOBJ: Generates sight path datasets to all fireballs, dust regions, and beta tubes in FOV



SUBROUTINE PATHS: Routine which determines number and position of paths to a specified region

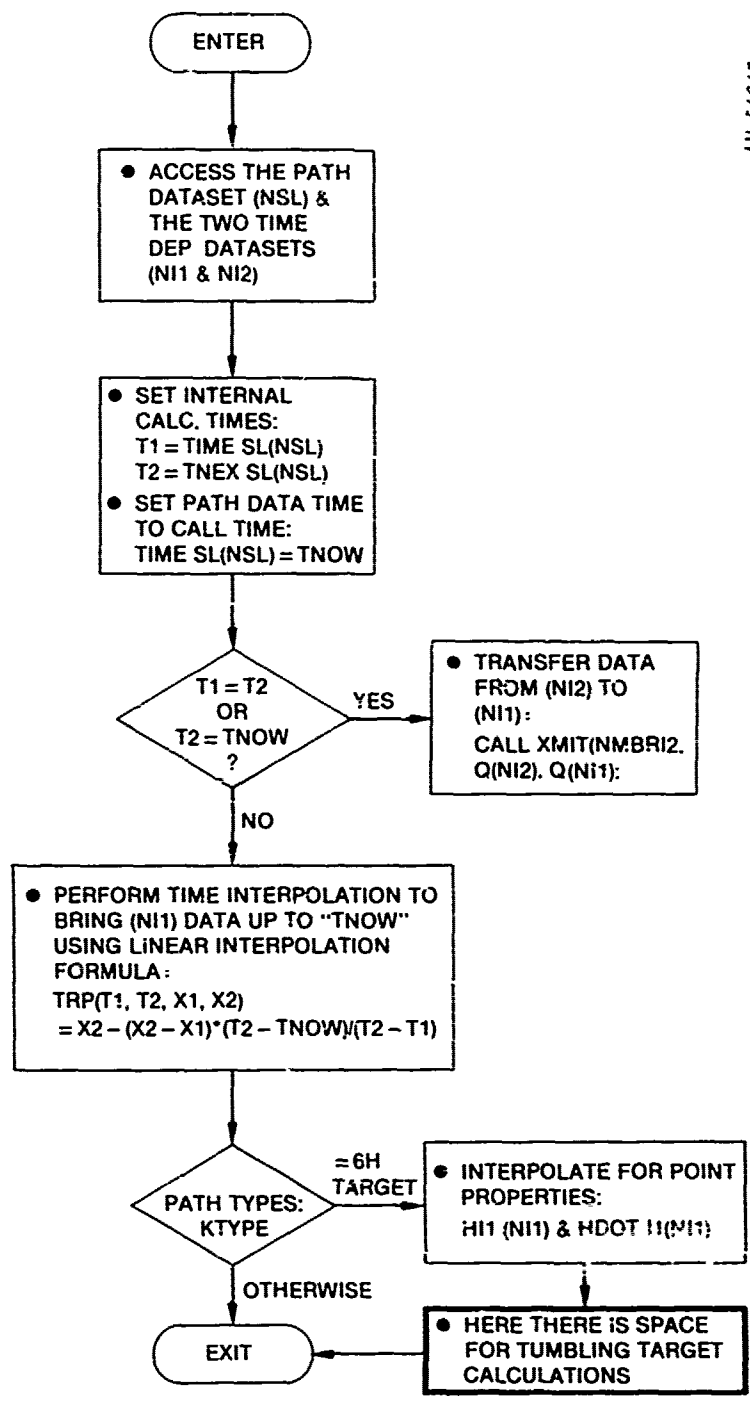


AN-56268

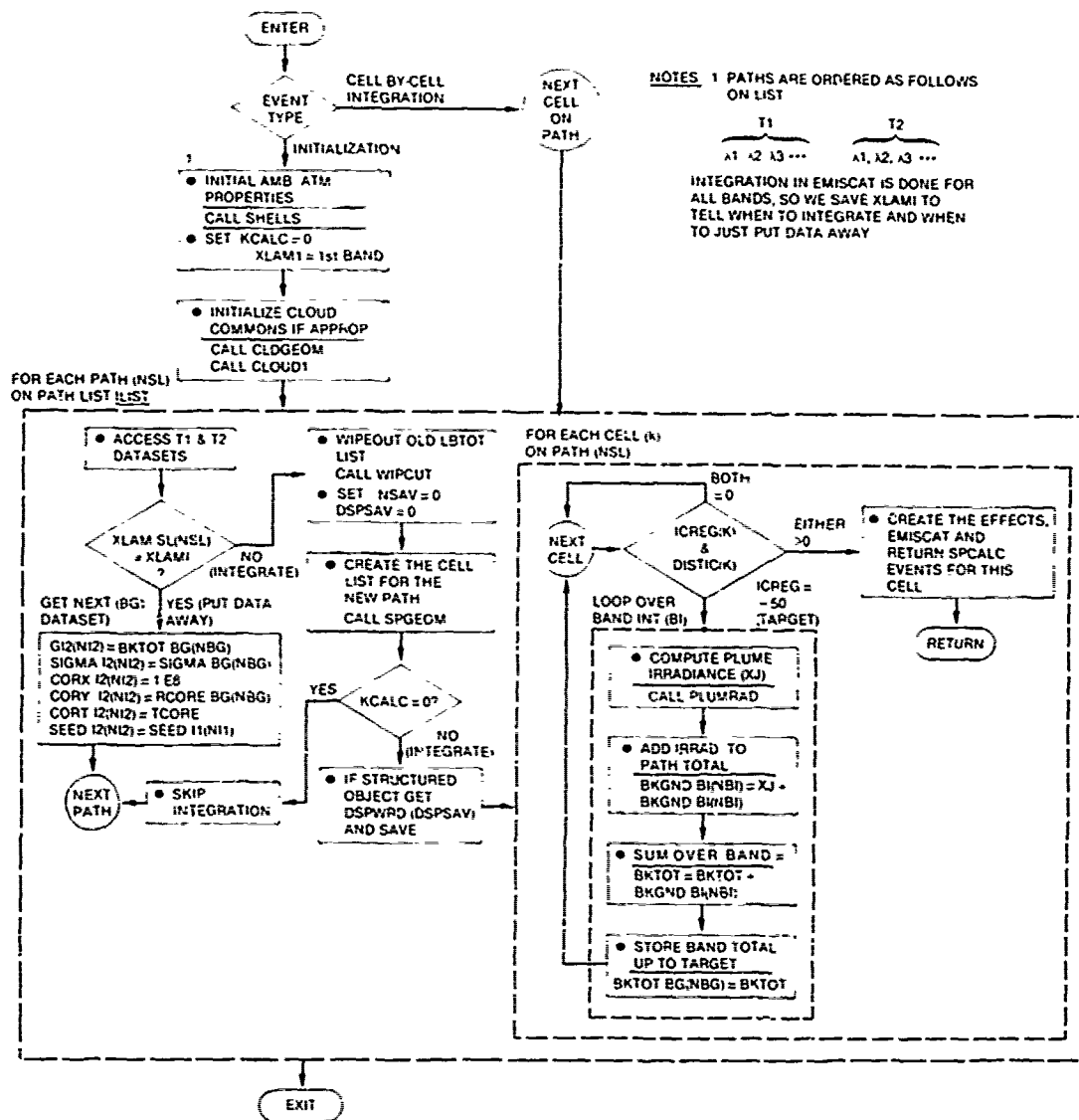


SUBROUTINE MRCUPD: Routine to determine next update time for path dataset

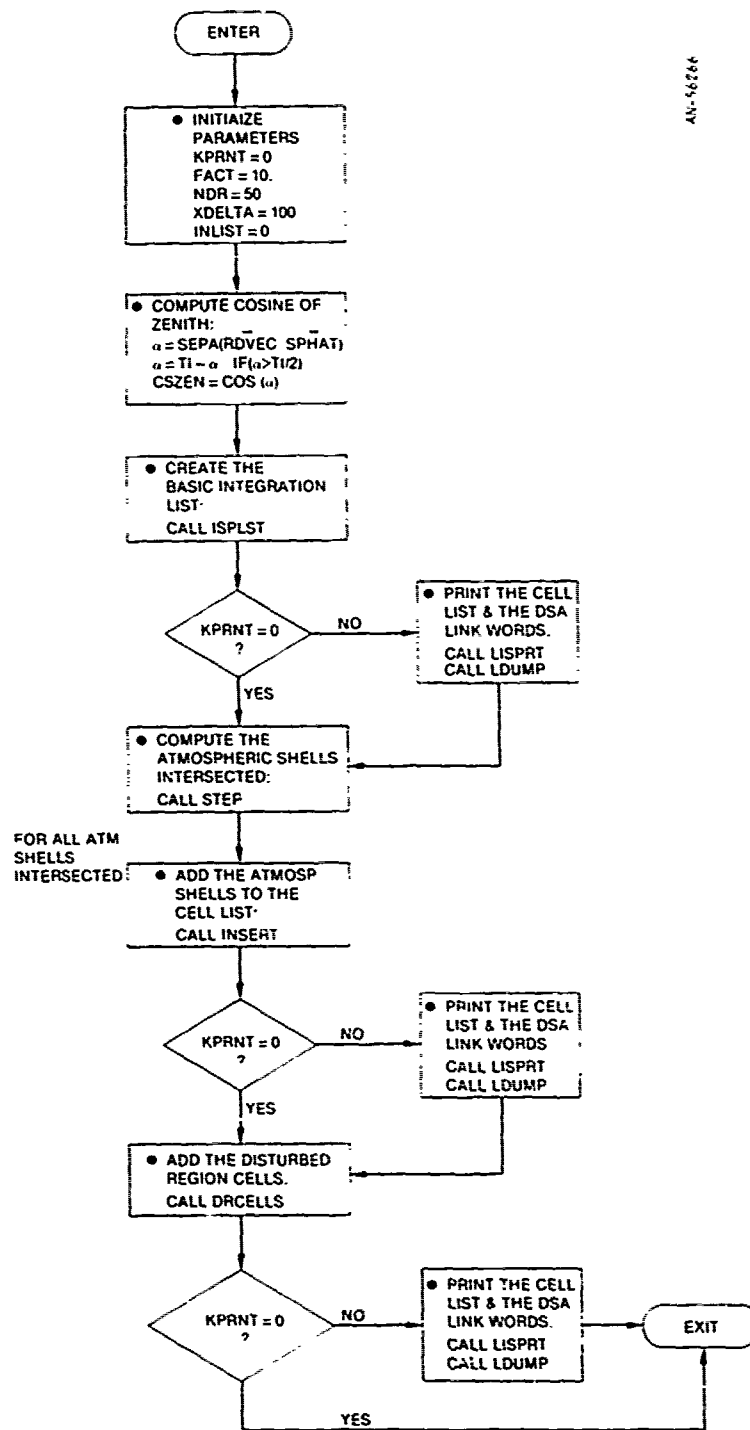
AN-56267



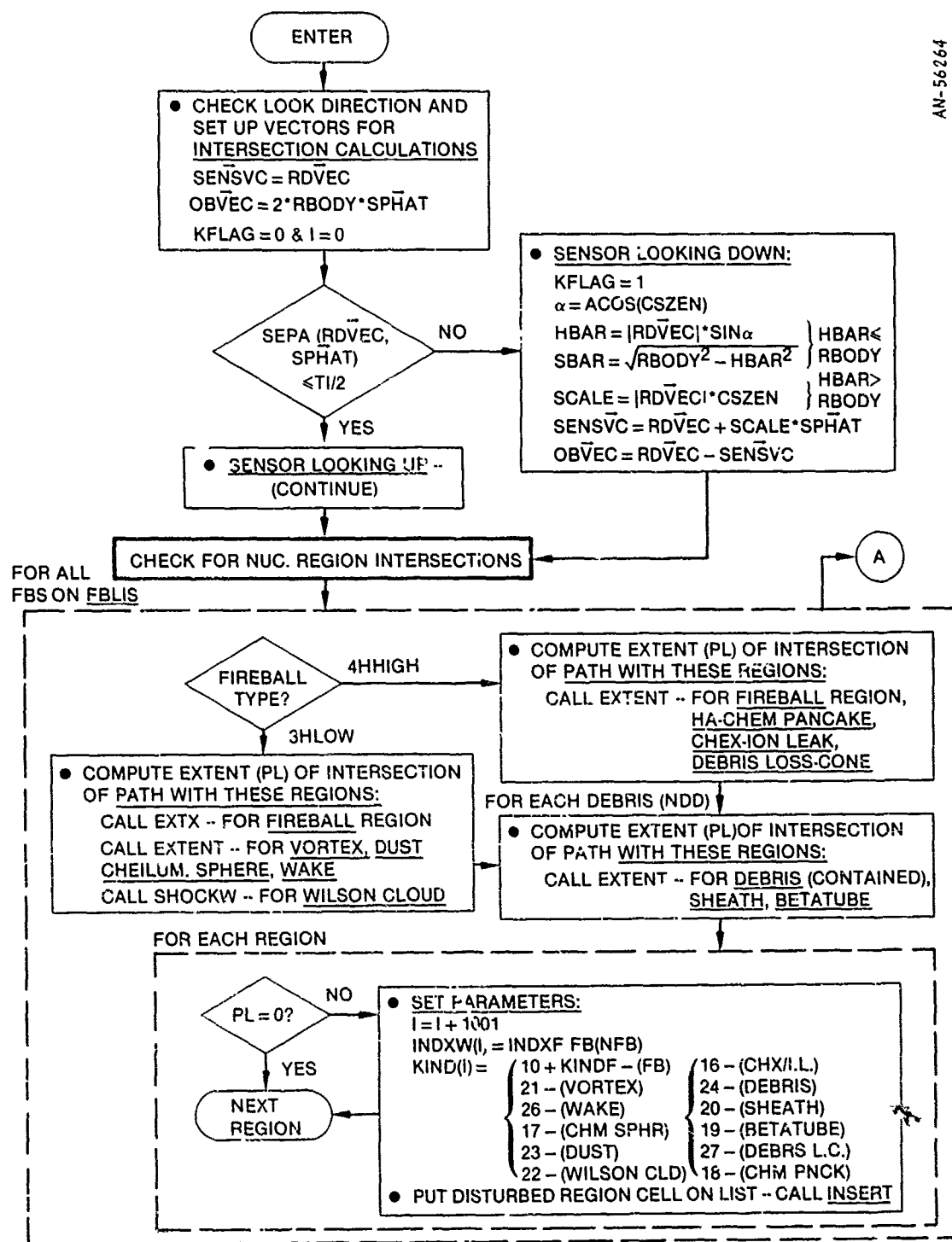
SUBROUTINE INTRPO: Routine which is used to interpolate path data to current time



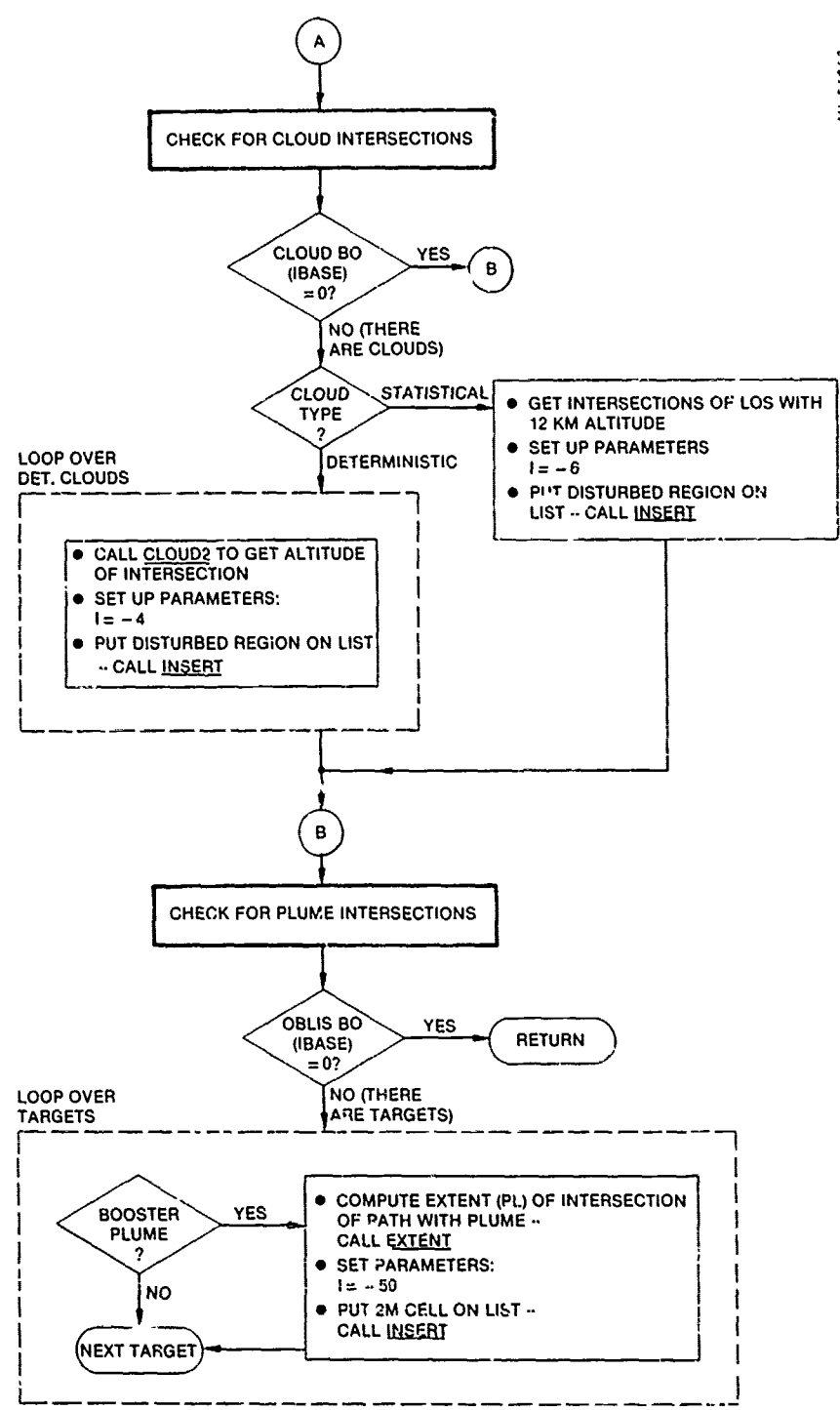
PROGRAM SPCALC: Sight path calculation event. Initializes sight path cell list and then creates EFFECTS and EMISCAT events to process data cell by cell



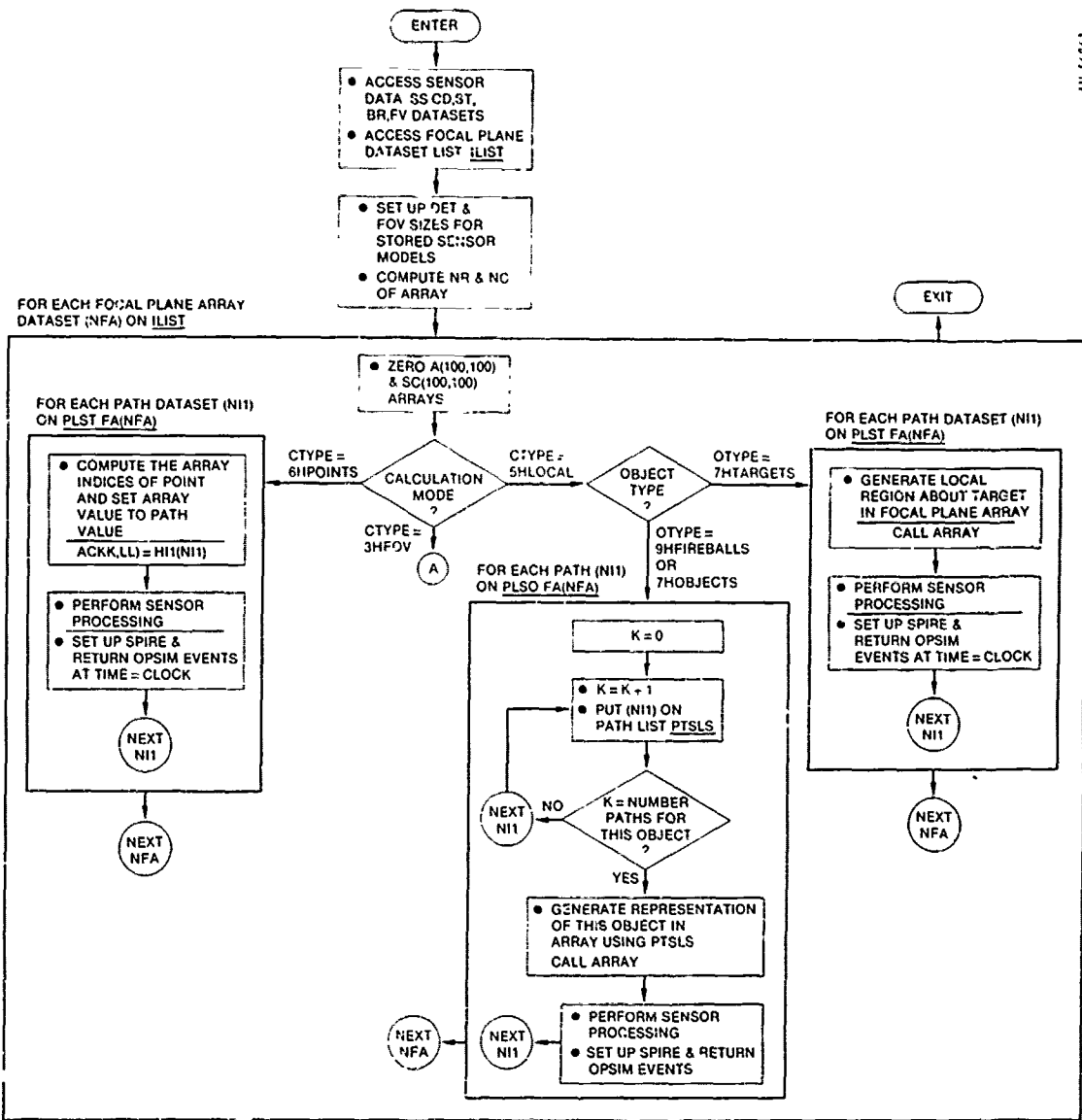
SUBROUTINE SPGEOM: This subroutine creates the cell integration list



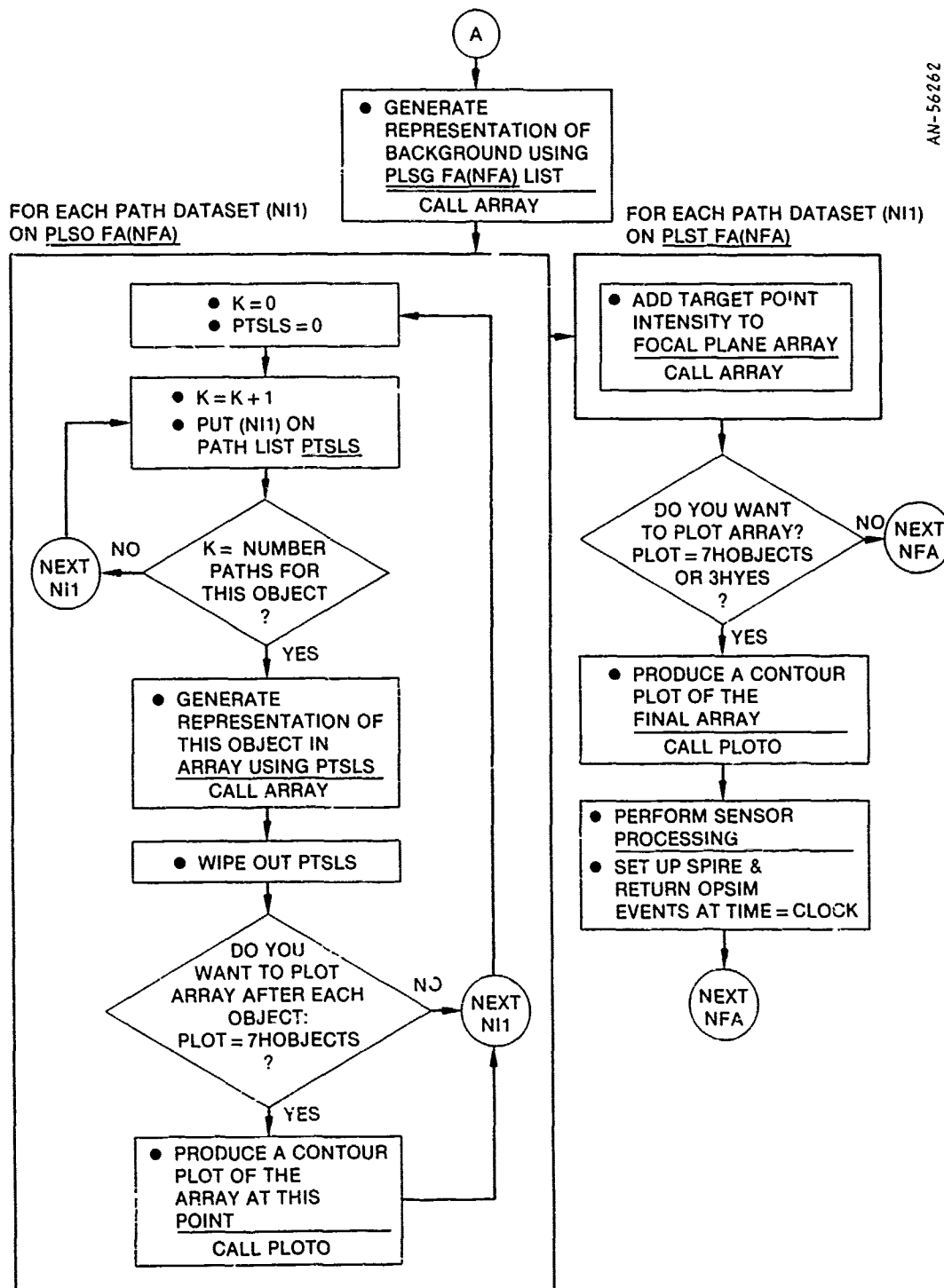
SUBROUTINE DRCELLS: Subroutine which creates disturbed region cells for specified path



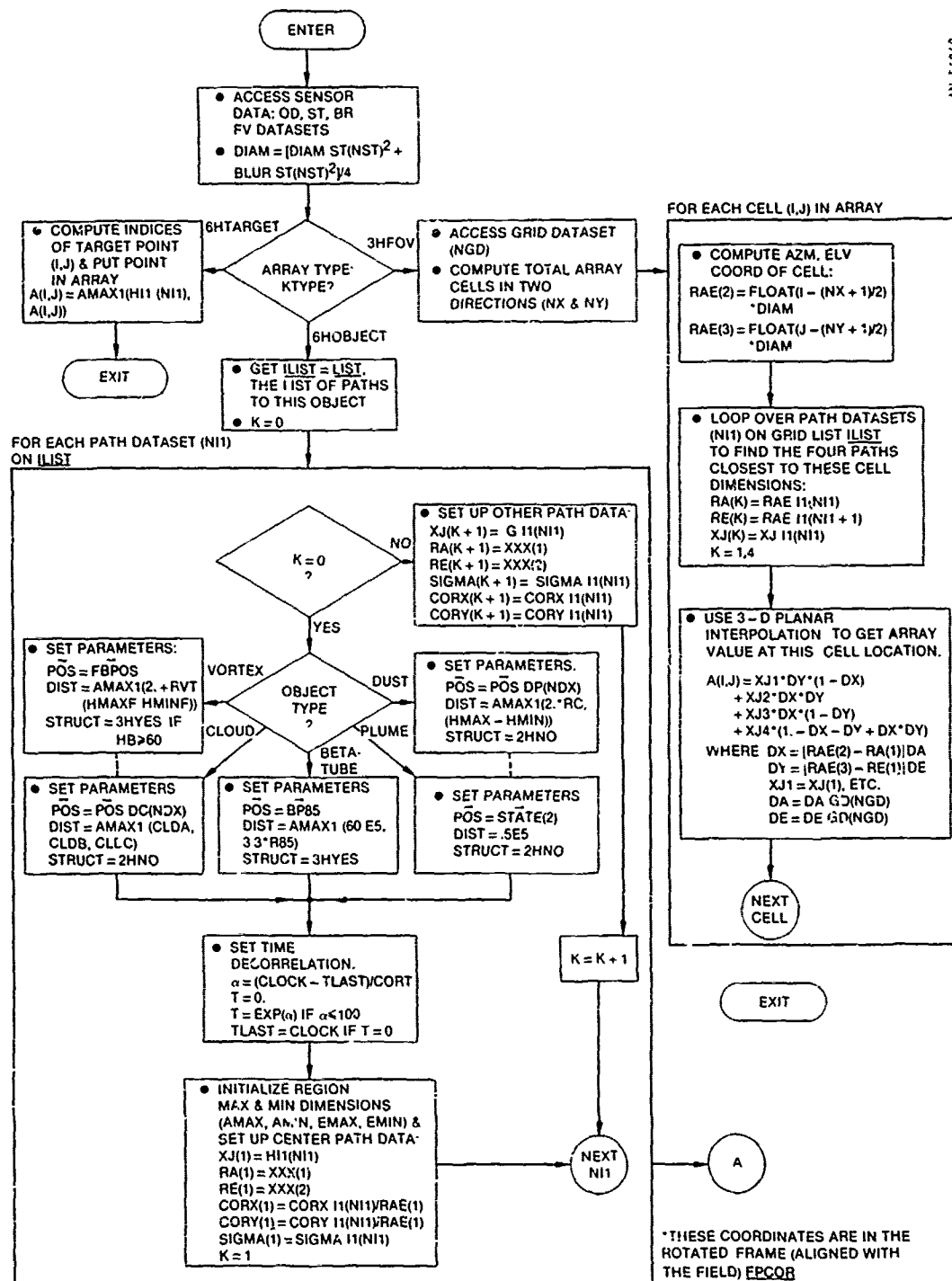
SUBROUTINE DRCELLS (continued)



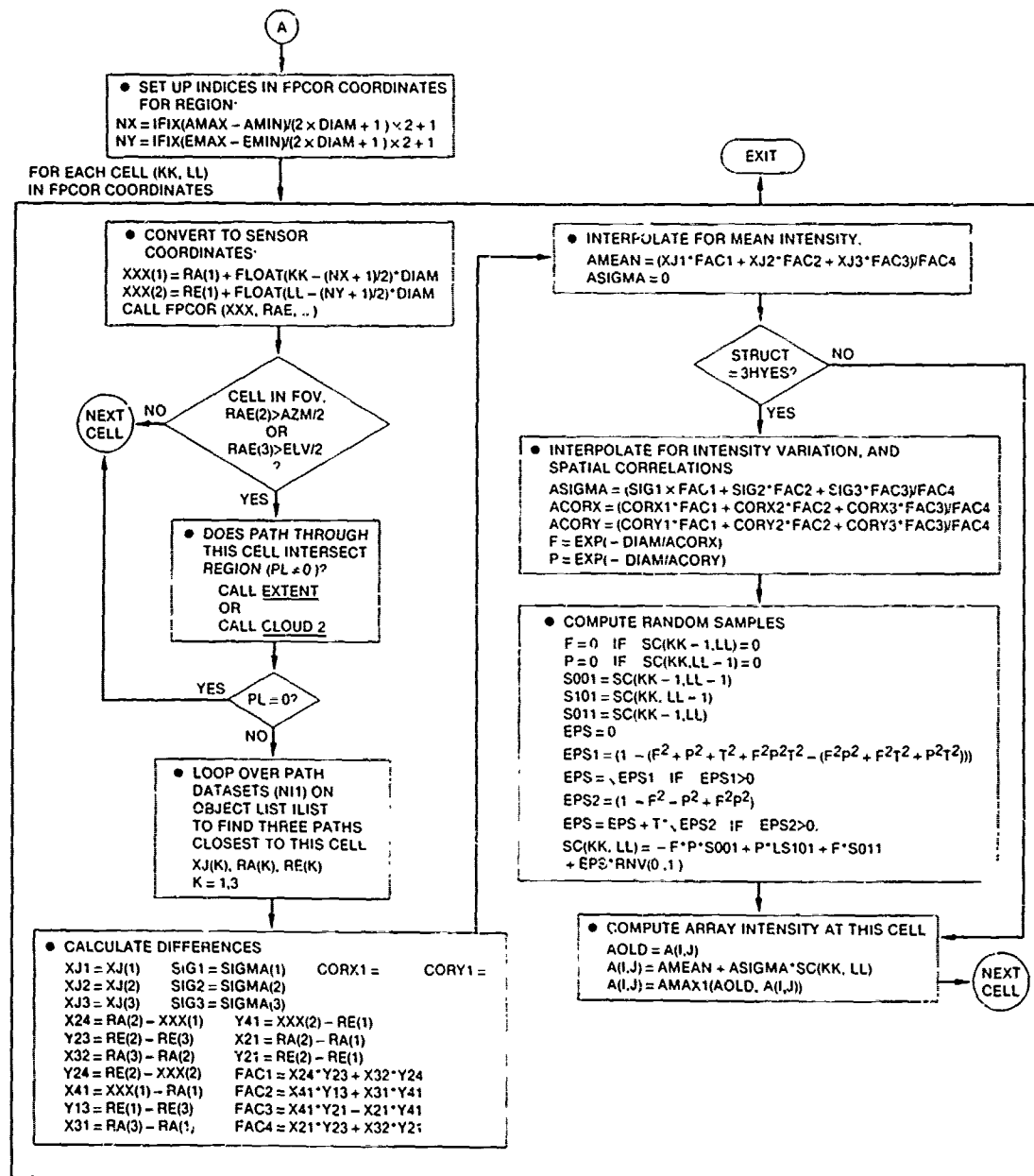
PROGRAM OPSIM: Optics simulation event. Generates focal plane array and calls processing routines



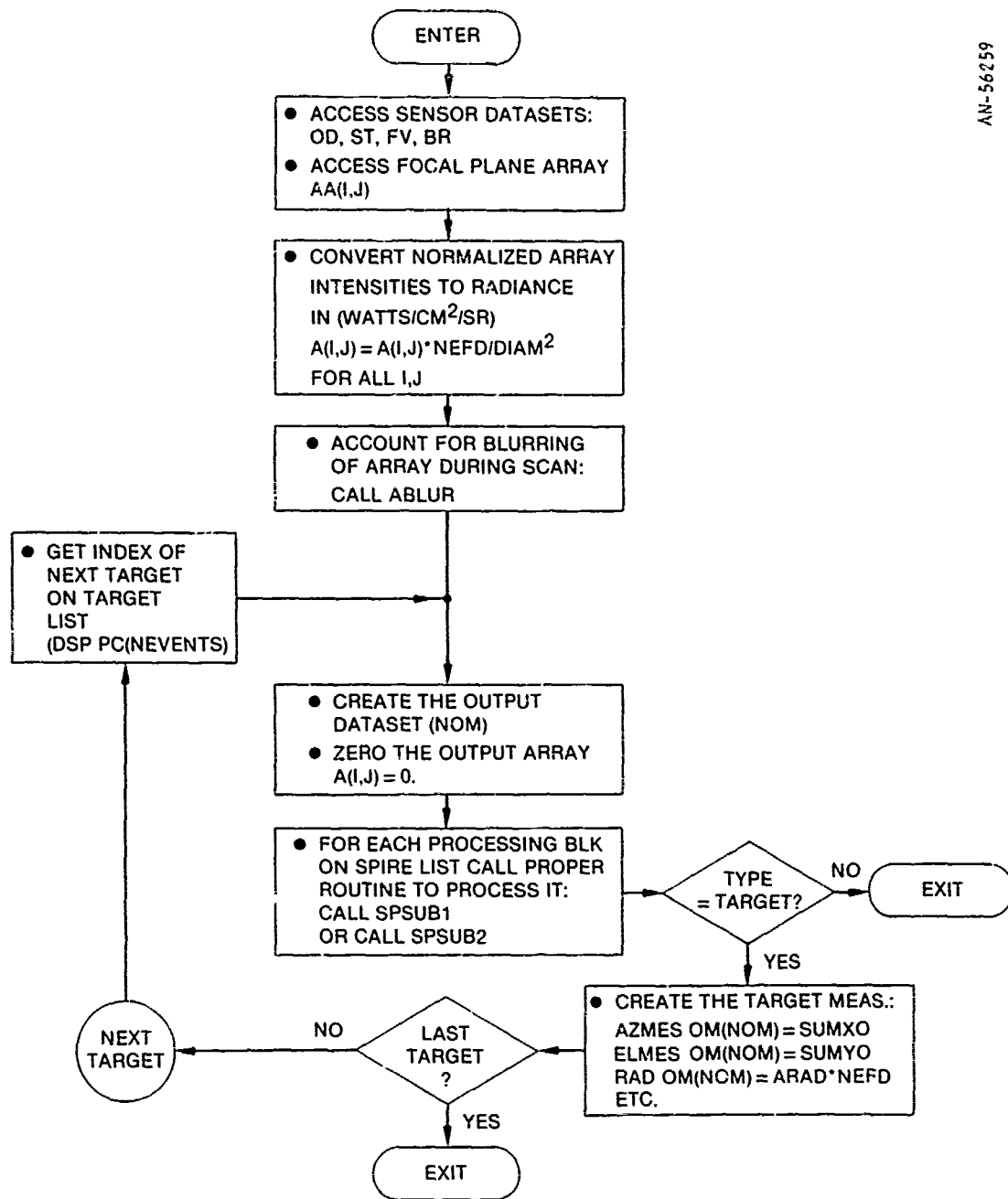
PROGRAM OPSIM (continued)



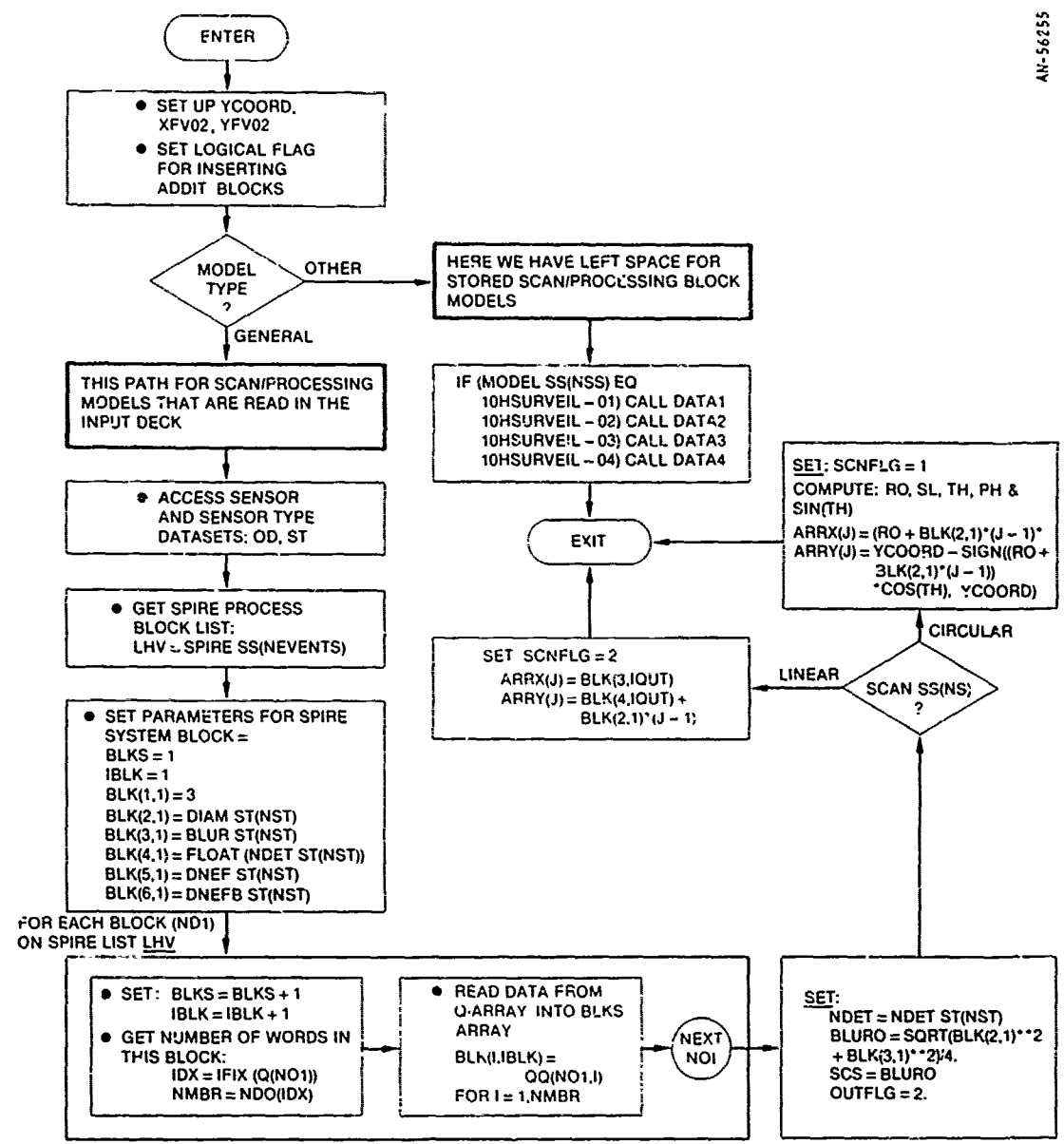
SUBROUTINE ARRAY: Constructs the focal plane intensity array, given path data describing target prints, objects, and grid



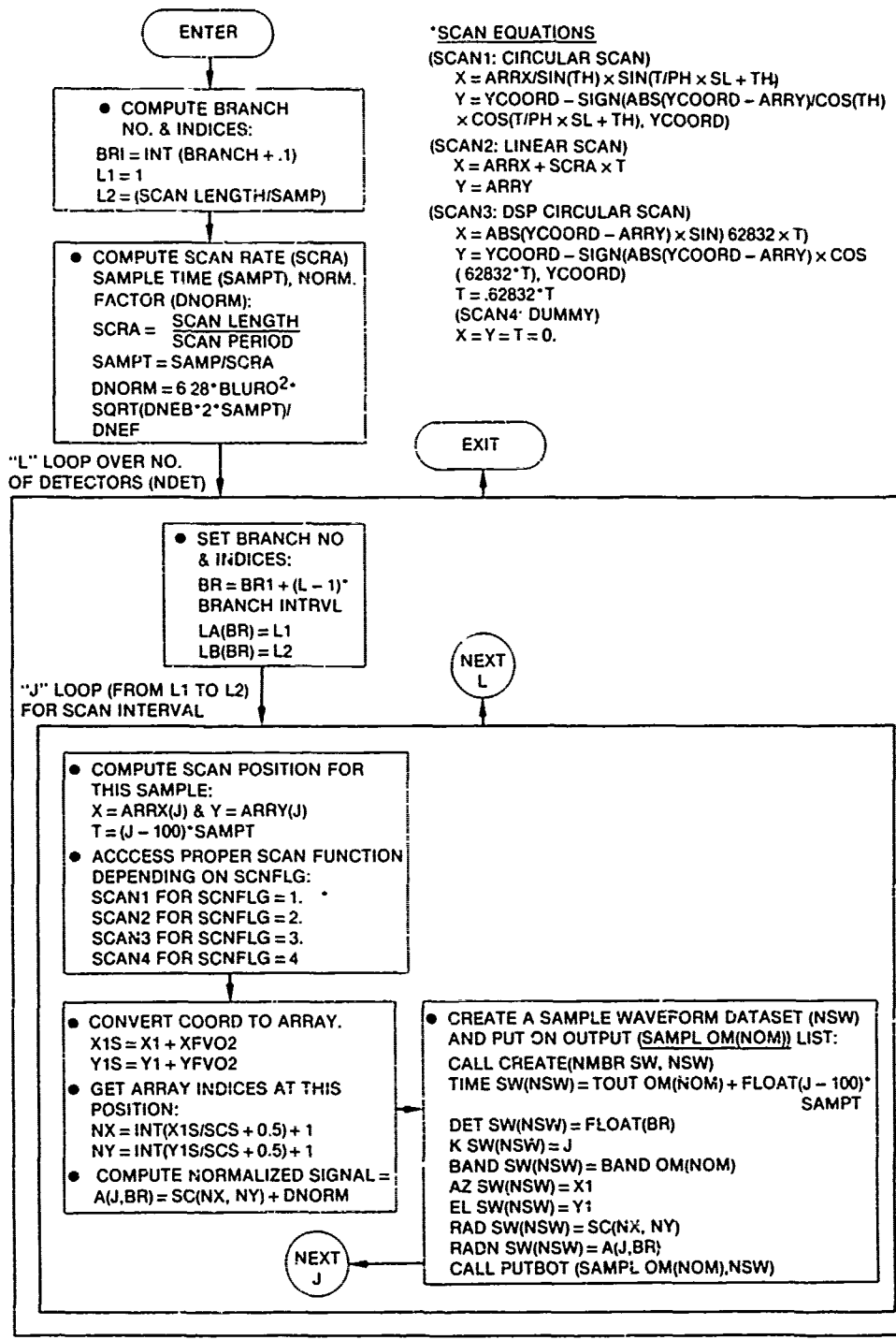
SUBROUTINE ARRAY (continued)



PROGRAM SPIRE: This program calls the subroutines to scan the focal plane and process the data. Also produces one output datasets



SUBROUTINE INSENS: Initializes SPIRE scan/processing computation blocks

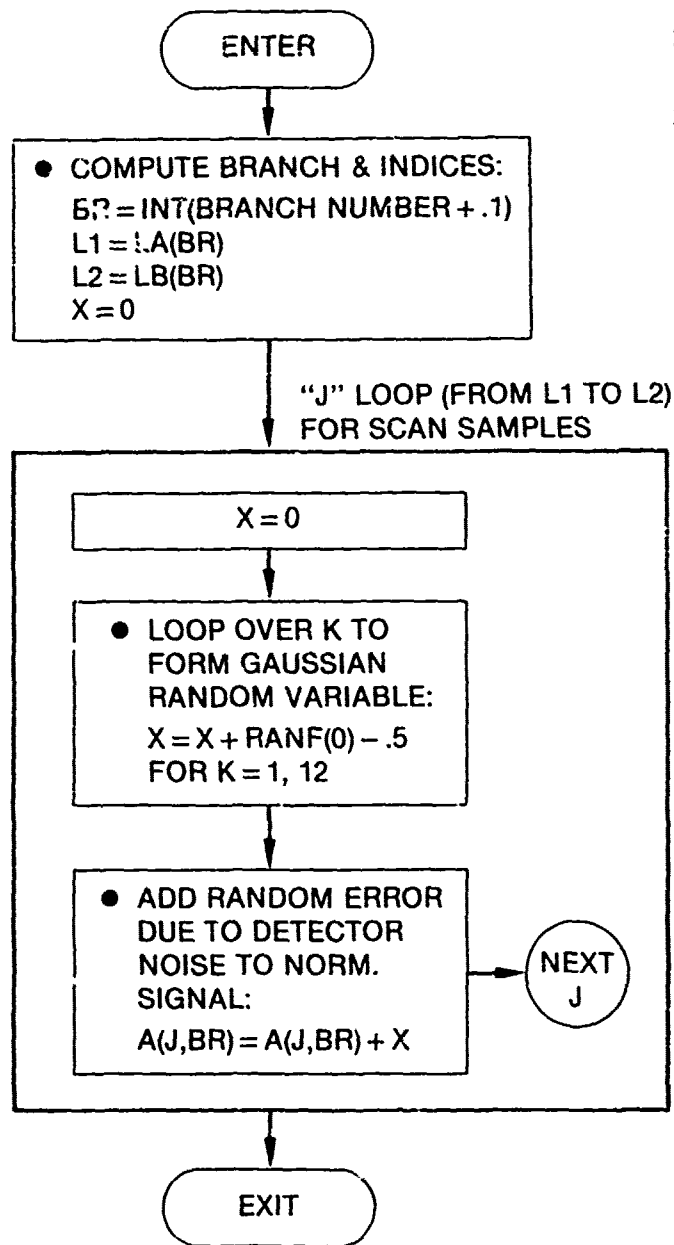


***SCAN EQUATIONS**
 (SCAN1: CIRCULAR SCAN)
 $X = ARR_X / \sin(\theta) \times \sin(\tau / \text{PH} \times SL + \theta)$
 $Y = YCOORD - \text{SIGN}(\text{ABS}(YCOORD - ARRY_Y) \cos(\theta)) \times \cos(\tau / \text{PH} \times SL + \theta), YCOORD)$
 (SCAN2: LINEAR SCAN)
 $X = ARR_X + SCRA \times T$
 $Y = ARRY$
 (SCAN3: DSP CIRCULAR SCAN)
 $X = \text{ABS}(YCOORD - ARRY) \times \sin(62832 \times T)$
 $Y = YCOORD - \text{SIGN}(\text{ABS}(YCOORD - ARRY) \times \cos(62832 \times T), YCOORD)$
 $T = .62832 \times T$
 (SCAN4: DUMMY)
 $X = Y = T = 0.$

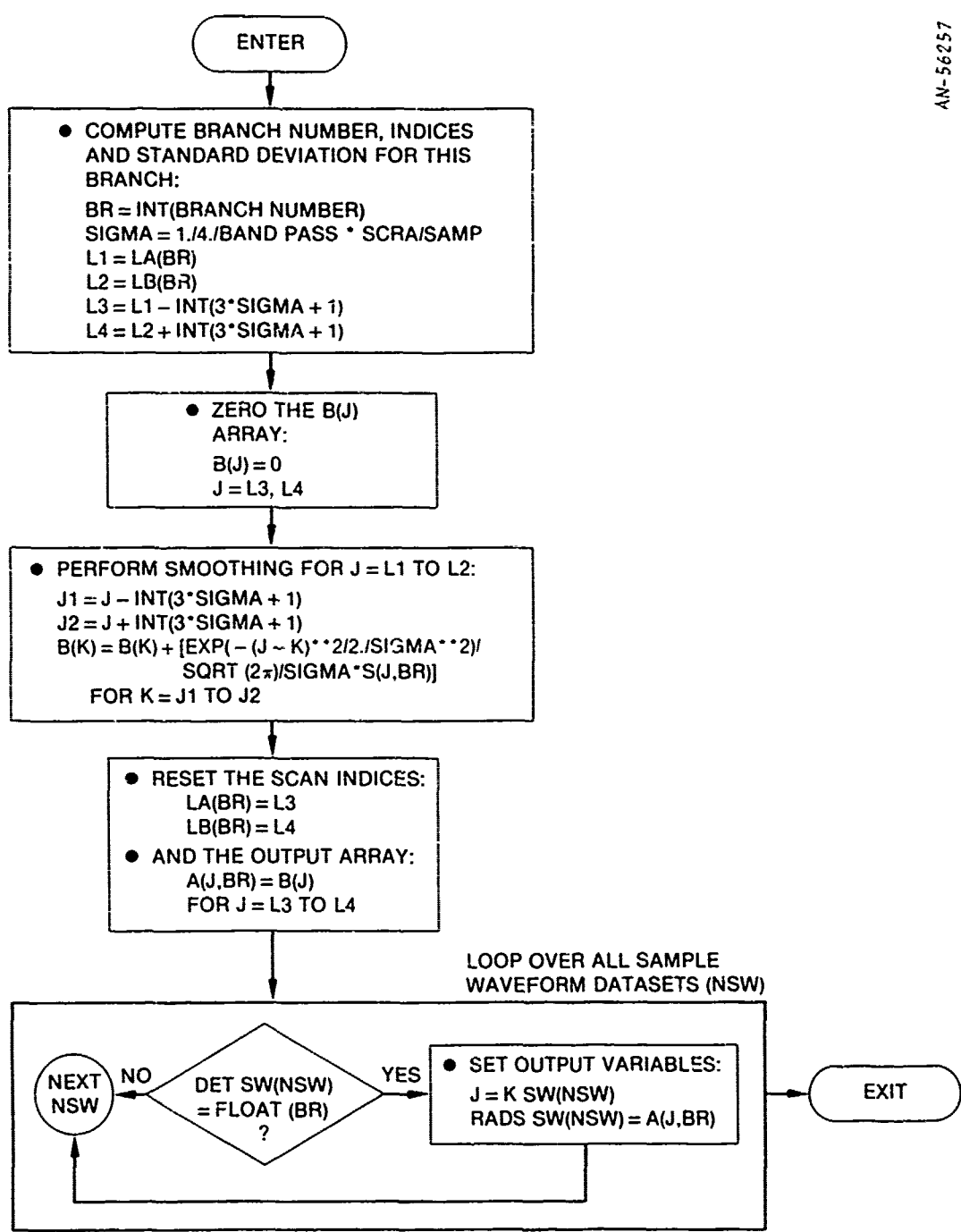
SUBROUTINE SPSUB1 --

(4) Scan Block--assuming square detector

AN-56256



SUBROUTINE SPSUB1 --
(5) Detector Noise Block



SUBROUTINE SPSUB2 ---
(6) Gaussian Smoothing Block

SUBROUTINE SPSUB1 --

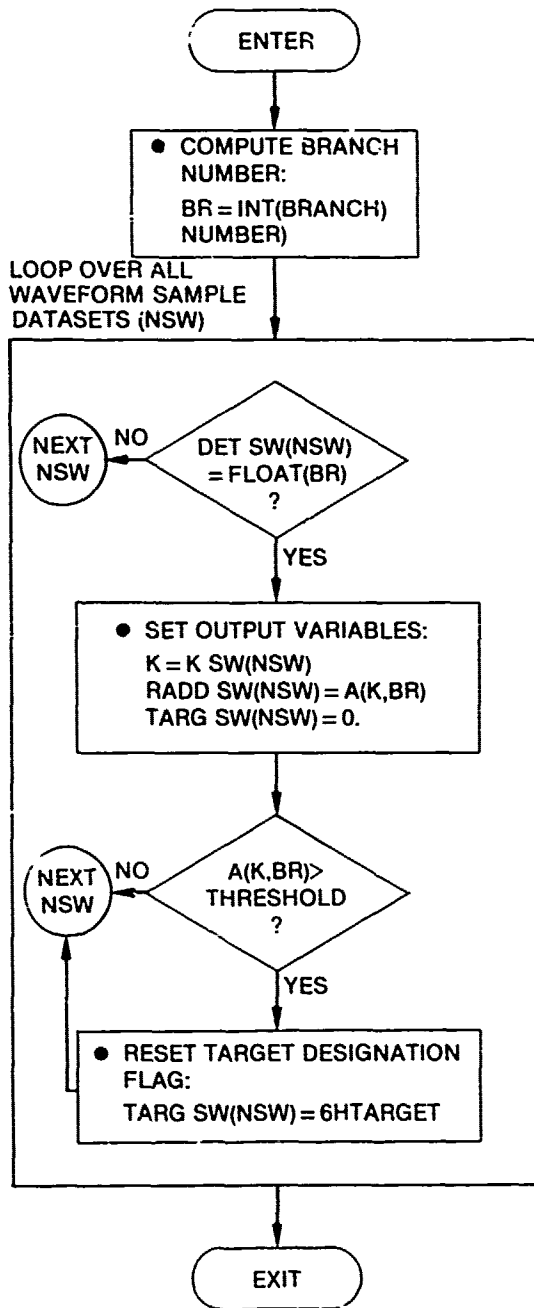
(26) OUTPUT BLOCK -- DESIGNATES SIGNALS ABOVE THRESHOLD VALUE AS TARGETS FOR OPTION OUT2 USED BY MODEL = SURVEIL-02; OTHER OPTIONS INCLUDE:

OUT1 -- TARG SW(NSW) = 9HBRIGHT PT FOR SAMPLES ABOVE THRESHOLD

OUT3 -- TARG SW(NSW) = 6HDIM PT FOR $A(K, BR) \geq 5.6$
TARG SW(NSW) = 9HBRIGHT PT FOR $A(K, BR) \geq 30$.

OUT4 -- TARG SW(NSW) = 6HBKGRND & IN ADDITION CREATES TARGET MEAS. IN SENSOR COORDINATES

AN-56252



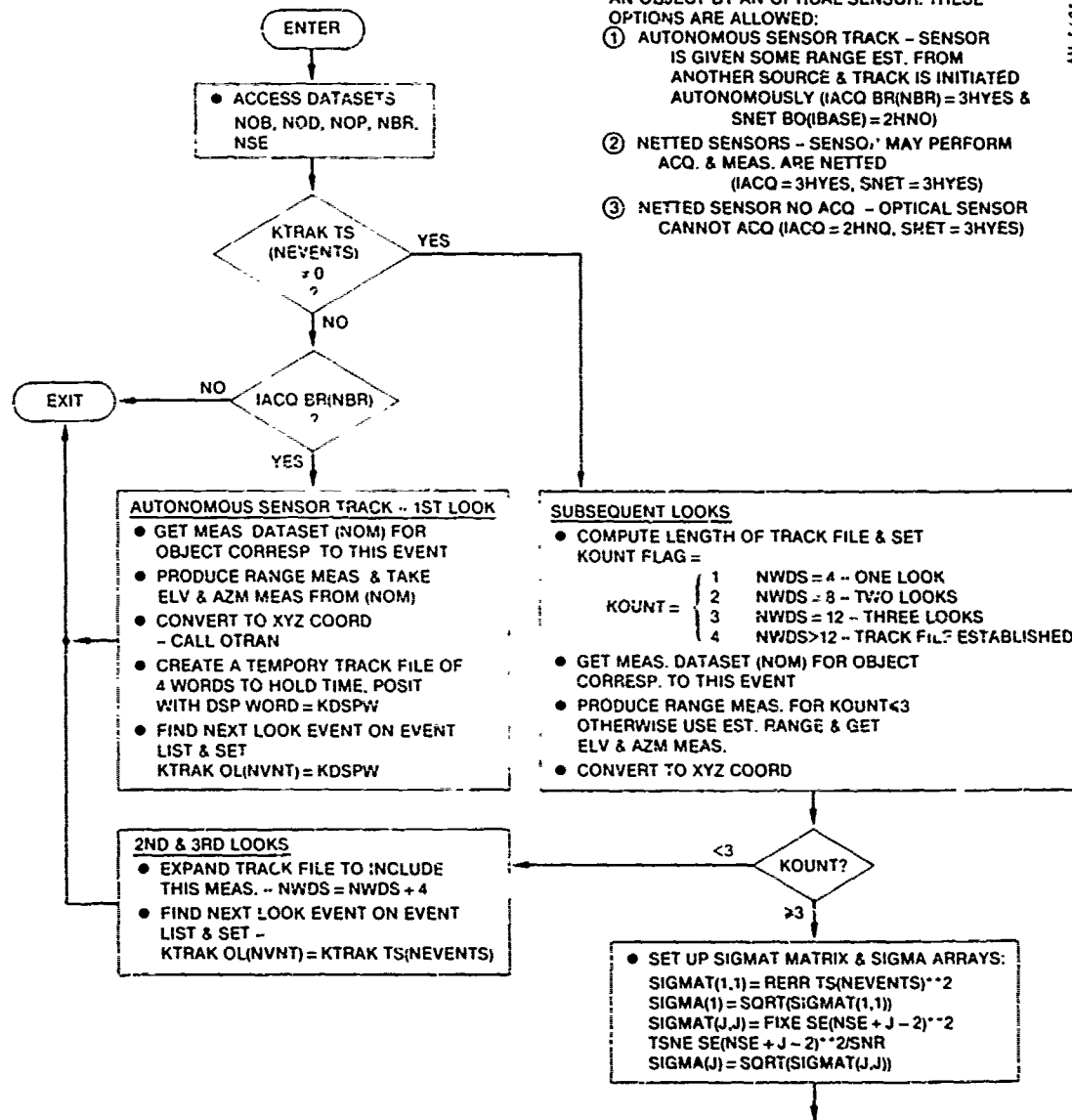
SUBROUTINE SPSUB1 --

(26) Designates signals above threshold value as targets for option OUT2 used by MODEL = SURVEIL-02

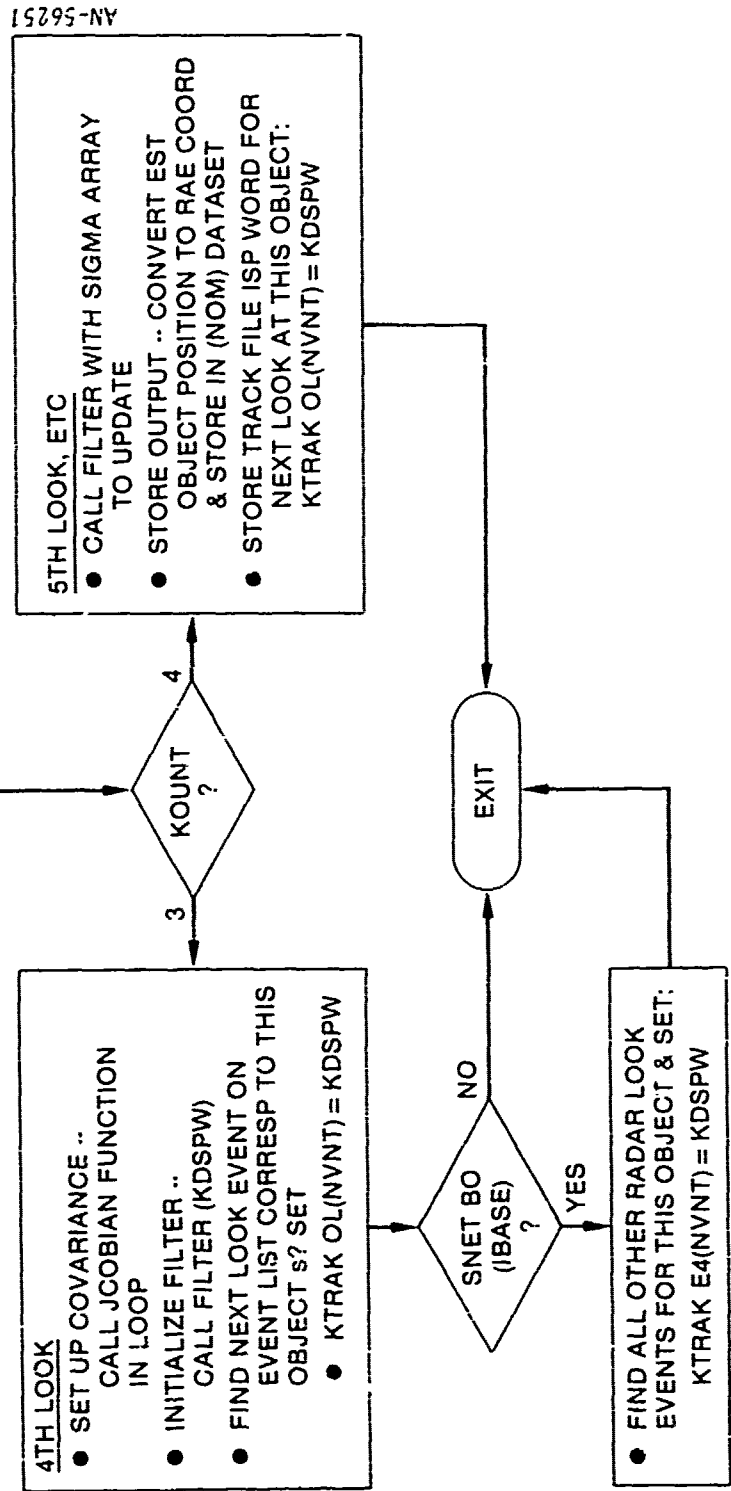
PROGRAM OTRACK -- THIS PROGRAM SIMULATES THE TRACKING OF AN OBJECT BY AN OPTICAL SENSOR. THESE OPTIONS ARE ALLOWED:

- ① AUTONOMOUS SENSOR TRACK -- SENSOR IS GIVEN SOME RANGE EST. FROM ANOTHER SOURCE & TRACK IS INITIATED AUTONOMOUSLY (IACQ BR(NBR)=3HYES & SNET BO(BASE)=2HNO)
- ② NETTED SENSORS -- SENSORS MAY PERFORM ACQ. & MEAS. ARE NETTED (IACQ=3HYES, SNET=3HYES)
- ③ NETTED SENSOR NO ACQ -- OPTICAL SENSOR CANNOT ACQ (IACQ=2HNO, SNET=3HYES)

AN-56253



PROGRAM OTRACK: Simulates the tracking of an object by an optical sensor



PROGRAM OTRACK (continued)

DISTRIBUTION LIST

DEPARTMENT OF DEFENSE

Assistant to the Secretary of Defense
ATTN: Executive Assistant

Defense Advanced Rsch Proj Agency
ATTN: TIO
ATTN: STO, S. Zakanycz

Defense Communications Engineer Center
ATTN: Code R410, J. McLean

Defense Nuclear Agency
ATTN: RAAE
ATTN: RAAE, P. Lunn
4 cy ATTN: TITL

Defense Technical Information Center
12 cy ATTN: DD

Field Command
Defense Nuclear Agency
ATTN: FCPR

Field Command
Defense Nuclear Agency
Livermore Branch
ATTN: FCPR

National Security Agency
ATTN: R-52, J. Skillman

Undersecretary of Def for Rsch & Engrg
ATTN: Strategic & Space Sys (OS)

WMCCS System Engineering Org
ATTN: R. Crawford

DEPARTMENT OF THE ARMY

Atmospheric Sciences Laboratory
U.S. Army Electronics R&D Command
ATTN: DELAS-EO, F. Niles

BMD Advanced Technology Center
Department of the Army
ATTN: ATC-T, M. Capps
ATTN: ATC-O, W. Davies

BMD Systems Command
Department of the Army
ATTN: BMDSC-HW, R. Dekalb

Harry Diamond Laboratories
Department of the Army
ATTN: DELHD-I-TL
ATTN: DELHD-N-P, F. Wimenitz

U.S. Army Foreign Science & Tech Ctr
ATTN: DRXST-SD

U.S. Army Missile Intelligence Agency
ATTN: J. Gamble

U.S. Army Missile R&D Command
ATTN: DRDMI-XS
ATTN: RSIC

U.S. Army Nuclear & Chemical Agency
ATTN: Library

DEPARTMENT OF THE ARMY (Continued)

U. S. Army Satellite Comm Agency
ATTN: Document Control

U.S. Army TRADOC Systems Analysis Activity
ATTN: ATAA-PL

DEPARTMENT OF THE NAVY

Naval Electronic Systems Command
ATTN: Code 501A
ATTN: PME 117-20

Naval Intelligence Support Ctr
ATTN: Document Control

Naval Ocean Systems Center
ATTN: Code 532

Naval Postgraduate School
ATTN: Code 1424 Library

Naval Research Laboratory
ATTN: Code 2627
ATTN: Code 4701, J. Brown
ATTN: Code 4700, T. Coffey
ATTN: Code 4780, S. Ossakow
ATTN: Code 4780, P. Palmadesso
ATTN: Code 4709, W. Ali

Naval Surface Weapons Center
ATTN: Code X211

Naval Surface Weapons Center
ATTN: Code F-14, R. Butler

Strategic Systems Project Office
Department of the Navy
ATTN: NSP-2722, F. Wimberly
ATTN: NSSP-2722, M. Meserole

DEPARTMENT OF THE AIR FORCE

Air Force Geophysics Laboratory
ATTN: OPR, A. Stair
ATTN: OPR, H. Gardiner
ATTN: SULL
ATTN: LKB, K. Champion

Air Force Systems Command
ATTN: Technical Library

Air Force Technical Applications Center
ATTN: Technical Library
ATTN: TFR, C. Meneely

Air Force Weapons Laboratory
Air Force Systems Command
ATTN: SUL
ATTN: DYC

Ballistic Missile Office
Air Force Systems Command
ATTN: MNX
ATTN: MNRC
ATTN: MNRTE

DEPARTMENT OF THE AIR FORCE (Continued)

Deputy Chief of Staff
Research, Development, & Acq
Department of the Air Force
ATTN: AFRDS

Headquarters Space Division
Air Force Systems Command
ATTN: SKX
ATTN: SKA, M. Clavin

Headquarters Space Division
Air Force Systems Command
ATTN: SZJ, P. Kelley

Rome Air Development Center
Air Force Systems Command
ATTN: OCS, V. Coyne
ATTN: TSLD
ATTN: OCSA, J. Simmons

Strategic Air Command
Department of the Air Force
ATTN: NRT
ATTN: XPFS, B. Stephan

DEPARTMENT OF ENERGY

Department of Energy
ATTN: OMA

OTHER GOVERNMENT AGENCIES

Department of Commerce
National Oceanic & Atmospheric Admin
ATTN: F. Fehsenfeld

Institute for Telecommunications Sciences
ATTN: G. Falcon
ATTN: W. Utlaut

DEPARTMENT OF DEFENSE CONTRACTORS

Aerojet Electro-Systems Co
ATTN: J. Graham

Aerospace Corp
ATTN: J. Reinheimer
ATTN: I. Garfunkel
ATTN: N. Stockwell
ATTN: V. Josephson
ATTN: N. Cohen
ATTN: J. Strauss

Berkeley Research Associates, Inc
ATTN: J. Workman

ESL, Inc
ATTN: J. Marshall

General Electric Co
ATTN: M. Bortner

General Electric Company—TEMPO
ATTN: T. Stephans
ATTN: J. Jordano
ATTN: DASIAC
ATTN: M. Stanton
ATTN: W. Knapp

DEPARTMENT OF DEFENSE CONTRACTORS (Continued)

General Research Corp
ATTN: J. Ise, Jr
ATTN: J. Garbarino

Jamieson Science & Engineering
ATTN: J. Jamieson

Kaman Sciences Corp
ATTN: N. Beauchamp
ATTN: D. Perio
ATTN: P. Tracy

Lockheed Missiles & Space Co, Inc
ATTN: D. Divis

Lockheed Missiles & Space Co, Inc
ATTN: M. Walt

M.I.T. Lincoln Lab
ATTN: D. Towle

McDonnell Douglas Corp
ATTN: R. Halprin
ATTN: H. Spitzer

Mission Research Corp
ATTN: D. Archer
ATTN: D. Sappenfield
ATTN: F. Fajen
ATTN: R. Hendrick
ATTN: R. Bogusch
ATTN: M. Scheibe
ATTN: R. Kilb

Nichols Research Corp
ATTN: N. Byrn

Pacific-Sierra Research
ATTN: H. Brode

Photometrics, Inc
ATTN: I. Kofsky

Physical Research, Inc
ATTN: R. Deliberis

University of Pittsburgh
ATTN: F. Kaufman

R & D Associates
ATTN: R. Lelevier
ATTN: F. Gilmore
ATTN: P. Haas
ATTN: B. Gabbard
ATTN: R. Turco

R & D Associates
ATTN: B. Yoon

Rand Corp
ATTN: C. Crain

Science Applications, Inc
ATTN: D. Hamlin

Science Applications, Inc
ATTN: W. Mendes

DEPARTMENT OF DEFENSE CONTRACTORS (Continued)

SRI International

ATTN: W. Chesnut
ATTN: W. Jaye

Teledyne Brown Engineering

ATTN: Technical Library
ATTN: G. Harney
ATTN: J. Cato

DEPARTMENT OF DEFENSE CONTRACTORS (Continued)

Visidyne, Inc

ATTN: C. Humphrey
ATTN: J. Carpenter
ATTN: H. Smith

Blount